1102 課

METALORGANIC MOLECULAR BEAM EPITAXY OF PHOSPHORUS-BASED III-V TERNARY SEMICONDUCTORS

Kazunari OZASA

Department of Electrical Engineering
Kyoto University

July 1989

METALORGANIC MOLECULAR BEAM EPITAXY OF PHOSPHORUS-BASED III-V TERNARY SEMICONDUCTORS

Kazunari OZASA

Department of Electrical Engineering
Kyoto University

July 1989

DOC
1989
1
電気系

ABSTRACT

This thesis describes the investigation on metalorganic molecular beam epitaxy (MOMBE) of phosphorus-based III-V ternary semiconductors (InGaP, InAlP, and AlGaP), using triethylindium (TEIn), triethylgallium (TEGa), triethylaluminum (TEAl), and phosphine. The effects of misfit strain on physical properties such as lattice parameters, photoluminescence, and electrical properties are also discussed for $In_{1-x}Ga_xP$ epilayers grown on GaAs(001) substrates by MOMBE. The main purpose of the present study is to make clear the characteristics and growth mechanism of MOMBE for phosphorus-based III-V ternary semiconductors, which give basis for further developing steps including photocontrolled and/or migration-enhanced MOMBE.

The thesis consists of six chapters. As introduction, the attractive properties of phosphorus-based III-V ternary semiconductors in realizing optoelectronic devices and high-speed devices are described in chapter 1, together with the advantages of MOMBE in preparing devices with fine microstructures, in comparison with other epitaxial growth techniques including molecular beam epitaxy (MBE) and metalorganic vapor phase epitaxy (MOVPE).

In chapter 2, low-vacuum MOVPE growth of InGaP is presented. Vapor-phase reactions such as decomposition of metalorganics and adduct formation, which are undesirable for the precise control of growth rate and epilayer composition, are observed even in a low vacuum of 0.03 Torr. Additionally, the immiscible growth of InGaP newly observed in this study is discussed to derive a growth model which can explain it.

Chapter 3 is devoted to a discussion of MOMBE growth of InGaP. The growth is limited by the incomplete decomposition of TEGa at lower temperatures below 390℃, and the shortage of

phosphorus at higher temperatures above 520℃. At moderate temperatures of 390-520℃, where the growth is governed by the supply of metalorganics, smaller phosphine fluxes improve the optical and electrical properties of the epilayers. The perfect selective growth of InGaP on SiO_2-masked GaAs substrates at 490℃ is also demonstrated.

Epitaxy of InAlP and AlGaP described in chapter 4 is a comparative study to analyze the temperature dependence of MOMBE growth. Co-decomposition of TEAl-TEIn and TEAl-TEGa is proposed to explain the enhanced decomposition of TEAl by TEIn or TEGa observed in InAlP and AlGaP epitaxy. The shortage of phosphorus at higher temperatures in MOMBE is clearly attributed to the evaporation of phosphorus from the epilayers.

In chapter 5, the effects of misfit strain on physical properties are discussed for InGaP epilayers grown by MOMBE on GaAs(001) substrates. The elastic accommodation of misfit strain is observed in the analysis of lattice parameters and energy-band-gap shift. Theoretical predictions of critical thickness for elastic-strain accommodation and of energy-band-gap shift agree well with experimental results. Photoluminescence and electrical properties are relatively insensitive to dislocations generated by the misfit strain.

The summary of the present study is given in chapter 6, together with prospects for future investigation on MOMBE of phosphorus-based III-V semiconductors.

ACKNOWLEDGMENTS

I would like to express my deep gratitude to Professor Hiroyuki Matsunami for his continuous guidance, encouragement, and critical supervision throughout this work. I am grateful to Professor Akio Sasaki for a critical reading of the manuscript and valuable comments on it. I thankfully acknowledge Professor Shigeo Fujita for his useful suggestions and criticism on the manuscript.

I am very indebted to Associate Professor Shigehiro Nishino (Kyoto Institute of Technology), who gave me powerful and stimulating encouragement through valuable discussions. I also wish to thank to Lecturer Takashi Fuyuki for his useful advice, and Dr. Masahiro Yoshimoto for his kind suggestions and for his efforts in SIMS analysis.

Special thanks are due to Mr. Masaaki Yuri, an excellent researcher, for his co-operation in various experiments including InGaP epitaxy in MOMBE. Thanks are also due to Mr. Shigehisa Tanaka for his experiments on the analysis of InGaP epilayers and on InP homoepitaxy in MOMBE.

I am grateful to Mr. Eiji Yamagishi in Rhom Co. for his efforts in EPMA analysis on immiscible samples. Experiments in this study were partially assisted by the use of facilities at Sasaki Laboratory (in double-crystal x-ray diffraction analysis), Takagi Laboratory (in stylus surface-profile measurement), and Kawabata Laboratory (in preparing SiO_2-mask patterns).

I am very thankful to Mr. Yoo Woo Sik and Mr. Takashi Saito for their kind help in preparing SiO_2-masked GaAs substrates. Useful advice and enjoyable discussions with my colleagues are fully appreciated.

I thankfully acknowledge Professor Robert W.Dutton from

Stanford University for his kind help to improve my English in this thesis.

I would like to thank Nippon Tylan Co. for offering a gas delivery system with specially made mass flow controllers, and Hokusan Co. for offering an exhaust gas neutralizing system. This work has been partially supported by the Housou-Bunka foundation and by the foundation "Hattori-Hokokai".

CONTENTS

METALORGANIC MOLECULAR BEAM EPITAXY OF PHOSPHORUS-BASED III-V TERNARY SEMICONDUCTORS

ABSTRACT
ACKNOWLEDGMENTS

1. INTRODUCTION
1-1. Phosphorus-based III-V Ternary Semiconductors 1
1-2. Metalorganic Molecular Beam Epitaxy 6

2. LOW-VACUUM METALORGANIC VAPOR PHASE EPITAXY OF InGaP
2-1. Introduction 16
2-2. Experiments 17
2-3. Epitaxial Growth of InGaP 20
2-3-1. Dependence on Temperature 20
2-3-2. Dependence on Source Flow 23
2-4. Immiscible Growth of InGaP 26
2-4-1. Observation of Immiscible Crystallites 26
2-4-2. Growth Model Including Immiscible Growth 31
2-5. Summary 36

3. METALORGANIC MOLECULAR BEAM EPITAXY OF InGaP
3-1. Introduction 41
3-2. Experimental Detail 43
3-2-1. MOMBE Apparatus and Growth Procedure 43
3-2-2. Cracking of Phosphine 49
3-2-3. Monitoring of Growth Rate 51
3-3. Temperature Dependence of InGaP Epitaxy 53
3-4. Growth at Lower Temperatures 56

3-5. Growth at Moderate Temperatures 59
3-5-1. Metalorganic Flux Dependence 59
3-5-2. Phosphine Flux Dependence 61
3-5-3. Optical and Electrical Properties 66
3-5-4. Selective Epitaxy 73
3-6. Growth at Higher Temperatures 76
3-6-1. Shortage of Phosphorus 76
3-6-2. Immiscible Defects 78
3-7. Summary 81

4. TEMPERATURE DEPENDENCE OF InAlP AND AlGaP GROWTH IN MOMBE
4-1. Introduction 86
4-2. Epitaxy of InAlP and AlGaP 87
4-3. Co-decomposition of Metalorganics 92
4-4. Phosphorus Evaporation 97
4-5. Impurity Incorporation 100
4-6. Summary 102

5. EFFECTS OF LATTICE MISMATCH
5-1. Introduction 105
5-2. Experiments 107
5-3. Strain Effects 107
5-3-1. Lattice Parameters 107
5-3-2. Photoluminescence 114
5-3-3. Electrical Properties 117
5-4. Summary 119

6. CONCLUSION 122

LIST OF PUBLICATION

1. INTRODUCTION

1-1. Phosphorus-based III-V Ternary Semiconductors

Silicon, the best semiconductor material for large scale integrated circuit (LSI) application, has made possible the developing of modern electronics. Remarkable development in Si-LSI technology has helped to realize memory-chips with a capacity of 16Mega-bits and central processing units (CPU's) with calculating speeds over several Giga-FLOPS (floating operation per second), which will soon be used in small computers for personal use as well as super computers[1]. The next stage in semiconductor technology is to connect localized computers with high-speed microwave/fiber-optic communication[2], and to develop artificial intelligence[3]. By these innovations, computers will be globally linked in real time, and will see, hear, and possibly even think as human beings do. For example, in the next generation of electronics, computers will forecast global weather automatically, by measuring climatic changes around the world, processing such data, and building a new forecast theory[4]. Based on improved weather forecasting, computers will predict crop yield, and even suggest how we could best deal with food crises.

Desirable materials for the next generation of electronics should have high electron mobility and highly effective light emission, which is necessary to achieve optoelectronic devices including optical logic circuits and optical neuro-chips[5,6]. These properties are not found in silicon, which has an indirect energy band structure (insufficient light emissivity) and low electron mobility, but they are found in III-V semiconductors. As listed in Table 1.1[7,8], many III-V binary semiconductors have direct energy band structures and high electron mobilities. Their

Table 1.1. Energy band gaps (upper parts, in eV) and mobilities (lower parts, in cm^2/Vs) in III-V semiconductors. Marks * represent indirect energy band gaps.

	Al	Ga	In
P	2.48* 80	2.261* 300	1.351 4600
As	2.163* 1200	1.424 8500	0.360 33000
Sb	1.58 200	0.726 4000	0.172 78000

Si
1.12 1500

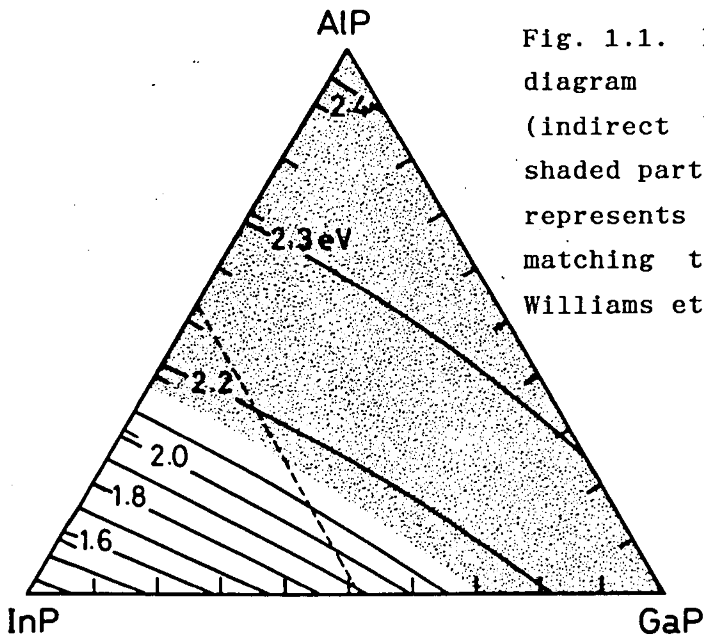

Fig. 1.1. Energy-band-gap diagram of InGaAlP (indirect band gap in a shaded part). Broken line represents lattice matching to GaAs. (After Williams et al.[12]).

conduction types are easily controlled by impurity doping, as in the case of silicon. The self-compensation of doped impurities, which impedes p-type doping in II-VI semiconductors[9], are not observed in III-V semiconductors. Moreover, high-quality semi-insulating substrates[10] of GaAs and InP are commercially available, but those of silicon are hard to prepare. Thus, device-isolation techniques to cut current paths through the substrate can be eliminated in the device-fabricating process of III-V semiconductors, while they are inevitably employed in silicon process[11]. This contributes to high-speed action with smaller currents in III-V semiconductor devices, by eliminating excess capacitances in pn-junction isolating structures. Another important characteristic which gives III-V semiconductors superiority over silicon is that energy band gap, the most important property of semiconductors, is widely controlled in III-V alloy semiconductors, as shown in Fig.1.1[12]. This allows us to tailor the material properties as we wish, and to make full use of the properties by preparing heterostructures. The basic concept of heterostructure devices was proposed in 1963[13], and found effective for the injection and confinement of minority carriers into active layers in device structures to enhance their radiative recombination[14]. In the intensive investigation of heterostructures in the AlGaAs/GaAs system, highly effective laser diodes and two-dimensional electron-gas field effect transistors (2DEG-FET's) for high-speed action have been successfully produced[15].

Phosphorus-based III-V ternary semiconductors (InGaP, InAlP, and AlGaP) studied in this thesis are wide gap materials, as shown in Fig.1.2[16]. Wide gap materials have been increasingly important as short-wavelength light sources to develop high-density memory/printing instruments, such as magneto-optic disk-memories, laser beam printers, and optical bistable devices.

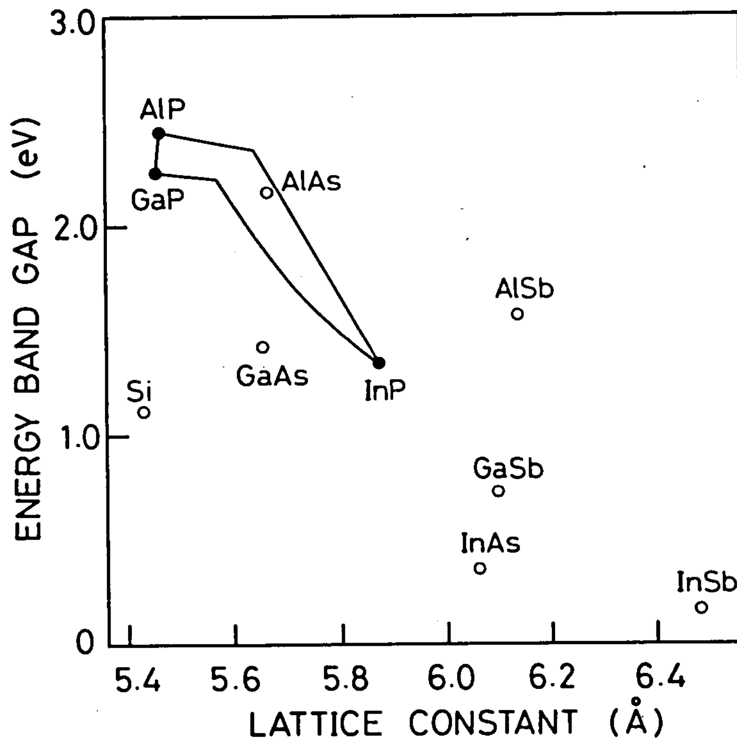

Fig. 1.2. Energy band gaps and lattice constants of III-V semiconductors. Phosphorus-based III-V semiconductors (InGaAlP) cover the surrounded area.

They are also useful for high-speed devices, such as 2DEG-FET's[17,18] or hetero-bipolar transistors (HBT's)[19]. However, the investigation on phosphorus-based III-V semiconductors runs far behind that of arsenic-based III-V semiconductors, especially in device application fields. Pulse operation at 77K of a visible InGaAlP laser using an InGaP active layer was reported in 1982[20], and continuous wave (CW) operation at room temperature was first achieved in 1985[21], while CW operation at room temperature of an AlGaAs laser with a threshold current density of 8.6 kA/cm^2 was achieved in 1969[22]. This comes mainly from the fact that the AlGaAs/GaAs system has almost no lattice mismatch in the entire range of aluminum content, while the careful control of epilayer composition x is required for $In_{1-x}Ga_xP$ to be lattice-matched to GaAs substrates (Fig.1.1). A large mismatch of lattice constant at the interface of heterostructures causes a number of dislocation defects in active layers, which are harmful to the reliability of devices[23], though strain-induced effects like energy-band-gap shift arisen from the tetragonal lattice deformation of epilayers[24,25] are useful in strained-layer devices. The problem of lattice mismatch is expected to be solved by introducing strained-layer superlattices[26] between substrates and active epilayers, and/or by the use of III-V ternary substrates. When the problem is removed, the ability of phosphorus-based III-V ternary is surely beyond that of arsenic-based ones, since they have larger energy band gaps (shorter wavelength in light emission), as shown in Fig.1.2, and generally, shorter wavelength is desirable to improve the recording density of magneto-optic disks or laser beam printers. Furthermore, lower efficiency of radiative recombination in indirect band-gap materials including GaP and AlP is expected to be improved by the indirect-to-direct transition of energy gap

caused by band-folding effects, recently predicted in $(GaP)_n(AlP)_n$ superlattices[27]. Phosphorus-based III-V ternary semiconductors, therefore, are certainly the most promising materials for the next generation of electronics.

1-2. Metalorganic Molecular Beam Epitaxy

The epitaxial growth of semiconductors is the most fundamental step to prepare various heterostructure devices. Recent progress of device design has come to require the fabrication of ultrafine microstructures in heteroepitaxy, such as multi-epilayers with abrupt change in composition, monolayer superlattices, or three-dimensional heterostructures.

Liquid phase epitaxy (LPE), which has been a main method to fabricate various semiconductor devices, has not sufficient ability to prepare heterostructures with atomic accuracy, especially superlattices. Moreover, large miscibility gaps in InGaP and InAlP[28], and the large distribution coefficient of aluminum[29] prevent the full use of LPE in preparing phosphorus-based III-V ternary semiconductors.

Molecular beam epitaxy (MBE) has excellent ability in controlling epilayer thickness and composition. Atoms and molecules evaporated from source effusion cells have large mean free path under high-vacuum in MBE, and they directly reach the substrate without collisions, as molecular beams. The growth rate in MBE can be reduced below to 0.1 μm/h, which corresponds to a few atomic layers per minute, without inducing residual impurity incorporation, since the residual gas molecules are very few in the high-vacuum condition. Therefore, the growth in MBE is controllable with atomic accuracy, by using mechanical chopping of molecular beams. Moreover, the degree of super-saturation in

source molecules at the substrate surface is lower in MBE growth, resulting in lower temperature epitaxy. Many instruments including reflection of high energy electron diffraction (RHEED) instruments, x-ray photoemission spectroscopes (XPS's), and quadrupole mass analyzers (QMA's) are available under high-vacuum in MBE in order to monitor the growth 'in-situ', contributing to the preparation of high-quality heterostructures. Remarkable progress in quantum-well physics and superlattice physics is owing to the development of MBE techniques, and a number of devices with double heterojunction (DH), multi quantum wells (MQW), and/or superlattices have been fabricated using MBE. Moreover, migration enhancing techniques, which utilize rapid-migration characteristics of metal atoms on metal-stabilized surfaces by means of the alternative supply of group-III atoms and group-V atoms, have proved very useful for growing GaAs and AlAs layers at temperatures as low as 200℃ in MBE[30,31]. The flatness and abruptness of heterointerfaces are also substantially improved in this migration enhanced epitaxy (MEE). However, some disadvantages of MBE listed below have been impeding its mass-productive use; (1) oval defects caused by gallium spitting from a gallium melting source are usually formed on epilayers[32,33], (2) selective epitaxy on insulator-masked substrates is imperfect (polycrystalline deposits on the insulator[34,35]), (3) recharge of solid sources involves the exposure of the growth chamber to ambient air, which is very harmful for the consistent production of high-quality semiconductors, (4) due to the high and different vapor pressures of allotropy in group-V solid sources, the intensity control of group-V beam is relatively difficult, resulting in a not precise ratio of group-V elements in multi-group-V semiconductors such as InGaAsP or AlGaAsP, and (5) fabricating a graded change in epilayer composition requires delicate temperature-control of

effusion cells.

In vapor phase epitaxial (VPE) methods, metalorganic vapor phase epitaxy (MOVPE) surpasses others (chloride VPE and hydride VPE) by employing group-III metalorganics and group-V hydrides; (1) since chemical reaction to make transportable group-III chemicals is not necessary, MOVPE does not need two temperature zones unlike other VPE methods, but only one to heat substrates, resulting in simple reaction furnaces, (2) epilayer thickness, composition, and doping profiles are precisely and easily controlled by employing mass flow controllers, and (3) substrate etching and auto-doping do not take place, since no hydrochloric is used. By using these advantages, many devices including AlGaAs and InGaAsP laser diodes, now widely used in laser-disk players and for fiber-optic communication, will soon be fabricated mass-productively in MOVPE. The high controllability of epitaxial growth in MOVPE was also demonstrated by succeeding in the preparation of monolayer superlattices like $(GaAs)_1(AlAs)_1$[36] and $(InAs)_1(AlAs)_1$[37], which had been believed to be preparable only by MBE methods. Furthermore, atomic layer epitaxy (ALE)[38], the ultimate technique to prepare superstructures, has been achieved for GaAs homoepitaxy in MOVPE systems by supplying group-III metalorganics and group-V hydrides alternatively, with and without laser assistance[39,40]. Disadvantages in this potential MOVPE technique are (1) large amounts of toxic gases such as arsine or phosphine are used[41,42], (2) efficiency of source utilization is very small as is the usual case in VPE methods, (3) epilayer composition is not proportional to source flow ratio, impeded by reaction between source gases including adduct formation of triethylindium and phosphine or arsine[43,44], and (4) thermal convection of gases on heated substrates disturbs homogeneous epitaxy.

Metalorganic molecular beam epitaxy (MOMBE) has been

recently developed as a new crystal growth technique with high ability in preparing heterostructures. The epitaxy in MOMBE is performed under high vacuum (<10^{-4} Torr) using group-III metalorganics and group-V hydrides (or solids) as molecular beam sources. In this thesis, the name of MOMBE is used for the epitaxy under high vacuum in which metalorganics are employed as group-III molecular beam sources (group-V sources are usually hydrides, but solid sources in some cases), and the name of gas-source MBE for those employ only group-V hydrides. MOMBE succeeds to the advantage of MBE and MOVPE, and is free from the disadvantages of both. The advantages of MOMBE, which have been confirmed mainly in GaAs homoepitaxy, are as follows[45,46]; (1) it has excellent controllability of epilayer thickness and composition, both being superior or comparable to MBE, (2) complicated heterostructures can be prepared by the easy change of source beam fluxes with mass flow controllers, (3) oval defects are not formed on epilayers, (4) perfect selectivity of epitaxy on insulator-masked substrates is achievable, (5) source metalorganics can be recharged easily without any contamination to the growth chamber, (6) beam fluxes of group-V hydrides are controlled as easily as group-III beam fluxes, and (7) harmful reaction of sources in MOVPE is eliminated with improving the efficiency of source utilization.

The essential difference of MOMBE growth from MBE or MOVPE growth is that the decomposition reaction of metalorganics takes place just on the heated substrates, as illustrated in Fig.1.3[46]. Since source molecules impinge directly onto the heated substrate without collisions as in MBE, harmful stagnant layers are not formed on the substrates, and thus, reactions between sources are completely removed. This leads to the highly precise control of epilayer thickness and composition in MOMBE. The decomposition reaction of metalorganics at the substrate

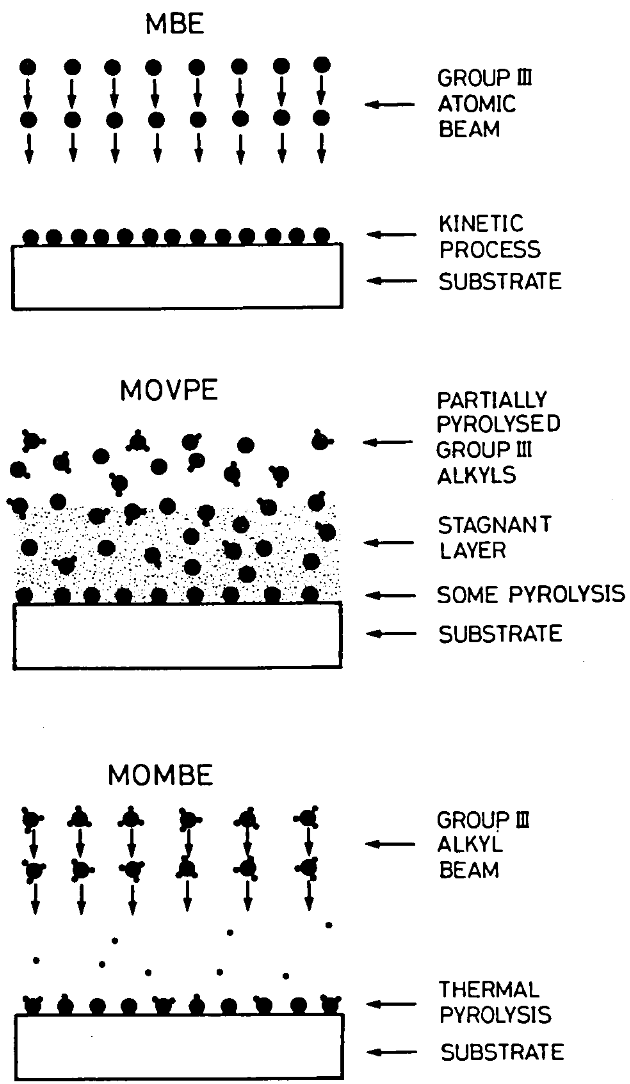

Fig. 1.3. Growth kinetics in MBE, MOVPE, and MOMBE. (After Tsang[46]).

surface is expected to be strongly influenced by surface condition and/or electron/photon irradiation. Selective epitaxy, electron-beam drawing epitaxy, or photocontrolled epitaxy will be practically available in MOMBE, by modulating the reaction with insulator-masking of substrates, electron-beam irradiation, or photo-excitation. These advanced techniques make it possible to fabricate new devices with three-dimensional heterostructures including quantum wires/boxes, which are predicted to have useful and unique characteristics in optical and electrical properties[47-49]. Moreover, by building focused ion-beam implantation (FIBI) equipment within the MOMBE system and by using various metalorganic sources for electrodes, the ultimate MOMBE process, in which heterostructure devices are completely fabricated without taking them out from the growth chamber, can be realized.

With a philosophy which holds that the fundamental investigation of growth mechanism in MOMBE gives the best basis for the advanced steps of MOMBE, various aspects of MOMBE growth of phosphorus-based III-V ternary semiconductors, especially its temperature dependence, are described in this thesis. The following topics are discussed in the next four chapters;

(1) influences of vapor-phase reaction in low-vacuum MOVPE (chapter 2),
(2) immiscible growth of InGaP observed in low-vacuum MOVPE (chapter 2),
(3) decomposition of metalorganics at lower temperatures in MOMBE (chapters 3 and 4),
(4) flux dependence of InGaP growth in MOMBE (chapter 3),
(5) optical and electrical properties of InGaP grown in MOMBE (chapter 3),
(6) selective epitaxy of InGaP in MOMBE (chapter 3),

(7) phosphorus evaporation at higher temperatures in MOMBE (chapters 3 and 4), and

(8) effects of lattice mismatch on physical properties of InGaP epilayers grown by MOMBE on GaAs(001) substrates (chapter 5).

References

[1] See recent issues of Electronics.

[2] See recent issues of Microw.J., Commun.Int., IEEE Trans.Microwave Theory Tech., IEEE Trans.Commun., or IEEE J.Lightwave Technol.

[3] See, for example, "The Handbook of Artificial Intelligence vols.1-3", Ed. A,Barr, E.A.Feigenbaum, and P.R.Cohen, Pitman (1982).

[4] See recent issues of Mon.Weather Rev. or Meteorol.Mag.

[5] P.Mandel, S.D.Smith, and B.S.Wherrentted, "From Optical Bistability Towards Optical Computing", North-Holland, Amsterdam (1987).

[6] N.H.Farhat, Appl.Opt. **26** (1987) 5093.

[7] M.Neuberger, "Handbook of Electronic Materials vol.2", IFI/Plenum (1971).

[8] H.C.Casey Jr. and M.B.Panish, "Heterostructure Lasers part B", Academic Press, New York (1978).

[9] B.Ray, "II-VI Compounds", Pergamon Press, Oxford (1969).

[10] "Semi-Insulating III-V Materials, Melmo 1988. Proceedings of the Fifth Conference", Adam Hilger (1988).

[11] L.C.Parrillo, "VLSI Technology", Ed. S.M.Sze, McGraw-Hill Int.Book Co. Chapter 11 (1983).

[12] C.K.Williams, T.H.Glisson, J.R.Hauser, and H.A.Littlejohn, J.Electron.Mater. **7** (1978) 639.

[13] H.Kroemer, Proc.IEEE **51** (1963) 1782.

[14] H.C.Casey Jr. and M.B.Panish, "Heterostructure Lasers part A", Academic Press, New York (1978).

[15] "Proc. 12th Int.Symp. Gallium Arsenide and Related Compounds, Karuizawa, 1985", Inst.Phys.Conf.Ser. No.79 (1986).

[16] M.Kazumura, I.Ohta, and I.Teramoto, Jpn.J.Appl.Phys. **22** (1983) 654.

[17] H.M.Cox, J.R.Hayes, R.N.Nottenburg, S.G.Hummel, and S.J.Allen, Electron.Lett. **22** (1986) 73.

[18] K.Kitahara, M.Hoshino, K.Kodama, and M.Ozeki, Jpn.J.Appl.Phys. **26** (1987) L1119.

[19] H.Kroemer, Proc.IEEE **70** (1982) 13.

[20] H.Asahi, Y.Kawamura, H.Nagai, and T.Ikegami, Electron.Lett. **18** (1982) 62.

[21] K.Kobayashi, S.Kawata, A.Gomyo, I.Hino, and T.Suzuki, Electron.Lett. **21** (1985) 931.

[22] I.Hayashi, M.B.Panish, and P.W.Foy, IEEE **QE-5** (1969) 211.

[23] P.J.Anthony, R.L.Hartman, N.E.Schumaker, W.R.Wagner, J.Appl.Phys. **53** (1982) 756.

[24] H.Asai and K.Oe, J.Appl.Phys. **51** (1983) 2052.

[25] C.P.Kuo, S.K.Vong, R.M.Cohen, and G.B.Stringfellow, J.Appl.Phys. **57** (1985) 5428.

[26] J.W.Matthews, A.E.Blakeslee, and S.Mader, Thin Solid Films **33** (1976) 253.

[27] M.Kumagai and T.Takagahara, Phys.Rev. **B37** (1988) 898.

[28] K.Onabe, Jpn.J.Appl.Phys. **22** (1983) 287.

[29] M.Kazumura, I.Ohta, and I.Teramoto, Jpn.J.Appl.Phys. **22** (1983) 654.

[30] Y.Horikoshi, M.Kawashima, and H.Yamaguchi, Jpn.J.Appl.Phys. **25** (1986) L868.

[31] Y.Horikoshi, M.Kawashima, and H.Yamaguchi, Appl.Phys.Lett. **50** (1987) 1686.

[32] P.D.Kirchner, J.M.Woodall, S.L.Wright, J.F.Freeous, and G.D.Pettit, Appl.Phys.Lett. **38** (1981) 427.

[33] K.Akimoto, M.Dohsen, M.Arai, and N.Watanabe, J.Cryst.Growth **73** (1985) 117.

[34] A.Y.Cho and W.C.Ballamy, J.Appl.Phys. **45** (1975) 783.

[35] S.Hiyamizu, K.Nanbu, T.Fujii, T.Sakurai, H.Hashimoto, and O.Ryusan, J.Electrochem.Soc. **127** (1980) 1562.

[36] A.Ishibashi, Y.Mori, M.Itabashi, and N.Watanabe, J.Appl.Phys. **58** (1985) 2691.

[37] T.Fukui and H.Saito, Jpn.J.Appl.Phys. **23** (1984) L521.

[38] T.Suntola and J.Anston, U.S.Patent No.4058430 (1977).

[39] Y.Aoyagi, A.Doi, S.Iwai, and S.Namba, J.Vac.Sci.Technol. **B5** (1987) 1460.

[40] M.Ozeki, K.Mochizuki, N.Ohtsuka, and K.Kodama, Appl.Phys.Lett. **53** (1988) 1509.

[41] "CRC Handbook of Laboratory Safety", Ed. N.V.Steere, Chemical Rubber Co., Cleaveland Ohio (1967).

[42] G.B.Stringfellow, J.Electron.Mater. **17** (1988) 327.

[43] R.Didchenko, J.E.Alix, and R.H.Toeniskoetter, J.Inorg.Nucl.Chem. **14** (1960) 35.

[44] H.M.Manasevit and W.I.Sympson, J.Electrochem.Soc. **120** (1974) 135.

[45] E.Tokumitsu, Y.Kudo, M.Kanagai, and K.Takahashi, J.Appl.Phys. **55** (1984) 3163.

[46] W.T.Tsang, J.Electron.Mater. **15** (1986) 235.

[47] Y.Arakawa and H.Sakaki, Appl.Phys.Lett. **40** (1982) 939.

[48] Y.Arakawa, K.Vahala, and A.Yaric, Appl.Phys.Lett. **45** (1984) 950.

[49] M.Asada, Y.Miyamoto, and Y.Suematsu, IEEE **QE-22** (1986) 1915.

2. LOW-VACUUM METALORGANIC VAPOR PHASE EPITAXY OF InGaP

2-1. Introduction

Metalorganic vapor phase epitaxy (MOVPE) of III-V semiconductors is being investigated intensively[1], since its excellent control of epitaxy (epilayer thickness and composition) makes it possible to prepare fine heterostructures such as multi quantum wells (MQW) or double hetero (DH) structures. The usual investigations on MOVPE of III-V semiconductors have been carried out under atmospheric pressure or under lower pressures of approximately 76 Torr. The reduction of reaction pressure and the fast flow of source gases are effective to make abrupt heterointerfaces by means of gas switching[2-4]. Low-vacuum MOVPE carried out in low-vacuum region (<0.1 Torr) is, therefore, expected to have an ability for making fine heterostructures, more so than conventional MOVPE.

In conventional MOVPE, crystals grow through two different kinds of process[5]; (1) vapor-phase reactive/kinetic process such as the thermal decomposition of source gases and the diffusion of decomposed species through a stagnant layer formed on a heated substrate, and (2) surface process such as the migration of adsorbed species on the substrate or their incorporation/desorption. Here, the vapor-phase process governs the main part of crystal growth (e.g., growth rate and crystal composition), and the surface process influences crystal quality. In low-vacuum MOVPE, the surface process plays a more important role than in conventional MOVPE, since smaller gas supply in the low-vacuum region makes the stagnant layer very thin. Fraas et al. reported vacuum chemical epitaxy (VCE) of GaAs at approximately $1x10^{-3}$ Torr[6,7], which is one of the vacuum MOVPE techniques. However, there have been few reports on MOVPE in the

low-vacuum region and no report on low-vacuum MOVPE of InGaP. Investigation on the low-vacuum MOVPE of InGaP will give useful information on the influence of vapor-phase/surface process on the epitaxy of phosphorus-based III-V ternary semiconductors, and contributes to the understanding of growth mechanism in metalorganic molecular beam epitaxy (MOMBE), where the stagnant layer is completely removed.

In this chapter, crystal growth of InGaP on GaAs(001) carried out by low-vacuum (0.03 Torr) MOVPE is described, together with a new observation of immiscible growth. The influence of vapor-phase/surface process is investigated from the temperature dependence and source-supply dependence of growth rate and epilayer composition. Additionally, the immiscible growth of InGaP newly observed in the low-vacuum MOVPE is discussed, and a growth model for the crystal growth in low-vacuum MOVPE, which can explain the occurrence of the immiscible growth, is proposed.

2-2. Experiments

Crystal growth was carried out in a stainless-steel chamber with a volume of 2000 cm^3 (Fig.2.1), which was evacuated by a rotary pump with a speed of 360 l/s, using triethylindium (TEIn), triethylgallium (TEGa), and phosphine (PH_3) without precracking. Since these ethyl-based metalorganics decompose in the way of β-elimination process[8-12], the products of their thermal decomposition are stable C_2H_4 and metal species like $Ga(C_2H_5)_2H$, resulting in less carbon contamination in MOVPE growth compared with methyl-based metalorganics, which inevitably provide CH_3 radicals[13-17]. To maintain the reaction pressure in the low-vacuum region, the total gas flow must be small compared with

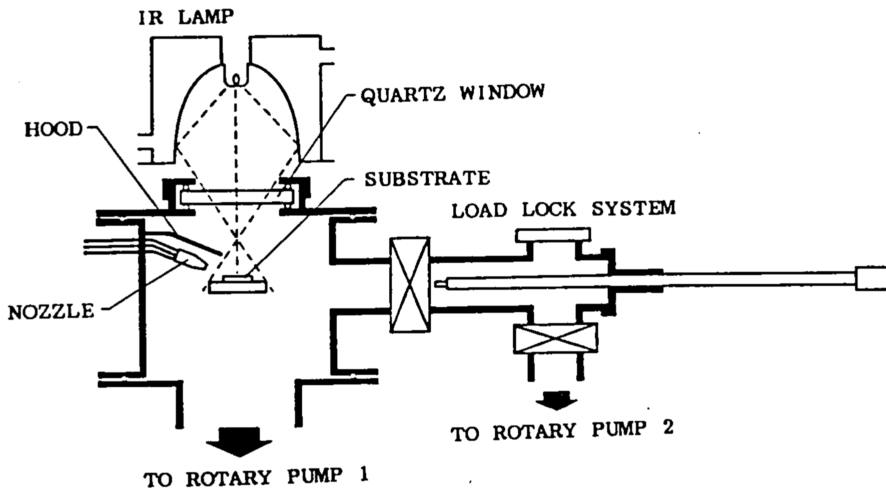

Fig. 2.1. Schematic drawing of low-vacuum MOVPE reactor.

Table 2.1. Growth condition for epitaxial growth of InGaP.

	Range	Typical
Substrate temperature (℃)	520-670	640
Source flow rate (sccm)		
TEIn	0.0291-0.0444	0.0294
TEGa	0.00-0.0798	0.0099
PH_3	0.250-1.000	1.000
V/III ratio	5.05-25.4	25.4
TEGa/(TEGa+TEIn)	0.00-0.729	0.252
Reaction pressure (Torr)	0.014-0.040	0.030

the pumping speed, and thus, hydrogen bubbling or any carrier/dilution gas was not employed. The metalorganics were kept warm in fan-heating boxes (80℃ for TEIn and 50℃ for TEGa; their vapor pressures are approximately 10 Torr), and their vapors were carried from their vessels to the reactor by the pressure difference. The source gases were led into the reactor separately after their flows were controlled by mass flow controllers, and carried onto a substrate through a mixing nozzle. The total amount of the three source gases that flowed into the reactor was very small (approximately 1.0 sccm), and the reaction pressure was kept in the low-vacuum region (approximately 0.03 Torr). A GaAs(001) substrate of 10x10 mm^2 was loaded through a loading chamber to prevent ambient contaminant gases from coming into the reactor. The substrate was heated by infrared irradiation from a halogen lamp (1000 W) set outside the reactor (Fig.2.1). The substrate temperature was measured by a thermocouple near the edge of the substrate, which was precalibrated by another thermocouple on the center of the substrate. Before the growth, the substrate was heated up to 700℃ for 1 min to remove the surface oxide layer. Under the high-vacuum conditions of MBE ($<10^{-5}$ Torr, with arsenic beam irradiation), the removal of surface oxide layers on GaAs substrates has been reported for temperatures as low as 550℃[18-21]. However, taking account of a background pressure of approximately $1x10^{-3}$ Torr in this low-vacuum MOVPE, a fairly high cleaning temperature was used.

The growth conditions for InGaP epitaxy is given in Table 2.1. The growth rate was determined from the epilayer thickness obtained by the cross-sectional observation of cleaved epilayers with a scanning electron microscope (SEM). The crystal quality of grown layers was examined by reflection high-energy electron diffraction (RHEED) observation. The epilayer

composition was determined by x-ray diffraction measurement.

2-3. Epitaxial Growth of InGaP

2-3-1. Dependence on Temperature

Figure 2.2 shows the improvement of crystal quality with increasing temperature as a change in RHEED patterns. When the temperature is 520℃, InGaP layers are still polycrystalline as indicated in Fig.2.2a by ring-patterns. By increasing the temperature above 550℃, the InGaP layers are improved to single crystalline as shown in Figs. 2.2b and 2.2c by the pattern change from rings to spots. At a temperature of 670℃, an epitaxial InGaP layer, which has a spot-pattern in RHEED (Fig.2.2d), is obtained. Similar temperature dependence of crystal quality is observed in the temperature change of full width at half maximum (FWHM) of x-ray rocking curves.

InGaP layers grown in the low-vacuum MOVPE at 600-670℃ are somewhat inferior in crystal quality and in surface morphology to those grown at same temperatures in conventional MOVPE[22-25], where high-quality epilayers are obtained for temperatures as low as 600℃. This is partly due to the unoptimized growth system and growth conditions in this study, but is mainly due to the fact that the growth interface in low-vacuum MOVPE differs much from that in conventional MOVPE. The stagnant layer in this low-vacuum MOVPE experiments is much heavier than in conventional MOVPE, since no carrier/dilution gas is employed. This makes the growth interface highly super-saturative with decomposed sources, and brings three-dimensional island-like growth, resulting in the inferior crystal quality. Higher temperatures are required to improve the crystal quality by promoting the migration of

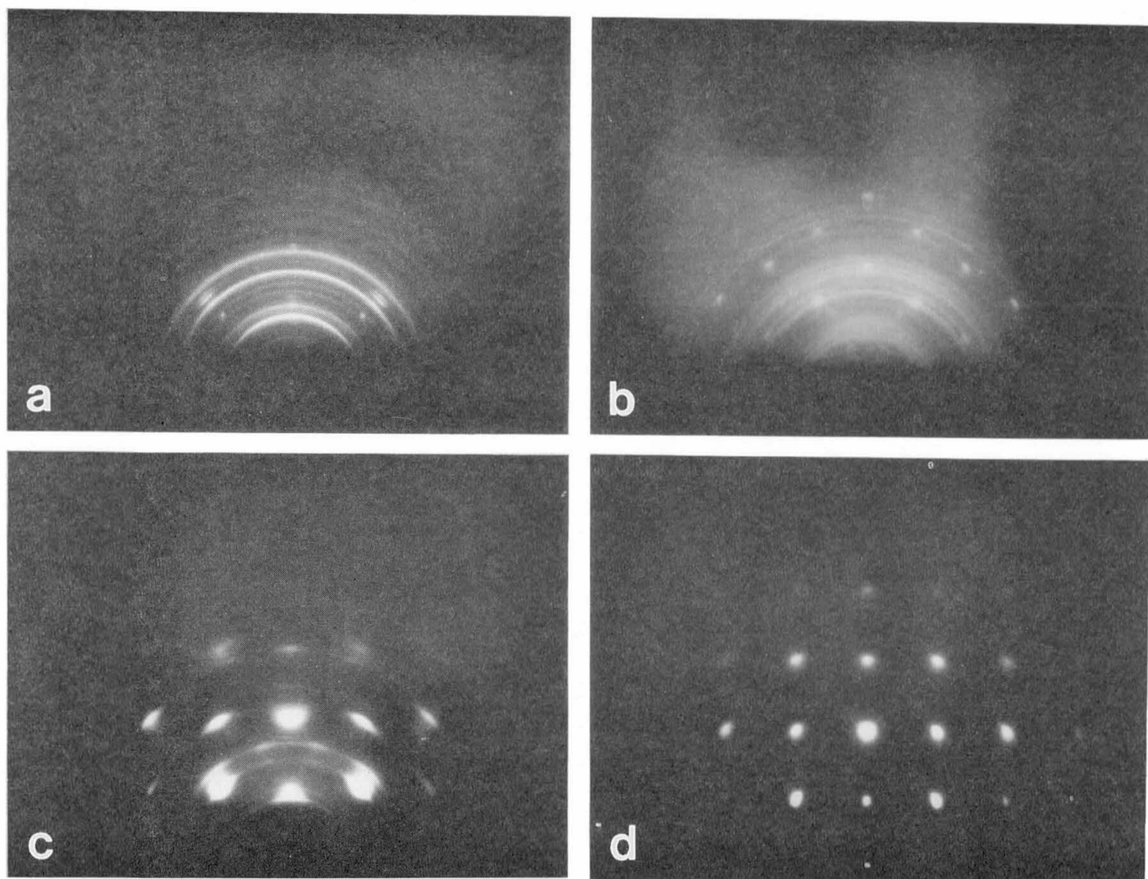

Fig. 2.2. Dependence of RHEED pattern on substrate temperature: (a) 520℃; (b) 550℃; (c) 640℃; (d) 670℃.

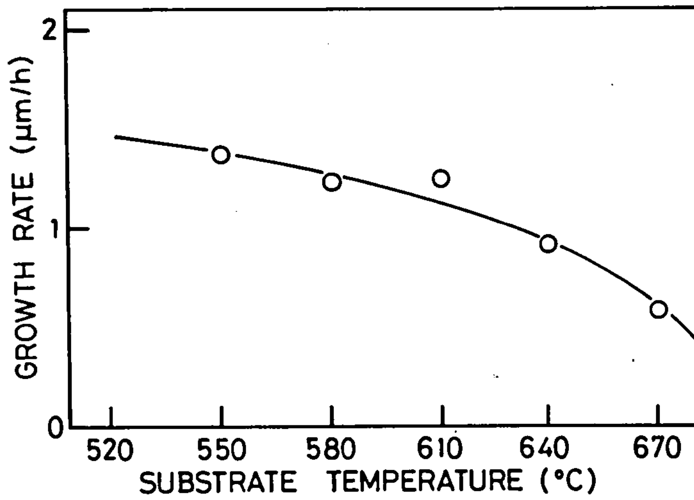

Fig. 2.3. Temperature dependence of growth rate.
(TEIn=0.029, TEGa=0.010, PH_3=1.00 sccm).

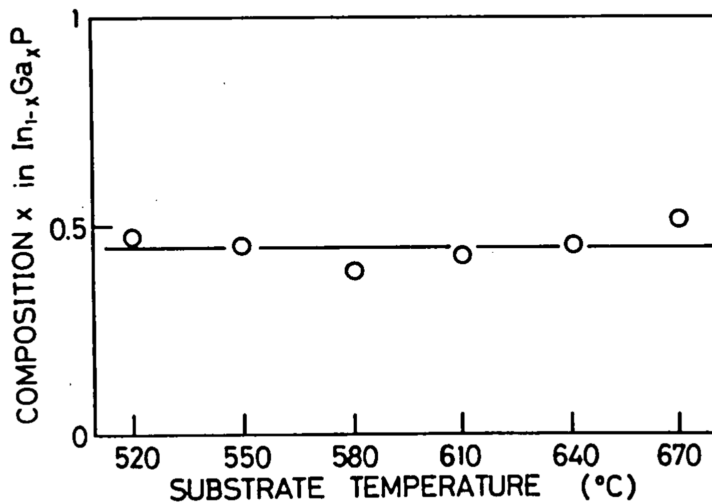

Fig. 2.4. Temperature dependence of composition x in $In_{1-x}Ga_xP$.
(TEIn=0.029, TEGa=0.010, PH_3=1.00 sccm).

adsorbed atoms.

The growth rate decreases with increasing temperature as shown in Fig.2.3. Two possible causes of this relation are (1) increase in power of infrared irradiation to raise the substrate temperature causes the decomposition of metalorganics before they reach the substrate, resulting in the reduction of effective supply of group-III sources, and (2) with the increase in substrate temperature, adsorbed atoms reevaporate from the substrate surface. The former is related to the vapor-phase reaction, and the latter to surface kinetics.

The composition x of $In_{1-x}Ga_xP$ layers is independent of temperature (Fig.2.4), even at the higher temperatures where the growth rate is reduced. This indicates that the growth rate of InP (involved in the growth rate of $In_{1-x}Ga_xP$) is reduced as much as that of GaP. The reevaporation of adsorbed atoms is smaller for gallium atoms than indium atoms, since Ga-P bonds are stronger than In-P bonds. Thus, the reduced growth rates of InGaP at higher temperatures are due to the thermal influence on the vapor-phase reaction as mentioned above (1), rather than that on the surface kinetics.

2-3-2. Dependence on Source Flow

The growth rate depends proportionally on the group-III total flow as shown in Fig.2.5, indicating that the growth in low-vacuum MOVPE is limited by the supply of group-III metalorganics as in conventional MOVPE. The crystal quality of InGaP layers grown at a constant temperature is not affected by the growth rate (group-III total flow). This suggests that the improvement of crystal quality with increasing temperature is not due to the reduced growth rates at higher temperatures.

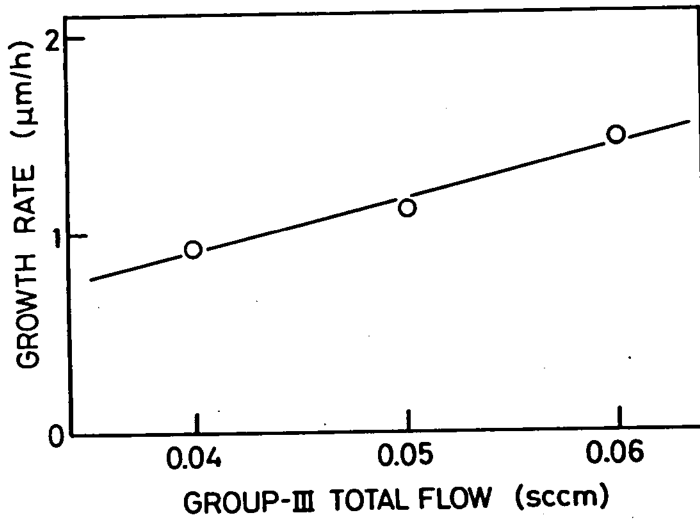

Fig. 2.5. Dependence of growth rate on group-III total flow of TEGa+TEIn.
(640℃, TEIn/TEGa=0.30, PH_3=1.00 sccm).

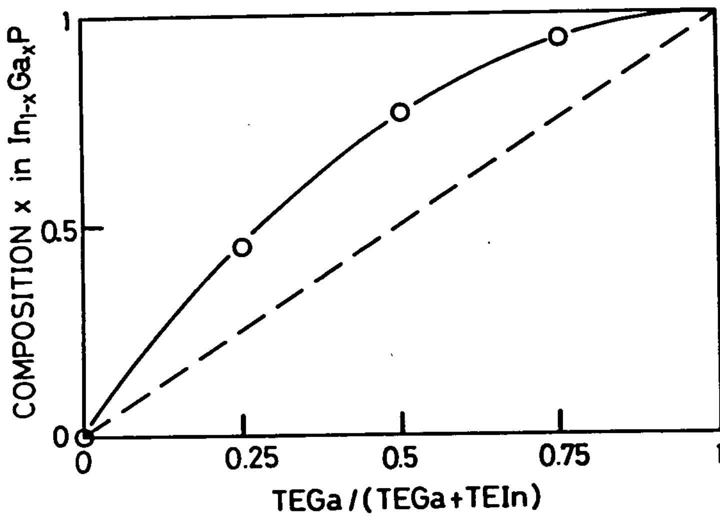

Fig. 2.6. Dependence of composition x in $In_{1-x}Ga_xP$ on flux ratio of TEGa/(TEGa+TEIn).
(640℃, TEIn=0.029, PH_3=1.00 sccm).

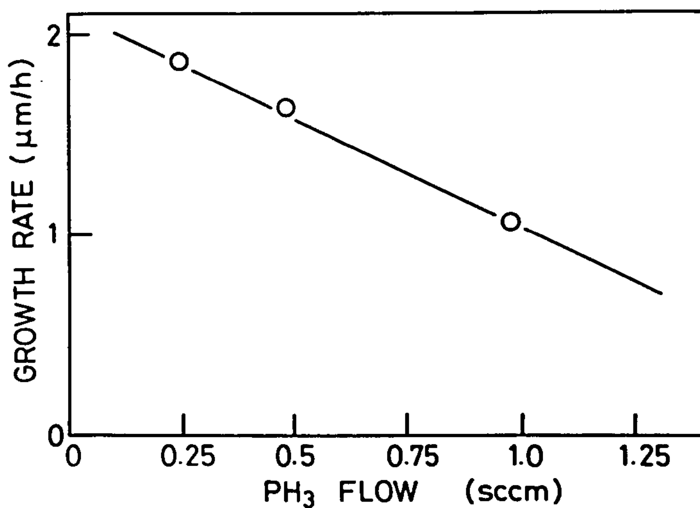

Fig. 2.7. Dependence of growth rate on phosphine flow. (580℃, TEIn=0.037, TEGa=0.012 sccm).

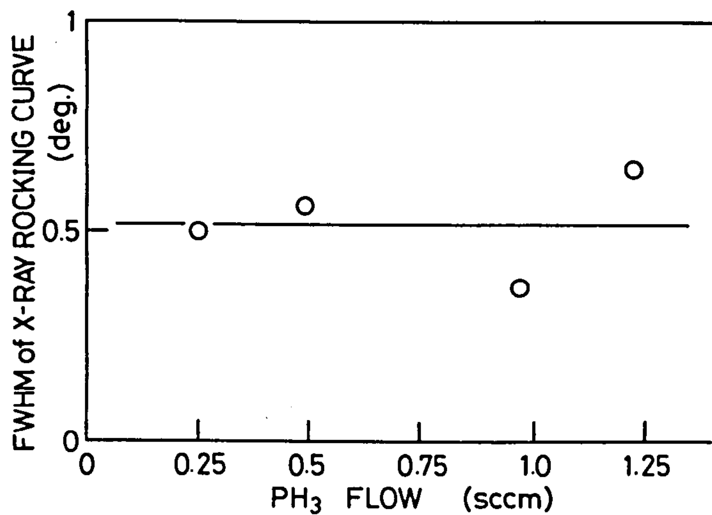

Fig. 2.8. Dependence of FWHM of x-ray diffraction rocking curve on phosphine flow.
(580℃, TEIn=0.037, TEGa=0.012 sccm).

The composition x of $In_{1-x}Ga_xP$ layers is controlled by the flow ratio of TEGa/(TEGa+TEIn), as given in Fig.2.6. The deviation from the proportional dependence shown in Fig.2.6 by a broken line reveals that the use of TEIn is highly ineffective compared with that of TEGa. The interpolation of experimental results (solid curve in Fig.2.6) shows that the InGaP layer will be lattice-matched to a GaAs substrate when the flow ratio of TEGa/(TEGa+TEIn) is 0.28, which corresponds to the TEIn/TEGa ratio of 2.6. The non-linear relation between the epilayer composition and the source flow ratio observed in this study is similar to that in conventional MOVPE[26-28], and is due to the formation of TEIn-PH_3 adduct. Since the adduct is decomposed easily by losing ethane to give an involatile polymeric material like $[-In(C_2H_5)PH-]_n$, it is not effective in achieving crystal growth[29-31].

Figure 2.7 shows the reductive influence of phosphine flow on the growth rate, which suggests that larger phosphine flows blow metalorganics away from the substrates. Phosphine flow has a small influence on the crystal quality, as indicated in Fig.2.8. This also supports the conjecture that the crystal quality is governed strongly by temperature, but not by the growth rate.

2-4. Immiscible Growth of InGaP

2-4-1. Observation of Immiscible Crystallites

In a few experiments of $In_{1-x}Ga_xP$ growth, a kind of immiscible growth was observed as two separate peaks of (002) diffraction in x-ray analysis, as shown in Fig.2.9, although most of the $In_{1-x}Ga_xP$ epitaxial layers grown in this low-vacuum MOVPE were single crystals of a single phase. The two peaks of (002)

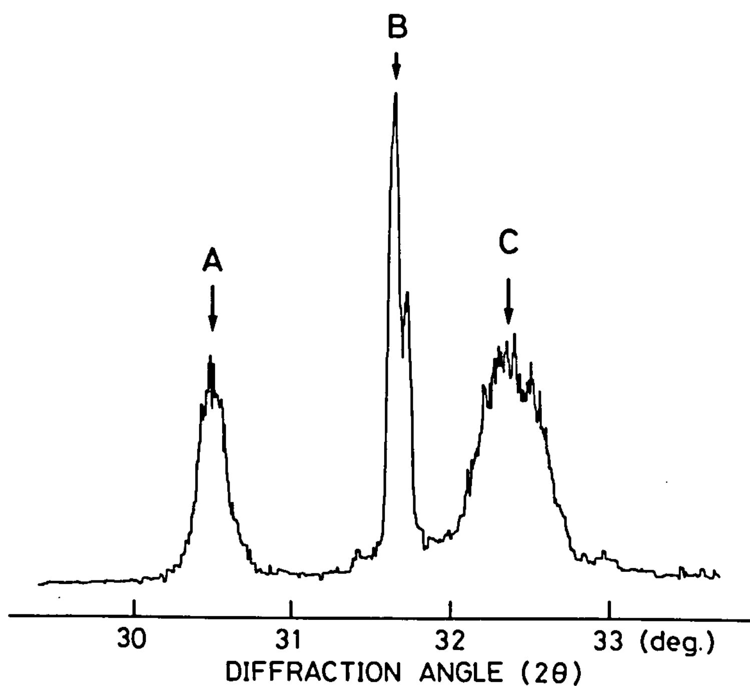

Fig. 2.9 X-ray diffraction pattern of immiscible $In_{1-x}Ga_xP$ layer. Peak A corresponds to $In_{0.99}Ga_{0.01}P$ (002), peak B to GaAs substrate (002), and peak C to $In_{0.20}Ga_{0.80}P$ (002).
(600℃, TEIn=0.048, TEGa=0.030, PH_3=1.00 sccm).

diffraction in Fig.2.9 (peaks A and C) cannot be attributed to polycrystalline peaks of a single solid composition. Moreover, the two solid compositions of immiscible $In_{1-x}Ga_xP$ layers, corresponding to the two peak positions in the abnormal x-ray diffraction pattern, varied from a largely separated pair of InP-rich and GaP-rich compositions (e.g., x = 0.01 and 0.84) to a pair of two close compositions (e.g., x = 0.37 and 0.41). On the surface of every immiscible $In_{1-x}Ga_xP$ layer with an abnormal x-ray diffraction pattern, there exist large oval-defect-like crystallites surrounded by a flat layer, as shown in Fig.2.10a, with a typical concentration of $1.2x10^6$ cm^{-2}. These crystallites were not observed on the surface of normally grown layers (Fig.2.10b), but very similar crystallites were observed on InP epitaxial layers grown on GaAs, as shown in Fig.2.10c. These crystallites in the immiscible $In_{1-x}Ga_xP$ layers were revealed to have an InP-rich composition compared with the surrounding flat layer by element (indium and gallium) distribution analysis using an electron-probe microanalyzer (EPMA). As clearly shown in Fig.2.11, the ratio of indium/gallium in EPMA signals was high at the crystallites and low at the flat area, indicating that peak A in Fig.2.9 corresponds to the composition of crystallites and peak C to that of the surrounding flat area. The conditions for the immiscible growth were not distinguished, except that the substrate temperature must be below 620℃. In fact, no immiscible growth occurred at 620℃, but it occurred once at 600℃. This temperature for the immiscible growth agrees with that predicted for a temperature below 608℃ by a calculation of excess enthalpy of mixing, as shown in Fig.2.12[32-35].

The immiscible growth of $In_{1-x}Ga_xP$ has not been reported in conventional MOVPE, and the immiscible growth newly found in this low-vacuum MOVPE is quite different from that of $InSb_xP_{1-x}$ reported by Fukui and Horikoshi in conventional MOVPE[36], since

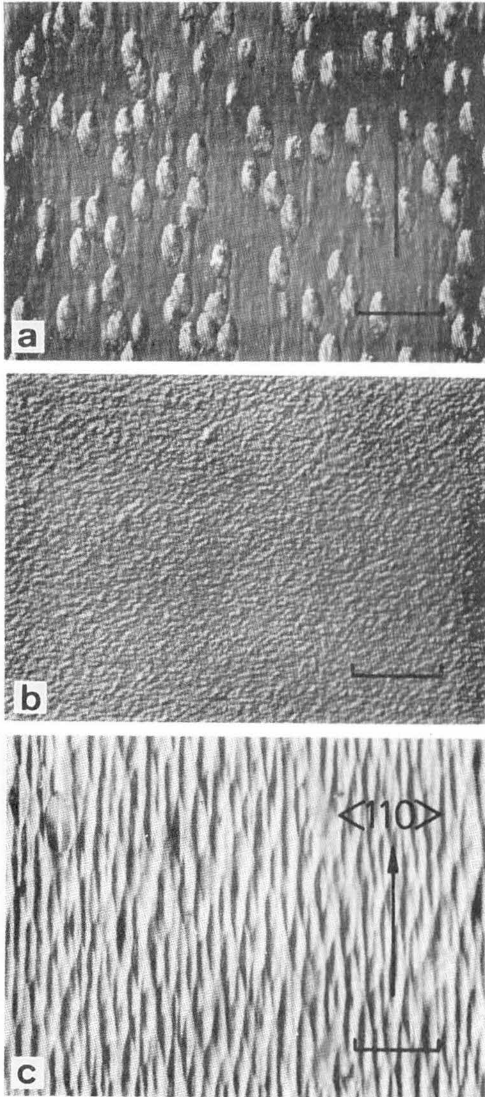

Fig. 2.10. Surface morphologies of
(a) immiscible layer of $In_{1-x}Ga_xP$ grown at 580℃,
(b) normal layer of $In_{1-x}Ga_xP$ grown at 610℃, and
(c) InP layer grown on GaAs,
observed by Nomarski phase contrast microscope. Markers in these pictures represent 20μm.

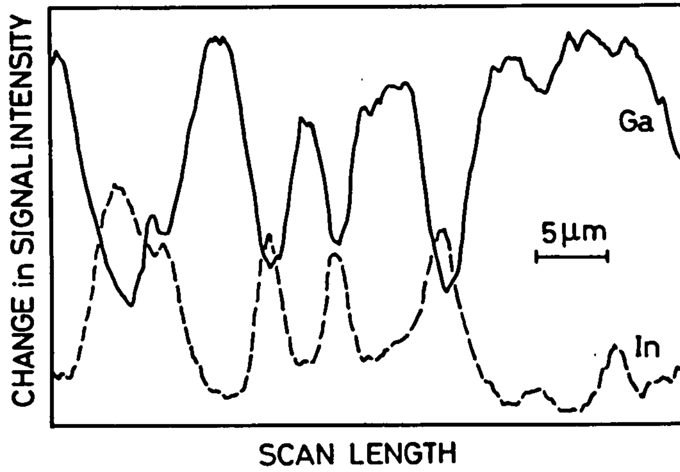

Fig. 2.11. Line-scan EPMA profile on surface of an immiscible layer.

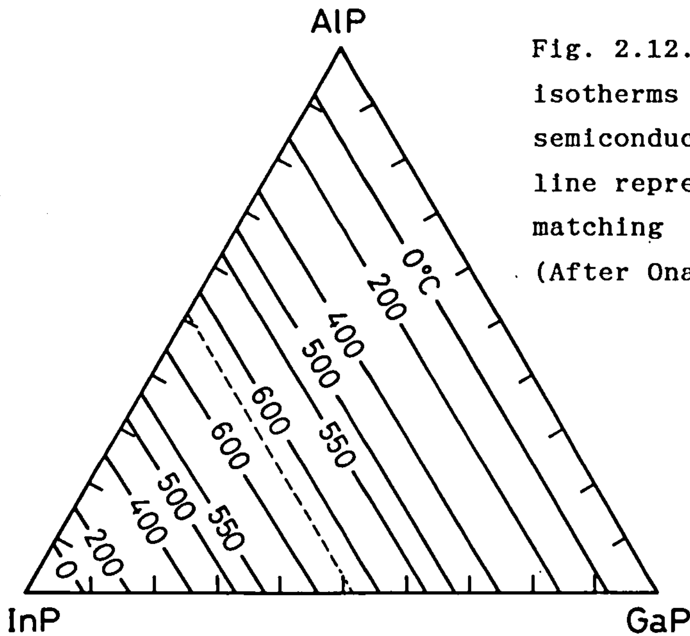

Fig. 2.12. Spinodal isotherms for InGaAlP semiconductor. Broken line represents lattice matching to GaAs. (After Onabe[35]).

they observed a single and fixed solid composition in their abnormal growth in the miscibility gap. Usually, homogeneous epilayers are obtained in conventional MOVPE for III-V semiconductors even in their miscibility gaps[37-39], since growth in MOVPE is far from thermal equilibrium unlike in liquid phase epitaxy (LPE), where the existence of miscibility gap has been experimentally confirmed[40-45].

2-4-2. Growth Model Including Immiscible Growth

The immiscible growth observed in this low-vacuum MOVPE has two unique characteristics; the compositional separation in the solid phase and the formation of InP-rich crystallites. The former seems to be due to the difference in the bond lengths of In-P and Ga-P, which causes a miscibility gap in the $In_{1-x}Ga_xP$ system, and the latter suggests that indium species (e.g., $InP_x(C_2H_5)_y$, where x and y are not clear) on the substrate surface do not migrate far enough to promote lateral growth compared with gallium species (e.g., $GaP_x(C_2H_5)_y$). By modifying the thermodynamic explanation of immiscibility in LPE, a growth model which can explain the above two characteristics simultaneously was constructed, as described in the following paragraphs.

In the $In_{1-x}Ga_xP$ system, the large lattice mismatch of 7.4% between InP and GaP results in a miscibility gap at lower temperatures, when InGaP growth is carried out with growth conditions close to thermal equilibrium like LPE growth. The interaction parameter (an index of interaction between constituent units in solution; zero for ideal solution) of 3500 cal/mol is calculated for InP-GaP with regular solution approximation, which corresponds to the critical temperature of

608℃ for equivalent mixing[32-35]. This indicates that the bonds of InP-InP and GaP-GaP are more stable than those of InP-GaP, since InP-GaP bonds cause the large mismatch stress, when InP and GaP molecules are assumed to be basic units in an In-Ga-P solution. Thus, the enthalpy of the In-Ga-P system increases with mixing. Near thermal equilibrium, the molecules of InP and GaP at the growth interface are mobile from the In-Ga-P solution to the growing InGaP solid, or from the solid to the solution, until they are finally incorporated into the solid. In this incorporation process, the bonds of InP-InP and GaP-GaP are formed much more than those of InP-GaP, resulting in two separated-composition phases in the solid.

Here, the similar incorporation process can be assumed at the growth interface in this low-vacuum MOVPE, though the degree of super-saturation is much larger than in LPE. As illustrated in Fig.2.13a, the bond between GaP (existing at the growth interface as the solid component) and gallium species (produced thermally in the vapor phase near the heated substrate, and adsorbed on the solid) is more stable than that between InP and gallium species, and the same holds for indium species. Moreover, the species at the growth interface are assumed to repeat adsorption and desorption, until they are fixed into growth nuclei.

When the substrate temperature is not high (below 620℃), the excess enthalpy of mixing due to the large difference of bond length between InP and GaP is not overcome by the entropy of mixing, and immiscible growth occurs as follows: At the initial stage, growth nuclei with a natural fluctuation of solid composition are formed on growth sites such as defects of the substrate. Moreover, the heated surface of the GaAs substrate is phosphoreted naturally by phosphorus ambient, resulting in a few monolayers of GaP. The gallium or indium species produced by thermal decomposition of metalorganics and phosphine, which

(a) adsorption

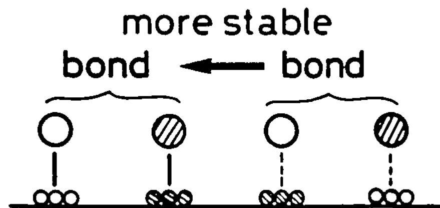

(b) GaP-rich nucleus growing laterally

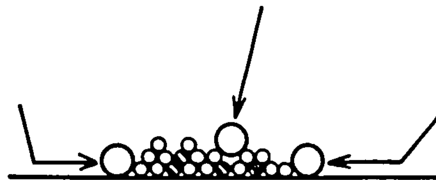

(c) InP-rich nucleus growing upward

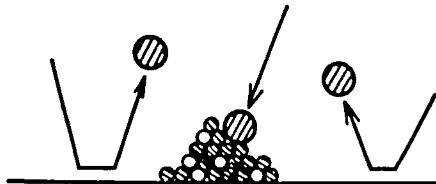

Fig. 2.13. Illustration of a model for immiscible crystal growth. Large circles are gallium or indium species in vapor phase, and small circles are gallium or indium atoms in solid (open circles for gallium and striped circles for indium). Phosphorus atoms are not indicated.

contribute to the crystal growth, are adsorbed on the growth nuclei and decompose there to be incorporated as GaP or InP. In this way, the gallium species are adsorbed by the GaP-rich nuclei more stably than by the InP-rich ones, and the same holds for the indium species. Thus, the gallium species are adsorbed selectively on GaP-rich nuclei and the indium species on InP-rich nuclei, promoting the separation of their solid compositions. The compositional separation of the solid phase observed in this low-vacuum MOVPE is derived through this process. The gallium or indium species which are adsorbed onto the substrate surface apart from the nuclei migrate or diffuse until they are incorporated into the nuclei, or reevaporate from the surface. Since the surface of the GaAs substrate is phosphoreted and covered with a few monolayers of GaP, gallium species are adsorbed stably onto the surface more than indium species, resulting in a farther migration or diffusion of gallium species. This causes the lateral growth of GaP-rich nuclei, because a number of migrating gallium species are incorporated into the side fronts of the nuclei, as illustrated in Fig.2.13b. The GaP-rich flat layer of the immiscible $In_{1-x}Ga_xP$ layer was formed by the coalescence of these GaP-rich nuclei growing laterally. On the other hand, InP-rich nuclei grow upward, keeping their angular shapes, and become crystallites at last, since their lateral growth is limited by the shorter migration (easier reevaporation) of indium species (Fig.2.13c). By this mechanism, the InP-rich crystallites were formed in the GaP-rich flat layer.

This model explains normal and immiscible $In_{1-x}Ga_xP$ growth, together with InP growth on GaAs, consistently with their surface morphologies. In normal $In_{1-x}Ga_xP$ growth, all growth nuclei grow laterally and coalesce with each other, resulting in a flat surface (Figs. 2.14a and 2.10b). The immiscible $In_{1-x}Ga_xP$ layer has InP-rich crystallites in GaP-rich flat layers as explained

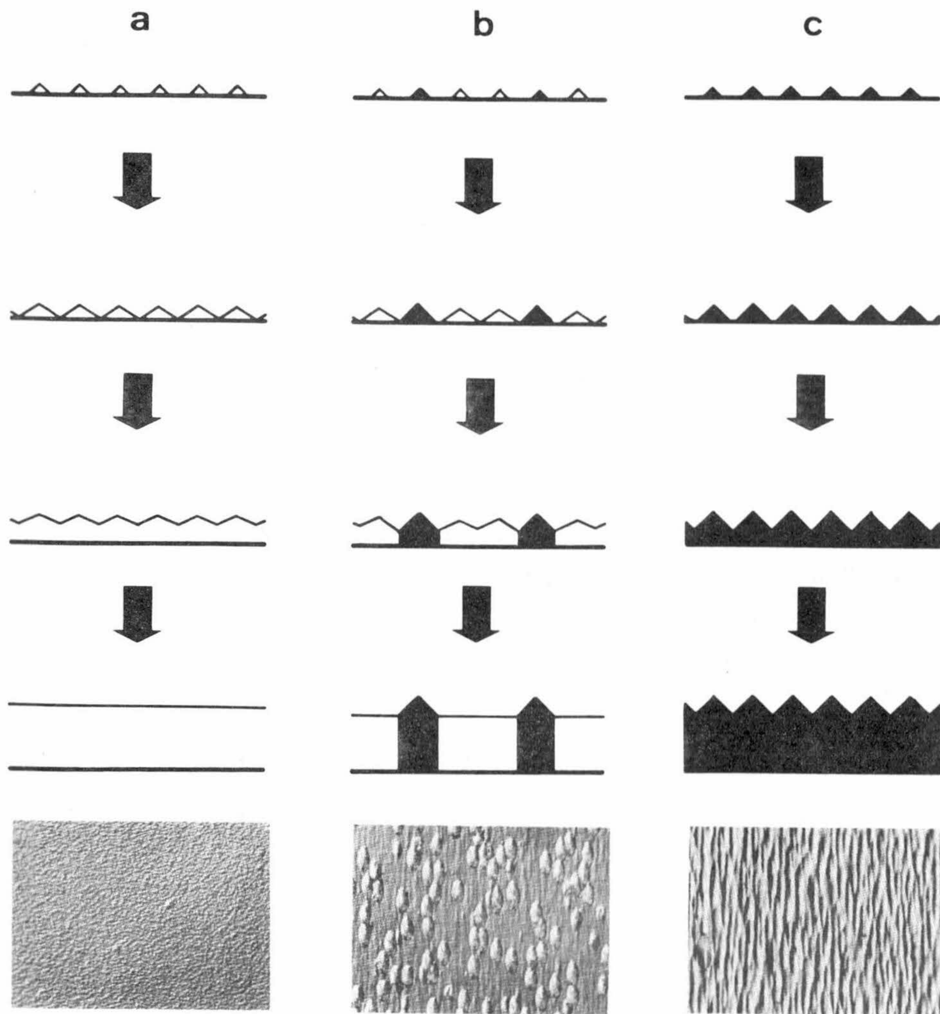

Fig. 2.14. Crystal growth model: (a) normal $In_{1-x}Ga_xP$ growth, white part represents uniform $In_{1-x}Ga_xP$ layer; (b) immiscible $In_{1-x}Ga_xP$ growth, white part represents GaP-rich $In_{1-x}Ga_xP$ and black part represents InP-rich $In_{1-x}Ga_xP$; (c) InP growth on GaAs, black part represents InP layer.

above (Figs. 2.14b and 2.10a). The fluctuation in the solid composition of growth nuclei at the initial stage changes in every experiment, causing poor reproducibility of immiscible growth and the variation in the two solid compositions of immiscible $In_{1-x}Ga_xP$ layers. In the case of InP growth on GaAs, all growth nuclei grow upward without coalescence, and cover all area of the epitaxial layer, making an irregular morphology of dense crystallites (Figs. 2.14c and 2.10c). This growth model suggests that the behavior of indium and gallium species at the growth interface in low-vacuum MOVPE is similar to the interface under thermal equilibrium in LPE.

As mentioned above, the immiscible growth of InGaP in conventional MOVPE has not been reported. It is not clear why the immiscible growth of InGaP was observed in this low-vacuum MOVPE. Here, it should be noticed that the stagnant layer on the heated substrate in the low-vacuum MOVPE is much heavier than in conventional MOVPE, and its main component is not hydrogen but phosphine. This seems to have much relation to the immiscible growth in the low-vacuum MOVPE.

The influence of lattice mismatch and phosphorus overpressure, however, is not clear in the above model, and more intensive investigations on the growth kinetics at the growth interface of MOVPE are required, together with the the identification of metal species produced thermally near the heated substrate.

2-5. Summary

By low-vacuum MOVPE, the following results were obtained.

(1) The crystal growth in low-vacuum MOVPE is limited by the

supply of group-III sources. The composition x in $In_{1-x}Ga_xP$ layers is controlled by the flow ratio of TEGa/(TEGa+TEIn), but gallium from TEGa is incorporated into the epilayers more effectively than indium from TEIn. This suggests that TEIn is wasted by vapor-phase reaction with phosphine to make involatile materials.

(2) The crystal quality is affected strongly by substrate temperature and improved with temperature increase, while it is not influenced by other factors such as growth rate or phosphine flow. Increase in temperature causes reduction in the effective supply of metalorganics by promoting their decomposition in the vapor phase, resulting in lower growth rates, while the composition is not affected by the temperature.

(3) In some growth experiments of InGaP below 620℃, immiscible growth was observed for the first time, as two separate peaks of (002) diffraction in x-ray analysis. The immiscible layers have many InP-rich crystallites in GaP-rich flat area. Based on the thermodynamic explanation of immiscibility, a growth model which explains the immiscible growth of InGaP and its surface morphology consistently was proposed.

(4) The vapor-phase reactions such as the decomposition of metalorganics and the adduct formation of TEIn-PH_3, which are undesirable for the precise control of growth rate and epilayer composition, are expected to be removed by reducing the growth pressure down to high vacuum and supplying the sources in the form of molecular beam.

References

[1] See, for example, proceeding of the Fourth International Conference on Metalorganic Vapor Phase Epitaxy, J.Cryst.Growth **93** (1988).

[2] J.P.Duchemin, M.Bonnet, G.Beuchet, and F.Koelsch, Inst.Phys.Conf.Ser. No.45 (1979) 10.

[3] M.Razeghi, "Semiconductors and Semimetals vol.22 part A", Ed. W.T.Tsang, Academic Press, Chapter 5 (1985).

[4] R.S.Sillmon, N.Bottka, J.E.Butler, and D.K.Gaskill, J.Cryst.Growth **77** (1986) 73.

[5] See, for example, J.Haigh, J.Vac.Sci.Technol. **B3** (1985) 1456.

[6] L.M.Fraas, P.S.McLeod, L.D.Partain, and J.A.Cape, J.Vac.Sci.Technol. **B4** (1986) 22.

[7] L.M.Fraas, P.S.McLeod, L.D.Partain, M.J.Cohen, and J.A.Cape, J.Electron.Mater. **15** (1986) 175.

[8] M.E.O'Neil and K.Wada, "Comprehensive Organometallic Chemistry vol.1", Ed. G.Wilkins, F.G.A.Stone, and E.W.Abel, Pergamon Press, New York (1982).

[9] J.W.Bruno, T.J.Marks, and L.R.Morss, J.Less-Common Met. **93** (1983) 357.

[10] M.Yoshida, H.Watanabe, and F.Uesugi, J.Electrochem.Soc. **132** (1985) 677.

[11] J.C.Traeger, C.E.Hudson, and D.J.McAdoo, Int.J.Mass Spectrom.Ion Process **82** (1988) 101.

[12] F.Maury and A.El Hammadi, J.Cryst.Growth **91** (1988) 105.

[13] C.Y.Chang, Y.K.Su, M.K.Lee, L.G.Chen, and M.P.Houng, J.Cryst.Growth **55** (1981) 24.

[14] T.F.Kuech and R.Potemski, Appl.Phys.Lett. **47** (1985) 821.

[15] S.Horiguchi, K.Kimura, K.Kamon, M.Mashita, M.Shimazu, M.Mihara, and M.Ishii, Jpn.J.Appl.Phys. **25** (1986) L971.

[16] N.Putz, H.Heinecke, M.Heyen, and P.Balk, J.Cryst.Growth **74** (1986) 292.

[17] C.Plass, H.Heinecke, O.Kayser, H.Luth, and P.Balk, J.Cryst.Growth 88 (1988) 455.

[18] A.Y.Cho, Thin Solid Films **100** (1983) 291.

[19] R.P.Vasquez, B.F.Lewis, and F.J.Grunthaner, J.Vac.Sci.Technol. **B1** (1983) 791.

[20] J.P.Contour, J.Massies, and A.Saletes, Appl.Phys. **A38** (1985) 45.

[21] J.Massies and J.P.Contour, J.Appl.Phys. **58** (1985) 806.

[22] I.Hino and T.Suzuki, J.Cryst.Growth **68** (1984) 483.

[23] Y.Ohba, M.Ishikawa, H.Sugawara, M.Yamamoto, and T.Nakanishi, J.Cryst.Growth **77** (1986) 374.

[24] M.Ikeda, K.Nakano, Y.Mori, K.Kaneko, and N.Watanabe, J.Cryst.Growth **77** (1986) 380.

[25] J.S.Yuan, M.T.Tsai, C.H.Chen, R.M.Cohen, and G.B.Stringfellow, J.Appl.Phys. **60** (1986) 1346.

[26] J.Yoshino, T.Iwamoto, and H.Kukimoto, J.Cryst.Growth **55** (1981) 74.

[27] Y.Ban, M.Ogura, M.Morisaki, and N.Hase, Jpn.J.Appl.Phys. **23** (1984) L606.

[28] J.S.Yuan, M.T.Tsai, C.H.Chen, R.M.Cohen, and G.B.Stringfellow, J.Appl.Phys. **60** (1986) 1346.

[29] R.Didchenko, J.E.Alix, and R.H.Toeniskoetter, J.Inorg.Nucl.Chem. **14** (1960) 35.

[30] H.M.Manasevit and W.I.Sympson, J.Electrochem.Soc. **120** (1974) 135.

[31] R.H.Moss and J.S.Evans, J.Cryst.Growth **55** (1981) 129.

[32] K.Onabe, Jpn.J.Appl.Phys. **21** (1982) L323.

[33] G.B.Stringfellow, J.Phys.Chem.Solids **33** (1972) 665.

[34] G.B.Stringfellow, J.Cryst.Growth **27** (1974) 21.

[35] K.Onabe, Jpn.J.Appl.Phys. **22** (1983) 287.

[36] T.Fukui and Y.Horikoshi, Jpn.J.Appl.Phys. **20** (1981) 587.

[37] G.B.Stringfellow, J.Cryst.Growth **65** (1983) 454.

[38] M.J.Cherng, R.M.Cohen, and G.B.Stringfellow, J.Electron.Mater. **13** (1984) 799.

[39] G.Bougnot, F.Delannoy, A.Foucaran, F.Pascal, F.Roumanille, P.Grosse, and J.Bougnot, J.Electrochem.Soc. **135** (1988) 1783.

[40] K.Nakajima, K.Osamura, K.Yasuda, and Y.Murakami, J.Cryst.Growth **41** (1977) 87.

[41] R.E.Nahory, M.A.Pollack, E.D.Beebe, J.C.DeWinter, and M.Ilegems, J.Electrochem.Soc. **125** (1978) 1053.

[42] K.Takahei and H.Nagai, Jpn.J.Appl.Phys. **20** (1981) L313.

[43] M.Quillec, C.Dagnet, L.Benchimol, and H.Launois, Appl.Phys.Lett. **40** (1982) 325.

[44] S.Tanaka, K.Hiramatsu, Y.Habu, N.Sawaki, and I.Akasaki, J.Cryst.Growth **79** (1986) 978.

[45] M.Kondo, S.Shirakata, T.Nishino, and Y.Hamakawa, J.Appl.Phys. **60** (1986) 3539.

3. METALORGANIC MOLECULAR BEAM EPITAXY OF InGaP

3-1. Introduction

Vapor-phase reactions, as described in chapter 2, have undesirable affects on the precise control of epitaxy, especially for phosphorus-based III-V semiconductors. The vapor-phase reactions can be eliminated when the epitaxy is carried out under high-vacuum condition, where source molecules are impinged to heated substrates without collisions.

The investigation on epitaxial growth by using gas molecules under high vacuum was started as an attempt to replace solid sources in conventional MBE by gas sources. The first report on the attempt was made in 1974 by Morris and Fukui[1]. They used arsine (AsH_3), phosphine (PH_3), and solid gallium in a high-vacuum system to deposit polycrystalline films of GaAs, GaP, and GaAsP on amorphous substrates. The advantages of using gas sources instead of solids pointed out in their work are better reproducibility of film deposition by easier control of gas flows, and larger scale production by inexhaustible gas sources. The investigation was taken over by Panish et al., who introduced the name of "gas-source MBE"[2-6]. They studied the accommodation coefficient of arsenic and phosphorus produced by the cracking of arsine and phosphine, and fabricated various heterostructure lasers of InGaAsP with threshold current density as low as approximately 2 kA/cm^2 at room temperature, indicating the high controllability of group-V beam flux in gas-source MBE. The cracking of group-V hydrides has been intensively investigated also by many other workers, and gas-source MBE has been spread widely as a new technique of high performance to prepare III-V semiconductors with multi group-V elements[7-11].

With respect to group-III sources, Veuhoff et al. reported

for the first time the epitaxy of GaAs using trimethylgallium (TMGa) and arsine under a high vacuum of $2x10^{-5}$ Torr, which they named "metalorganic molecular beam epitaxy (MOMBE)"[12]. Their work stimulated many workers, and the unique advantages and characteristics of MOMBE have been reported successively. Vodjdani et al. investigated the decomposition of TMGa and arsine by mass spectrometry, and demonstrated the perfectly selective epitaxy of GaAs on insulator-masked GaAs substrates in MOMBE[13]. Carbon incorporation into GaAs epilayers grown by MOMBE has been investigated intensively by Putz et al.[14-17] and by Tokumitsu et al.[18-22], and it has been made clear that the carbon contamination can be drastically reduced by the use of triethylgallium (TEGa) instead of TMGa. By using TMGa intentionally, p-type GaAs epilayers heavily doped with carbon up to 10^{20} cm^{-3} have been prepared in MOMBE. The elimination of oval defects has been reported for MOMBE grown GaAs by many workers[23]. Kawaguchi et al. have prepared high-quality InP epilayers with electron mobility up to 10^5 cm^2/Vs at 77K, by MOMBE using triethylindium (TEIn) and phosphine, and high-quality InGaAs/InP multi quantum wells using trimethylindium (TMIn), TEGa, arsine, and phosphine[24-26]. Tsang et al. succeeded to fabricate double heterostructure lasers of AlGaAs/GaAs with very low threshold currents and InP/InGaAsP/InGaAs avalanche photodiodes with good performance by using a MOMBE technique (what they call chemical beam epitaxy, CBE)[27-32]. Through these works and many others, MOMBE has been solidly recognized as a powerful technique to prepare III-V semiconductor devices with high quality heterostructures.

As mentioned in chapter 1, the decomposition of metalorganics on the heated substrate is expected to be modified by many factors including photon/electron irradiation, which leads to advanced steps like photo-controlled MOMBE. The

investigation on the pyrolysis of metalorganics at the growth interface has just been started for GaAs MOMBE, and some interesting aspects of growth mechanism such as the desorption of gallium alkyls at higher temperatures have been found[33,34]. In this chapter, the growth mechanism of InGaP MOMBE, especially the difference from GaAs MOMBE, is discussed mainly from the analysis of temperature dependence of growth rate, epilayer composition, and surface morphology.

3-2. Experimental Detail

3-2-1. MOMBE Apparatus and Experimental Procedure

The schematic drawing and a photograph of an originally designed MOMBE system used in this study are given in Figs. 3.1 and 3.2, respectively. The growth chamber with a volume of approximately 15 liters was evacuated by an oil-diffusion pump (1500 l/s) through a liquid-nitrogen trap. The background pressure was approximately 4×10^{-9} Torr. Source materials used in the MOMBE experiments were triethylindium (TEIn), triethylgallium (TEGa), triethylaluminum (TEAl), and phosphine (PH_3). Triethylarsine (TEAs) was employed to supply arsenic to a GaAs substrate under a thermal cleaning process. The vapors of metalorganics were transported from their vessels (warmed in individual fan-heating boxes; 60℃ for TEIn, 35℃ for TEGa, and 90℃ for TEAl; their vapor pressures are approximately 5-10 Torr) to the growth chamber by the pressure difference. Each source flux was controlled precisely by an individual mass flow controller (Fig.3.3). Phosphine and TEAs were precracked by passing them through simple thermal cracking cells in the chamber (the detail is described in the next section). Source fluxes of

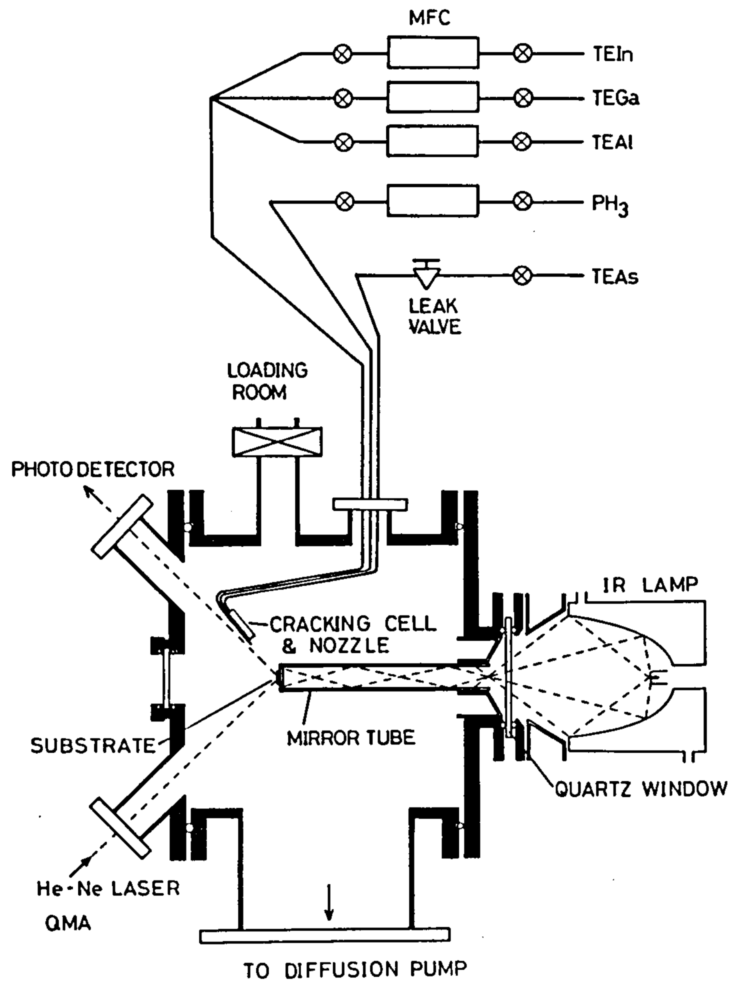

Fig. 3.1. Schematic drawing of MOMBE system.

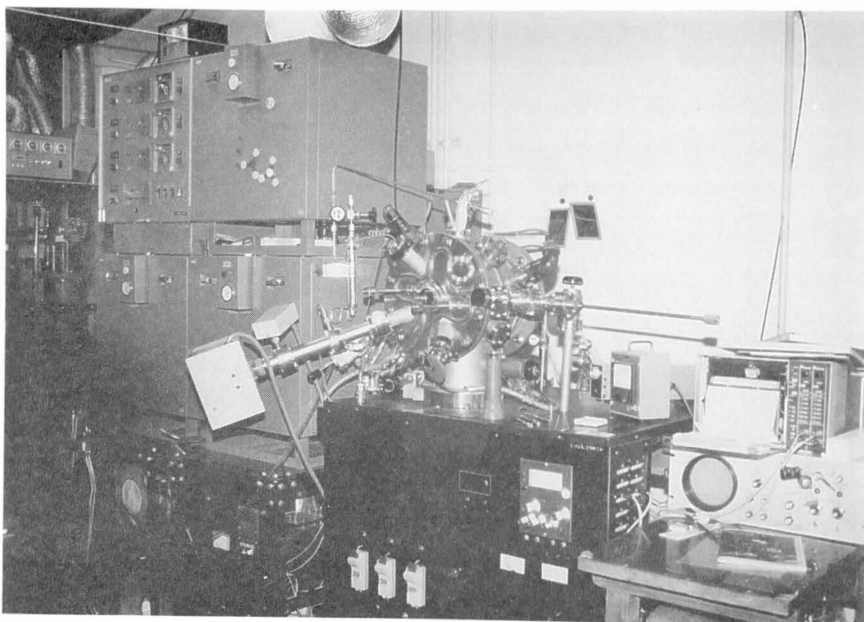

Fig. 3.2. Photograph of MOMBE system.

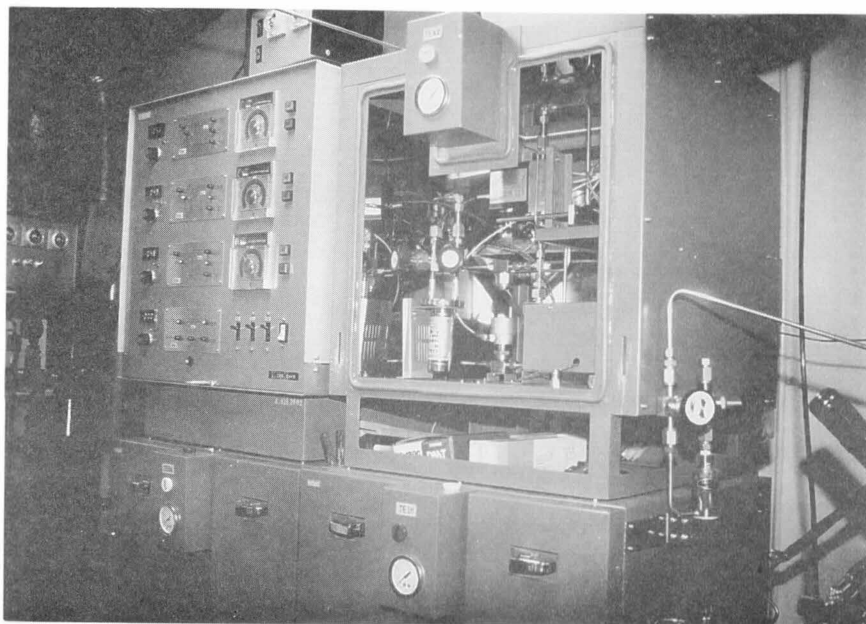

Fig. 3.3. Mass flow controllers and fan-heating box.

metalorganics were mixed together before impinging onto the heated substrate to guarantee the uniform composition of epilayers. Phosphine and metalorganics were provided to the substrate as two individual fluxes to avoid adduct formation. Metalorganics were supplied to the heated substrate from a nozzle with a 3 mm^2 aperture, and phosphine was supplied from a cracking cell with a 12 mm^2 aperture. The distance of the nozzle and the cell from the substrate was 40 mm. A thermal shield was set between the nozzle and the cracker.

Each substrate of GaAs(001), prepared with a normal etching solution of $4H_2SO_4:1H_2O_2:1H_2O$, was mounted on a molybdenum (Mo) disk with indium solder (Figs. 3.4 and 3.5). The disk was fitted into a stainless holder, and loaded into the growth chamber through a loading room. The substrate on the Mo disk was heated from its backside by infrared irradiation from a halogen lamp (1000 W) set outside of the chamber. The substrate temperature was measured by a thermocouple which was brought into contact with an indium pool on the Mo disk every time after loading the holder into the chamber. The thermocouple was precalibrated using the eutectic points of Al/Si (577.2℃) and Al/Ge (424℃). Before the epitaxial growth, the substrate was heated up to 700℃ under precracked TEAs flux to remove the surface oxide layer. An optimum cleaning temperature of 700℃ was determined from the cleaning temperature dependence of epilayer quality examined by the full width at half maximum (FWHM) of x-ray rocking curves.

As the in-situ monitoring of the growth, the reflection of a He-Ne laser beam at the epilayer surface was monitored by a photodetector.. The growth rate was calculated from the interference oscillation period of this reflection intensity (section 3-2-3 describes its detail). The epilayer composition was determined by x-ray diffraction measurement. The growth conditions used in this study is given in Table 3.1.

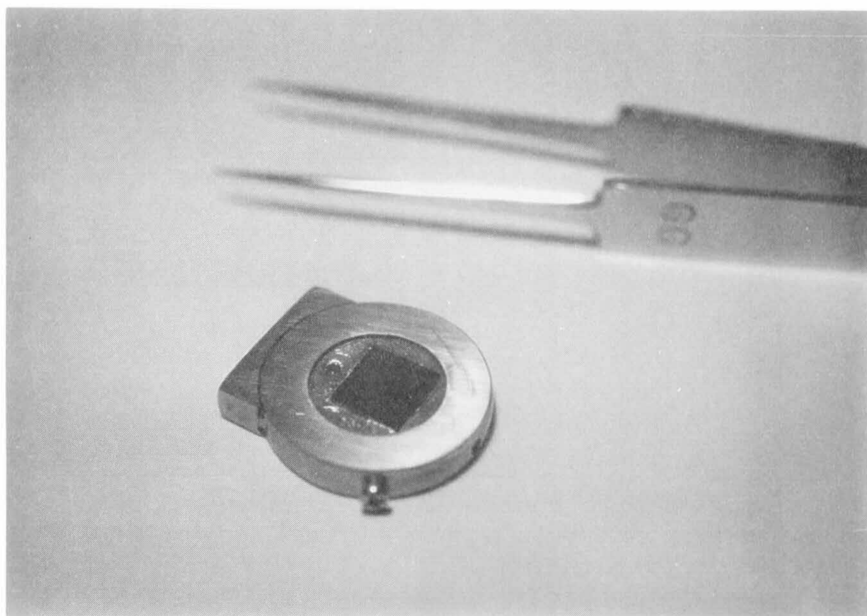

Fig. 3.4. Substrate on Mo disk fitted into holder.

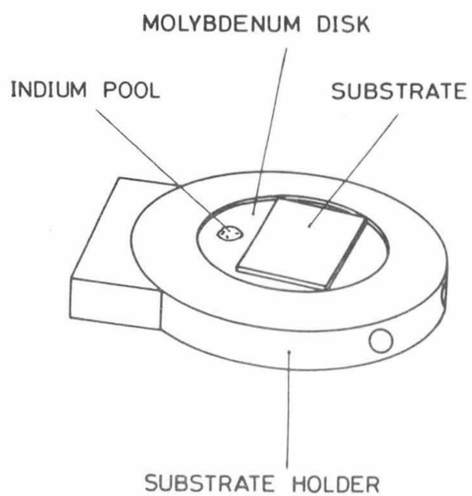

Fig. 3.5. Illustration of substrate holder.

Table 3.1. Growth condition for epitaxial growth of InGaP in MOMBE.

	Range	Typical
Substrate temperature (℃)	290-600	490
Source flow rate (sccm)		
TEIn	0.0000-0.0600	0.0160
TEGa	0.0000-0.0600	0.0200
PH_3	0.0250-0.5000	0.1000
V/III ratio	3.50-12.5	3.50
TEGa/(TEGa+TEIn)	0.00-1.000	0.550
Reaction pressure ($\times10^{-5}$ Torr)	0.20-1.20	0.30

3-2-2. Cracking of Phosphine

In MOMBE, the growth of III-V semiconductors is generally impossible without the precracking of group-V hydrides. Even at a high temperature of 500℃, only metal droplets are deposited on the substrate when phosphine was used without precracking in MOMBE, while crystals grow at the same temperature in low-vacuum MOVPE, as shown in chapter 2. This indicates that growth kinetics in MOMBE largely differ from that in low-vacuum MOVPE, at least for the decomposition of source chemicals, and that phosphine is much more difficult to decompose by surface reaction than group-III metalorganics. Phosphine molecules which impinged onto the heated substrate under the high vacuum of MOMBE are desorbed without pyrolysis, since they do not stay there long enough to receive sufficient thermal energy to be decomposed. In the low-vacuum MOVPE, phosphine molecules are decomposed by many collisions with the heated substrate or with high-energy molecules in the stagnant layer. Additionally, it is clear that group-III metalorganics are decomposed by surface reaction in MOMBE, and by vapor-phase reaction in MOVPE.

Figure 3.6 shows the structure of thermal cracking cells employed to precrack phosphine and TEAs. Each cell has a heating coil of a tantalum (Ta) ribbon in a quartz guiding tube (8.6 O.D., 40 mm long). Phosphine molecules are cracked by many collisions with a high-temperature Ta heater. The fragment pattern of phosphine cracking was investigated by the use of a quadrupole mass analyzer (QMA) at various cell temperatures of 20-1400℃. The temperature dependence of fragment intensity is given in Fig.3.7, where every intensity of QMA signal except that of PH_3 (amu.=34) was corrected as follows to remove the influence of electron-impact dissociation in the QMA;

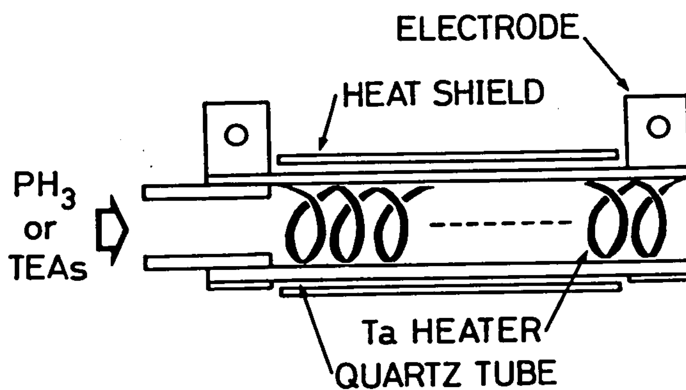

Fig. 3.6. Structure of thermal cracking cell.

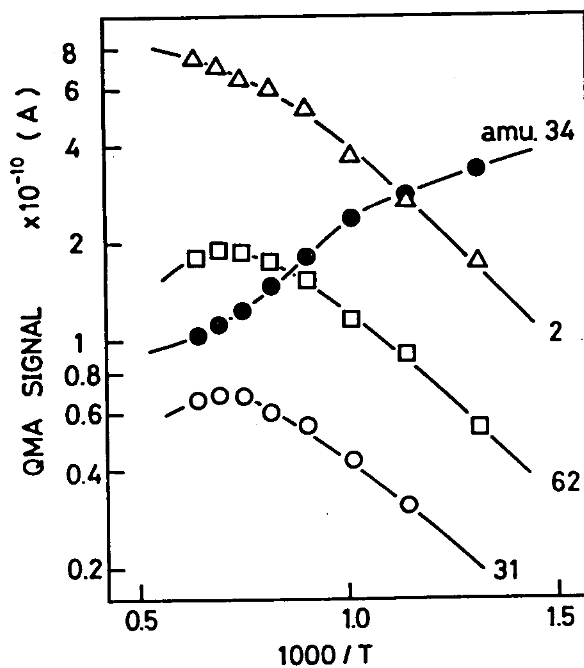

Fig. 3.7. Temperature dependence of phosphine cracking.

$$I(M,T_c) = I_o(M,T_c) - I_o(34,T_c)\cdot\frac{I_o(M,r.t.)}{I_o(34,r.t.)} , \qquad (2\text{-}1)$$

where $I_o(M,T_c)$ is the output of QMA for the fragment of amu.=M at cell temperature T_c, and $I(M,T_c)$ is corrected intensity.

In the epitaxial growth experiments, the cracking temperature of 830℃ was used for phosphine, and 1050℃ for TEAs. The efficiency of phosphine cracking at 830℃ is relatively small (58%, estimated from decrease in QMA output for amu.=34), since some amount of phosphine molecules pass through the cell without collision.

3-2-3. Monitoring of Growth Rate

Figure 3.8 shows the interference intensity oscillation of a He-Ne laser beam reflected at the epilayer surface during the epitaxy of InGaP. The oscillation is caused by that the beam passing through the epilayer and being reflected at the substrate surface interferes with the beam reflected at the epilayer surface. The absorption coefficient of the epilayer depends on the epilayer composition. The larger absorption for InP-rich epilayers causes the damping of the oscillation, while the random reflection at the rough surface brings the weaker reflection intensity, as shown in Fig.3.8.

The linear relation between the period T and the growth rate γ is given as below;

$$\gamma = \frac{\lambda}{2nT\cos\theta} , \qquad (2\text{-}2)$$

where n is the refractive index of epilayer, θ is the incident

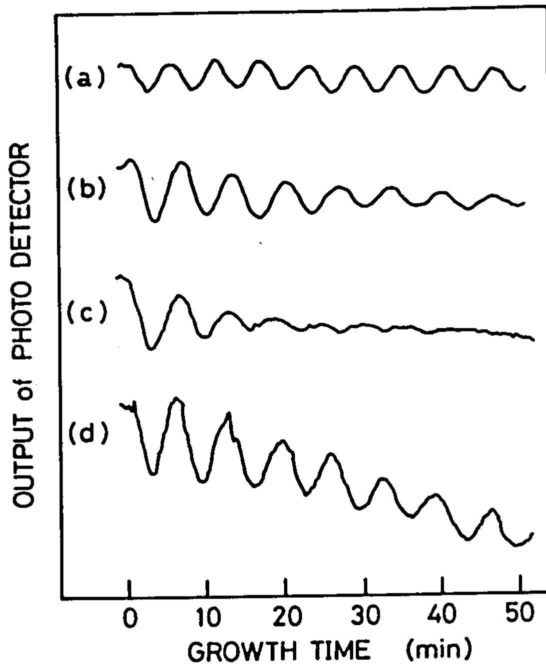

Fig. 3.8. Examples for interference intensity oscillation of a He-Ne laser beam reflected at epilayer surface during growth. In growth of (a) GaP, (b) $In_{0.43}Ga_{0.57}P$, (c) InP, (d) $In_{0.27}Ga_{0.73}P$ with surface roughening.

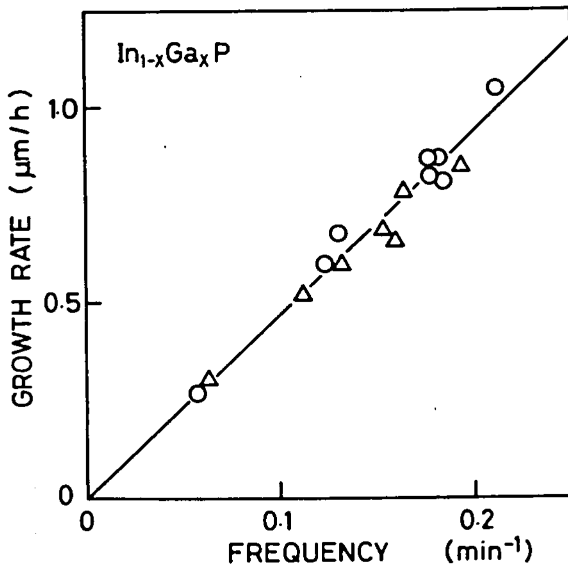

Fig. 3.9. Relation between growth rate and interference oscillation frequency.

angle of laser beam (45° in this system), and λ is the wavelength of He-Ne laser (632.8 nm). Since the refractive index of the epilayer at growth temperatures is unclear and the effect of multiple reflection is not taken into the equation, the growth rate was confirmed by the cross-sectional observation of cleaved epilayers with a scanning electron microscope (SEM), and by the measurement of the step height between the epilayer surface and the substrate surface masked with a small GaAs piece during the epitaxial growth. Figure 3.9 shows the proportional relation between the growth rate and the frequency of interference oscillation. The relation is expressed as follows;

$$\gamma(\mu m/h) = \frac{4.73}{T(min)} \quad . \qquad (2\text{-}3)$$

Though epilayer compositions widely varied in Fig.3.9, its influence is negligible, suggesting a little difference of the refractive index between InP and GaP. Thus, the growth rate of every epilayer in this study was determined from the oscillation period using the equation (2-3).

3-3. Temperature Dependence of InGaP Epitaxy

The temperature dependence of growth rate, epilayer composition x, surface morphology, and RHEED patterns of $In_{1-x}Ga_xP$ epilayers were investigated with TEIn=0.016sccm, TEGa=0.020sccm, and PH_3=0.1sccm (Figs. 3.10, 3.11, and 3.12). Three distinct stages are clearly observed in the temperature dependence. In the low-temperature region below 390℃, both the growth rate and the epilayer composition x increase with temperature, accompanied with no severe adverse affects on

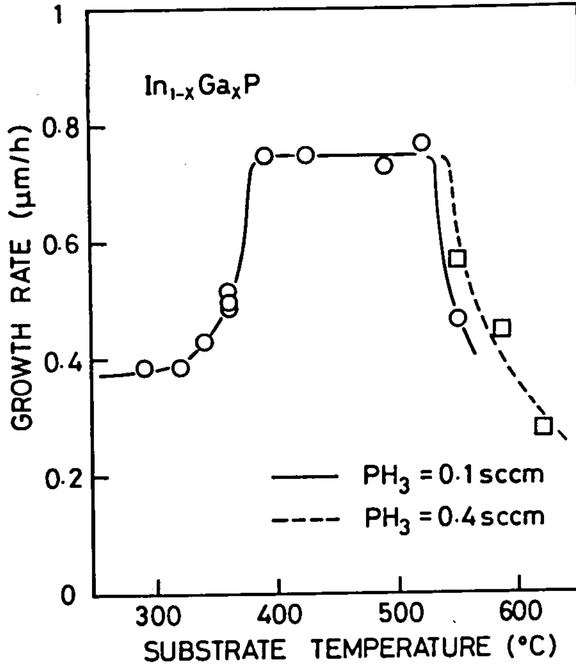

Fig. 3.10. Temperature dependence of growth rate of InGaP. (TEIn=0.016, TEGa=0.020 sccm).

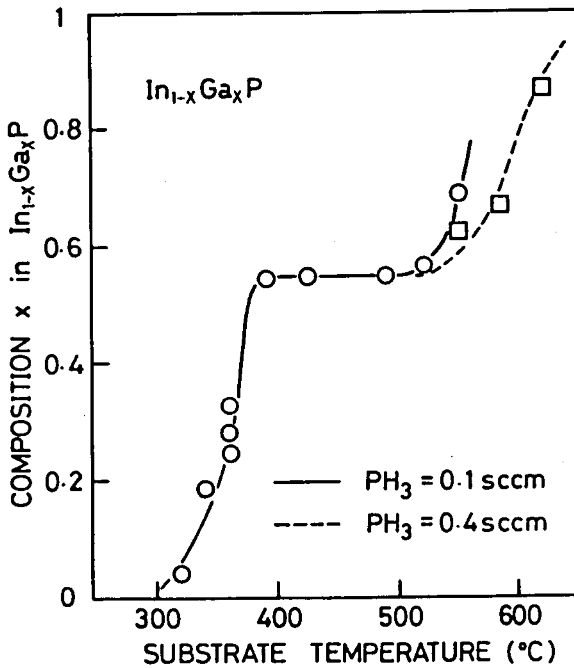

Fig. 3.11. Temperature dependence of epilayer composition x in $In_{1-x}Ga_xP$. (TEIn=0.016, TEGa=0.020 sccm).

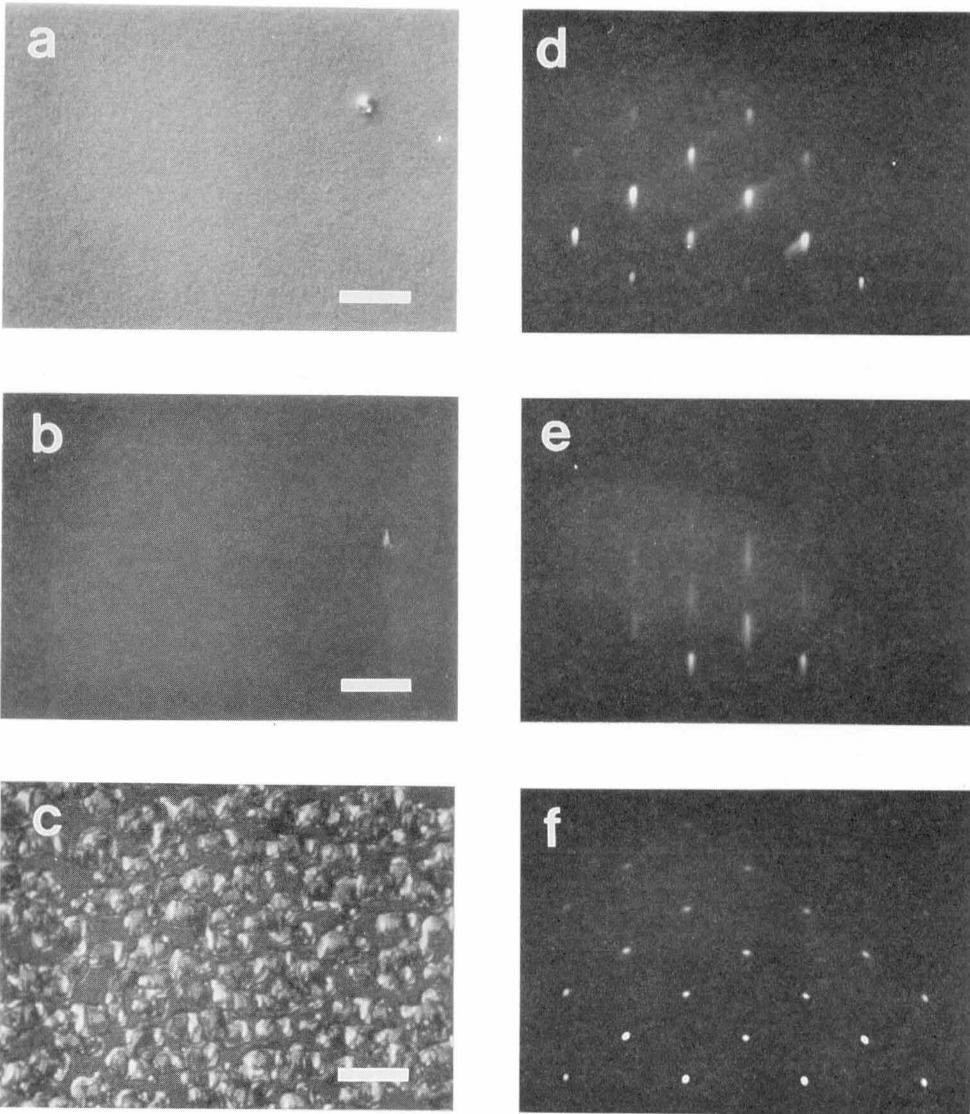

Fig. 3.12. Temperature dependence of surface morphology observed by a Nomarski phase contrast microscope (a)-(c), and RHEED patterns (d)-(f). (a),(d) 360℃; (b),(e) 490℃; (c),(f) 550℃. Markers in (a)-(c) represent 10μm.

surface morphology and RHEED patterns. These changes at lower temperatures are not observed in conventional MBE, suggesting that the decomposition of metalorganics governs the growth below 390℃. In the moderate-temperature region of 390-520℃, the growth rate, and the epilayer composition do not depend on temperature, as in conventional MBE, indicating that the supply of metalorganics limits the growth, since all the metalorganics impinged onto the substrate are completely decomposed and incorporated into the epilayer. At higher temperatures above 520℃, the remarkable change of growth rate and epilayer composition was observed, together with defect (droplet) formation on the epilayer surface. This differs much from the result that improved epilayers were obtained above 600℃ in low-vacuum MOVPE, suggesting that the lower pressure of phosphine causes the degradation of epilayers at higher temperatures in MOMBE.

In the next three sections (3-4, 3-5, and 3-6), the characteristics of MOMBE growth in each temperature region are discussed in detail.

3-4. Growth at Lower Temperatures

The reduced growth rates with lower gallium composition observed below 390℃ suggest the imperfect decomposition of TEGa in the low-temperature region. For the quantitative analysis of the factors which govern the growth at lower temperatures, the growth rate γ of $In_{1-x}Ga_xP$ epilayers was divided into the two growth rates of quasi-binaries ($x\gamma$ for GaP and $(1-x)\gamma$ for InP), and plotted in the Arrhenius' relation (Fig.3.13). It is clearly shown in Fig.3.13 that the pyrolysis of TEGa with an apparent activation energy (E_{act}) of 39 kcal/mol causes the temperature

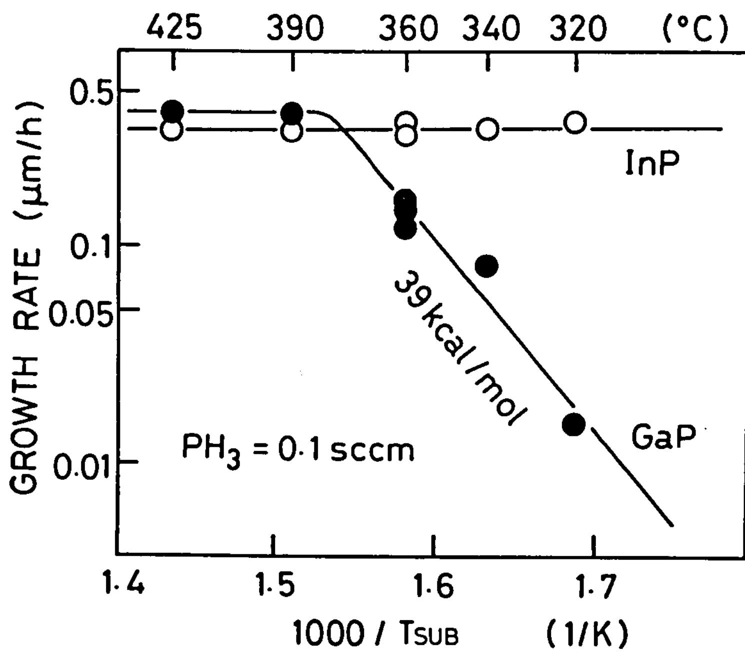

Fig. 3.13. Arrhenius plot of growth rates of quasi-binaries (InP and GaP) at lower temperatures. (TEIn=0.016, TEGa=0.020 sccm).

dependence of growth rate and epilayer composition below 390℃. The activation energy obtained in this experiment is somewhat lower than that measured by direct pyrolysis (carrier gas system, 48 kcal/mol)[35], but far from that reported in GaAs MOMBE (15 kcal/mol)[33]. Moreover, in this study, a similar small E_{act} of 20 kcal/mol was obtained in GaAs MOMBE using TEGa and cracked TEAs. This significant difference indicates that phosphorus at the growth interface does not have a strong surface-catalytic effect on TEGa decomposition, while arsenic does[33]. This imperfect pyrolysis of TEGa at lower temperatures has the same effect as the reduction of TEGa flux, and has no adverse influence on the RHEED pattern of epilayers (Fig.3.12d). Therefore, the slightly inferior surface morphology obtained at 360℃ (Fig.3.12a) compared with the perfectly smooth surface grown at 490℃ (Fig.3.12b) seems to be due to poorer migration at lower temperatures and/or due to the lattice mismatch between the InP-rich epilayer and the substrate.

In GaAs atomic layer epitaxy (ALE) in MOVPE system, TEGa molecules on arsenic atoms decompose more speedily than those on gallium atoms, resulting in layer-by-layer growth by the alternative supply of TEGa and arsine[36,37]. The speedy decomposition of TEGa on arsenic atoms corresponds to the smaller E_{act} of TEGa decomposition in GaAs MOMBE than in direct pyrolysis. Not so small E_{act} of TEGa decomposition in InGaP MOMBE as in GaAs MOMBE indicates that GaP ALE is much difficult to achieve, since the slow decomposition of TEGa molecules on phosphorus atoms as on gallium atoms easily brings three dimensional growth, but not layer-by-layer growth. The precise control of the TEGa period in alternative beam supply[38] is required for the layer-by-layer growth of GaP. No information on the E_{act} of TEIn decomposition was obtained in this study.

The incomplete pyrolysis of TEGa at lower temperatures is

expected to be improved by photon/electron irradiation. The enhanced growth rate of GaAs by ArF excimer laser irradiation (193 nm) has been reported in MOMBE using TEGa and solid arsenic, arising from the laser pyrolysis of adsorbed TEGa molecules[39]. The photochemical decomposition of TMGa induced by the irradiation of Ar-ion laser (458-515 nm) has been observed as the growth enhancement of GaAs homoepitaxy in MOVPE[40,41]. An electron-transfer mechanism has been proposed for the photochemical assistance, in which the transfer of electrons from adsorbed metalorganic molecules to the hole-accumulated substrate plays an important role to reduce the dissociation energy of metalorganics. In this study, however, the improved growth rate was not observed in the experiments of laser-assisted MOMBE of InGaP, carried out on n-type GaAs substrates at 300-360℃ with Ar-ion laser irradiation (20 mW). The electron-transfer mechanism probably does not work well for TEGa in InGaP/GaAs heteroepitaxy, since the conditions of the growth interface, such as adsorption energy-level and charge trapping defects like dislocation, differ much from those in GaAs homoepitaxy. The weaker laser power is partly responsible for the results. The photon number in the experiments was approximately 7×10^{17} $cm^{-2}s^{-1}$ estimated from the beam diameter of 3 mm on the substrates, which is 10^4 times larger than the arrival of TEGa molecules to grow GaP with a growth rate of 0.1 μm/h, but considerably smaller than that employed in the successful laser-assisted MOVPE experiments.

3-5 Growth at Moderate Temperatures

3-5-1. Metalorganic Flux Dependence

In the moderate-temperature region of 390-520℃, the growth

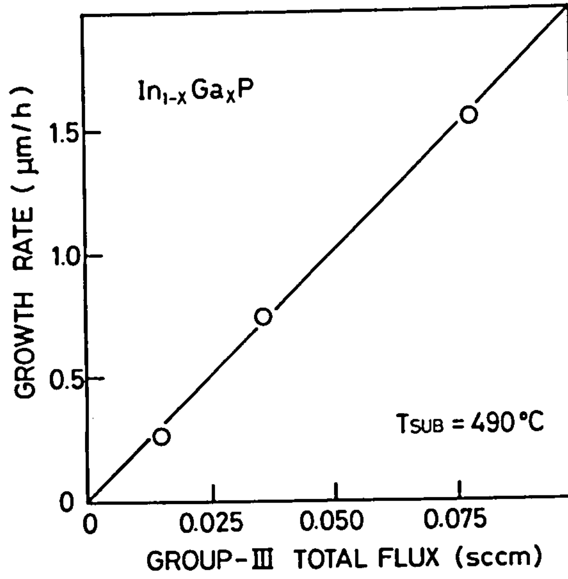

Fig. 3.14. Dependence of growth rate on group-III total flux of TEGa+TEIn.

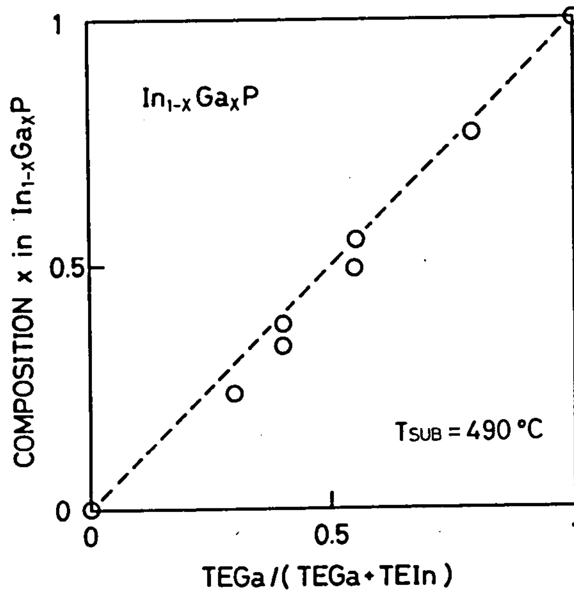

Fig. 3.15. Dependence of epilayer composition x in $In_{1-x}Ga_xP$ on flux ratio of TEGa/(TEGa+TEIn).

rate, and the epilayer composition do not depend on temperature. Moreover, the growth rate is proportional to the group-III total flux of TEGa+TEIn, and the composition x in $In_{1-x}Ga_xP$ epilayer is proportional to the flux ratio of TEGa/(TEGa+TEIn), as shown in Figs. 3.14 and 3.15, respectively. This indicates that the adduct formation between TEIn and PH_3 observed in low-vacuum MOVPE does not take place in MOMBE. These proportional relations are desirable for the precise control of growth rate and epilayer composition. Since the source nozzles have relatively small apertures and are arranged close to the substrates, very effective source utilization is achieved in this study, as indicated by smaller metalorganic fluxes compared with growth rates in Fig.3.14.

3-5-2. Phosphine Flux Dependence

The influence of phosphine flux on the epitaxy was examined at 490℃ with the group-III total flux of 0.036 sccm. A small V/III flux ratio of near unity was found to be sufficient to grow smooth epilayers in MOMBE unlike in conventional MOVPE where a large V/III ratio such as 100 is required. Moreover, smaller phosphine fluxes as low as 0.05 sccm improve the FWHM of x-ray rocking curves of epilayers, as shown in Fig.3.16. However, when the phosphine flux was reduced below 0.05 sccm, the growth rate decreased rapidly, the FWHM of x-ray rocking curves of epilayers became worse, and many indium droplets were formed on the surface of epilayers which grew to be GaP-rich. These results suggest that strong Ga-P bonds are preferentially formed at the growth interface than In-P bonds, which results in GaP-rich epilayers and in indium-droplet formation when phosphorus is insufficient for normal growth.

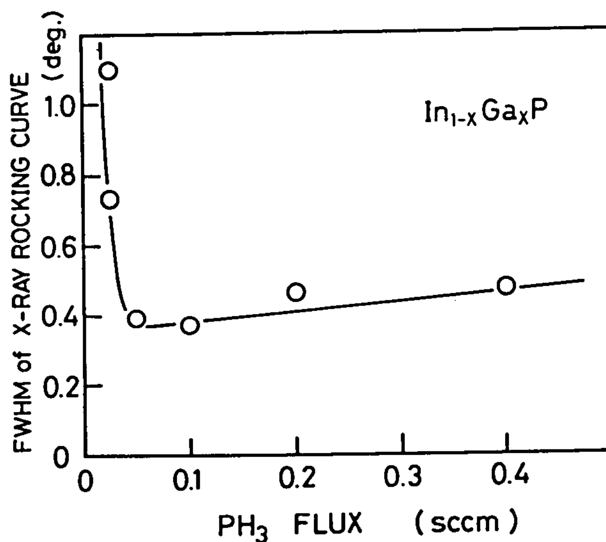

Fig. 3.16. Dependence of FWHM of x-ray rocking curves on phosphine flux. Poor resolution of x-ray instrument caused relatively large FWHM.

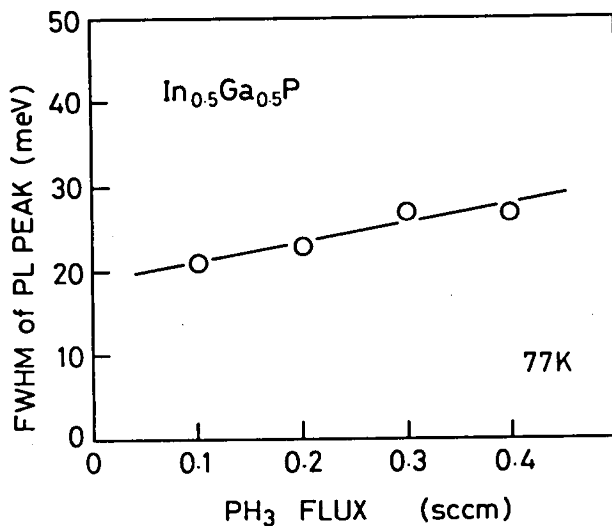

Fig. 3.17. Dependence of FWHM of band-edge PL peak on phosphine flux.

The phosphine flux dependence of photoluminescence (PL) was investigated for $In_{0.5}Ga_{0.5}P$ epilayers grown at 490℃, using a conventional grating monocromator and a photomultiplier. An Ar-ion laser of 6 mW was used as an excitation beam. Figure 3.17 shows that the band-edge PL peak is slightly narrower in lower phosphine fluxes. More drastic improvement in the PL peak width by smaller phosphine fluxes is observed for InP homoepitaxial layers grown in this MOMBE system. By reducing phosphine flux from 0.4 sccm to 0.1, the FWHM of band-edge PL peak of InP epilayers grown at 490℃ is lowered by a factor of 4.2.

The electrical properties of $In_{0.5}Ga_{0.5}P$ epilayers (n-type), examined by Hall measurements at room temperature, are also better when smaller phosphine fluxes are used, as shown in Figs. 3.18 and 3.19. The electron mobility of epilayers is improved slightly by smaller phosphine fluxes. Low carrier concentration around $2x10^{13}$ cm^{-3} with a small mobility of approximately 600 cm^2/Vs obtained with phosphine flux above 0.2 sccm indicate that carriers in these epilayers are largely compensated. With a phosphine flux of 0.1 sccm, a relatively high carrier concentration of $5x10^{15}$ cm^{-3} was obtained. This suggests that smaller phosphine fluxes reduce the compensation. However, the phosphine flux dependence of carrier concentration was not reproducible, indicating the complicated origin of compensators.

Three possible factors which probably induce the degradation of epilayer quality by higher phosphine fluxes are the suppressed migration of adsorbed atoms/molecules, the incorporation of phosphorus clusters, and increase in deep-level impurities attributed to the contamination of the phosphine source or the cracking process. Excess phosphorus atoms at the growth interface arising from higher phosphine fluxes suppress the migration of group-III adsorbed atoms/molecules, and cause phosphorus clustering in epilayers. Another unclear factor is natural atomic

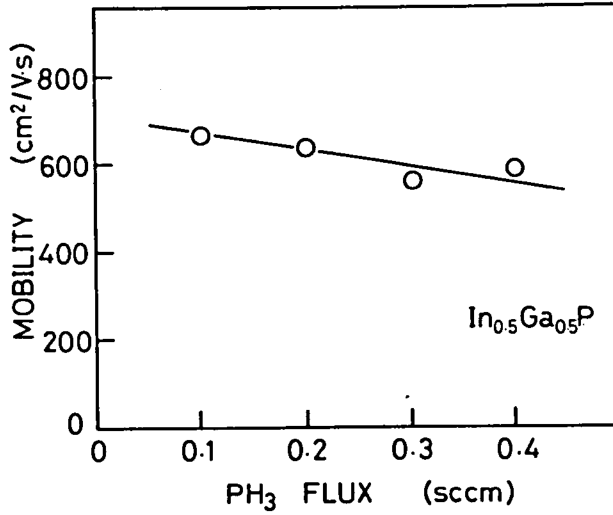

Fig. 3.18. Dependence of electron mobility on phosphine flux.

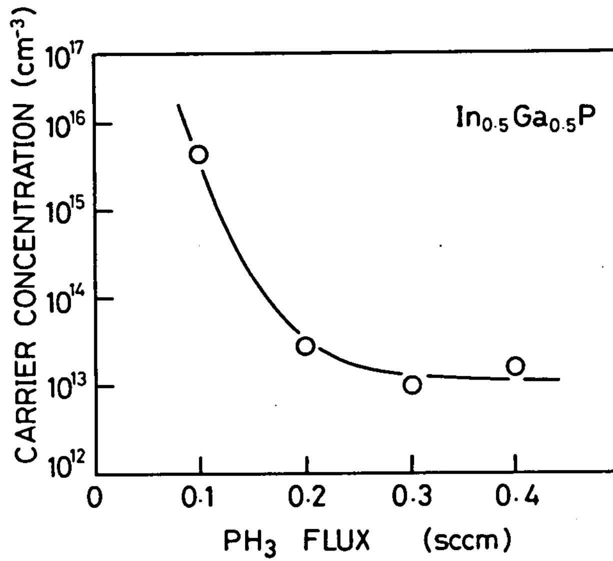

Fig. 3.19. Dependence of carrier concentration on phosphine flux.

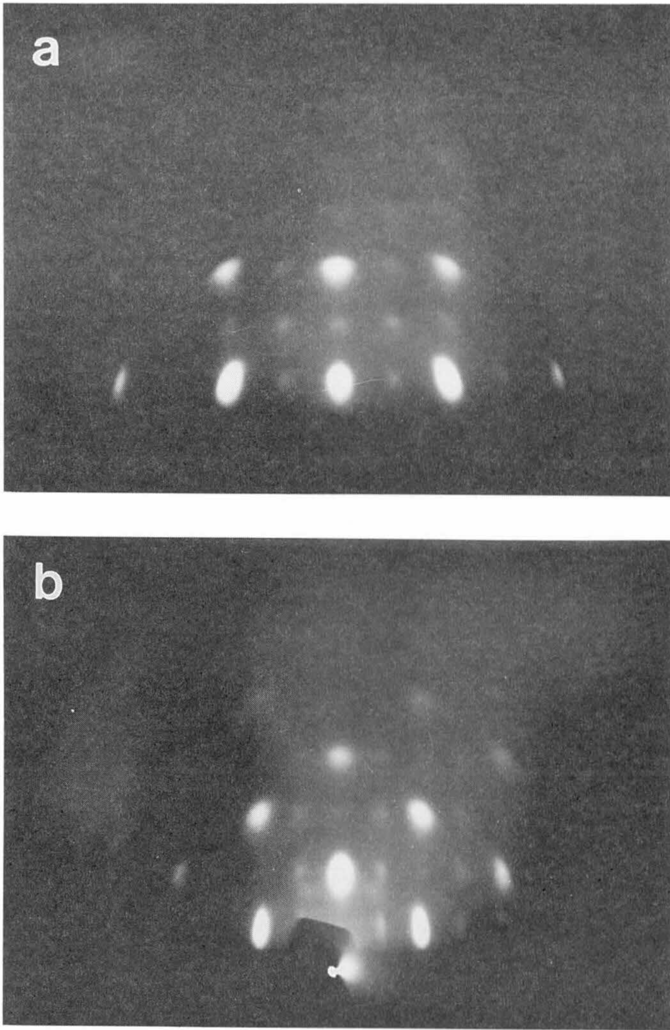

Fig. 3.20. Abnormal RHEED patterns. (a) <100> incidence, (b) <110> incidence.

ordering reported for InGaP lattice matched to GaAs grown in conventional MOVPE[42.43]. In this study, any abnormal PL peak shift due to the atomic ordering was not observed, but in the RHEED patterns of some epilayers, super spots usually forbidden for zincblende-type crystals were found, as shown in Fig.3.20. The super spots in Fig.3.20 suggest that indium atoms and gallium atoms are ordering on group-III sublattice-planes of (111), by turns like ···/In/Ga/In/Ga/In/Ga/···. The influence of such atomic ordering on the physical properties of epilayers has not been elucidated yet. More microscopic investigations are required to make clear the dominant factor responsible for the phosphine flux dependence of epilayer quality.

3-5-3. Optical and Electrical Properties

Most $In_{1-x}Ga_xP$ epilayers with x of 0.4-0.55 grown at moderate temperatures show quite sharp PL peaks of band edge, as shown in Fig.3.21. The dependence of PL spectrum on measuring temperature is given in Fig.3.22. The band-edge peak energy (E_g) shifts to lower energy as the temperature increases. When the temperature is lowered to 4.2K, the band-edge peak is weakened, and an impurity-related peak appears clearly, which is approximately 30 meV lower than E_g.

Figure 3.23 gives the dependence of PL peak on excitation intensity for a typical epilayer with many defect-related peaks. Three defect-related peaks named E_1, E_2, and E_3 for identification are observed clearly. The E_1 peak (approximately 20 meV lower than E_g) is sharp, but appears in only a few epilayers. It seems to originate from unreproducible factors such as growth ambience and interval period between each growth. The E_2 peak is independent of excitation intensity, but the peak E_3

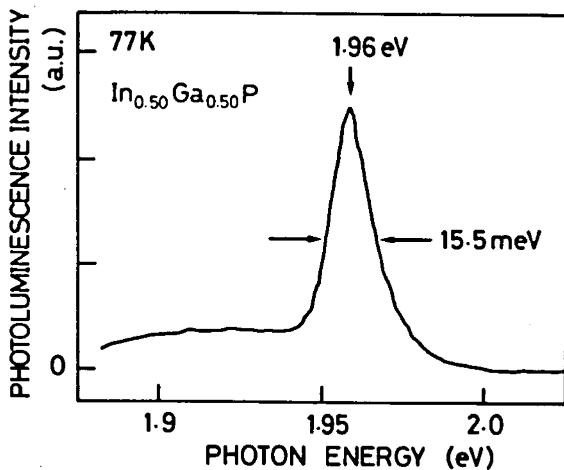

Fig. 3.21. Band-edge PL peak of typical $In_{0.5}Ga_{0.5}P$ epilayer grown at 490℃.

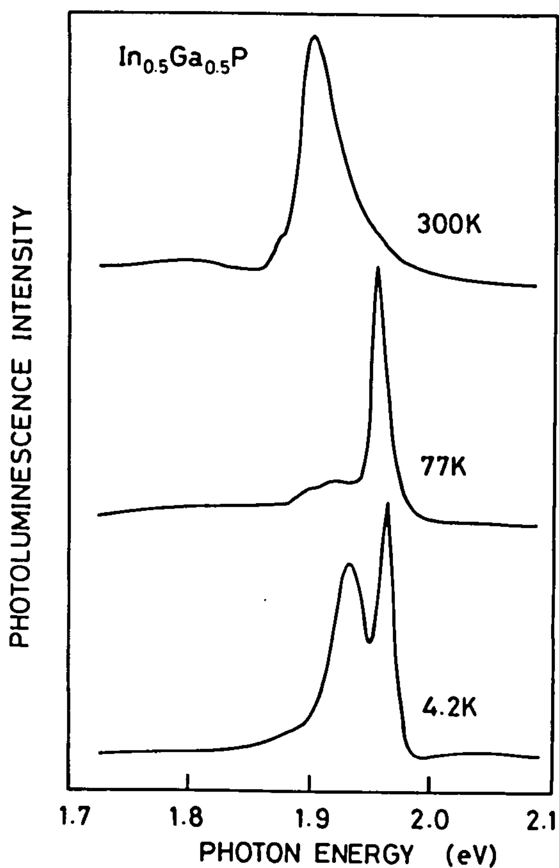

Fig. 3.22. PL spectra measured at 4.2K, 77K, and 300K.

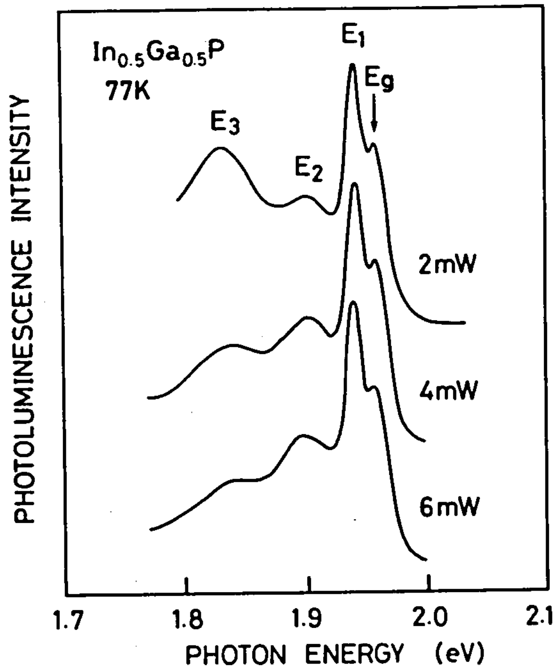

Fig. 3.23. Dependence of PL spectrum on excitation intensity.

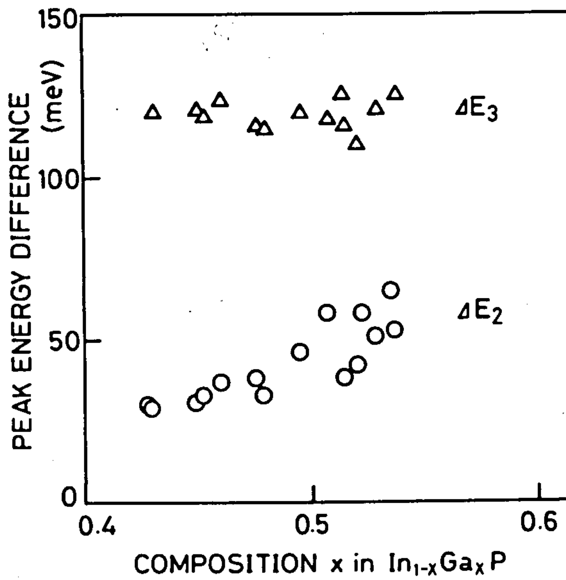

Fig. 3.24. Dependence of ΔE_2 and ΔE_3 on epilayer composition.

is saturated at higher excitation. The energy difference of $\Delta E_2=E_g-E_2$ and $\Delta E_3=E_g-E_3$ is plotted versus epilayer composition in Fig.3.24. The E_2 peak is possibly related with impurities (like donor-acceptor pairs), since ΔE_2 varies with epilayer composition (i.e., energy band gap), and its values are small. In contrast with ΔE_2, the relatively large ΔE_3 of approximately 120 meV is independent of epilayer composition, while the origin of the E_3 peak is unclear.

The InGaP epilayers grown in this study exhibit n-type conduction, or are highly resistive. Figures 3.25 and 3.26 show the temperature dependence of electrical properties for a typical $In_{0.5}Ga_{0.5}P$ epilayer with relatively high conductivity. The temperature dependence of electron mobility agrees well with a simple fitting calculation assumed $T^{-0.5}$ and $T^{1.5}$ dependence (Fig.3.25). As shown in Fig.3.26, carrier traps at a relatively deep level of 140 meV are responsible for the temperature dependence of carrier concentration. The value of 140 meV is close to ΔE_3, indicating that the origin of the E_3 peak relates deeply with the carrier traps. Moreover, the existence of other deep levels is suggested by photocurrent spectrum given in Fig.3.27. The photocurrent appears when the epilayers are illuminated by photons with energy higher than 1.4 eV. The deep levels with an activation energy of approximately 1.5 eV seems to catch most of electrons released from donor impurities, and cause the photocurrent. Similar deep level (1.3 eV) has been reported in MBE-grown InGaAlP[44].

Figure 3.28 shows the energy levels of impurities and carrier traps, which are suggested by the results discussed above. For MBE-grown Sn-doped $In_{0.5}Ga_{0.5}P$, an electron mobility of 3500 cm^2/Vs and a carrier concentration of 2×10^{16} cm^{-3} without compensation was reported[45]. In comparison with the report, the InGaP epilayers grown in this study are considerably inferior in

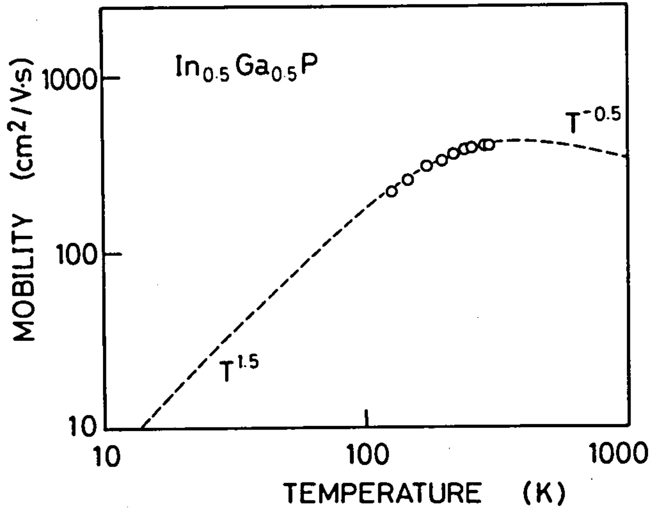

Fig. 3.25. Temperature dependence of mobility. Broken line is a fitting curve by $T^{-0.5}$ and $T^{1.5}$ slopes.

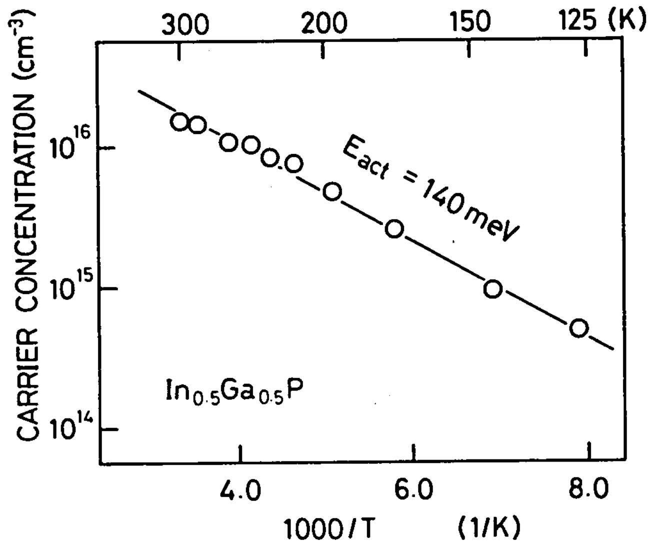

Fig. 3.26. Temperature dependence of carrier concentration.

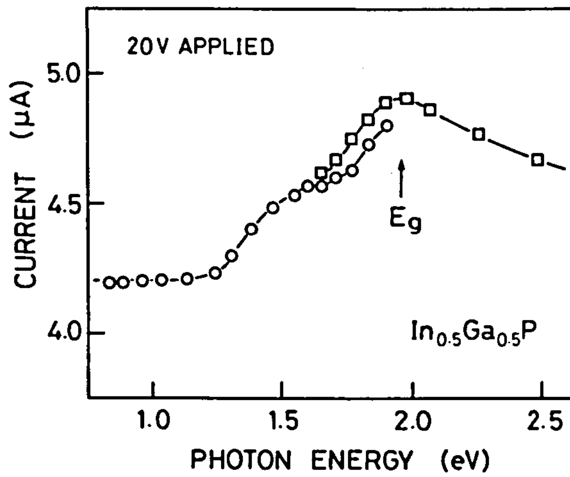

Fig. 3.27. Photon energy dependence of current under illumination. Two monocromators were used for measurements, causing two branches.

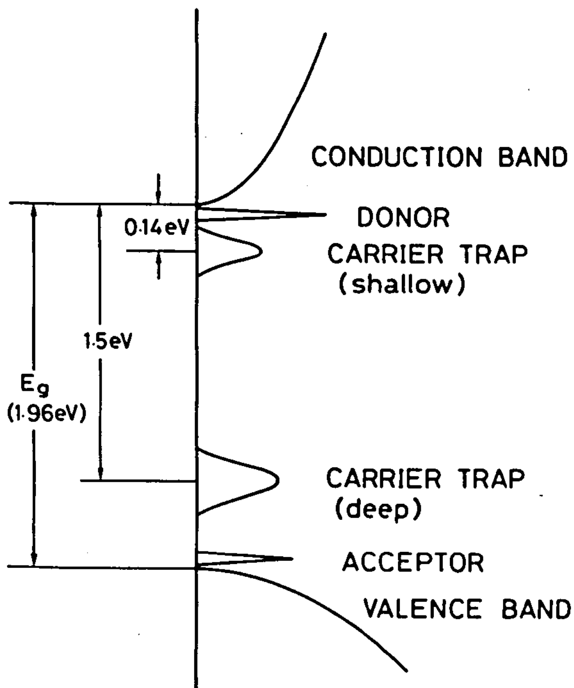

Fig. 3.28. Illustration of energy levels.

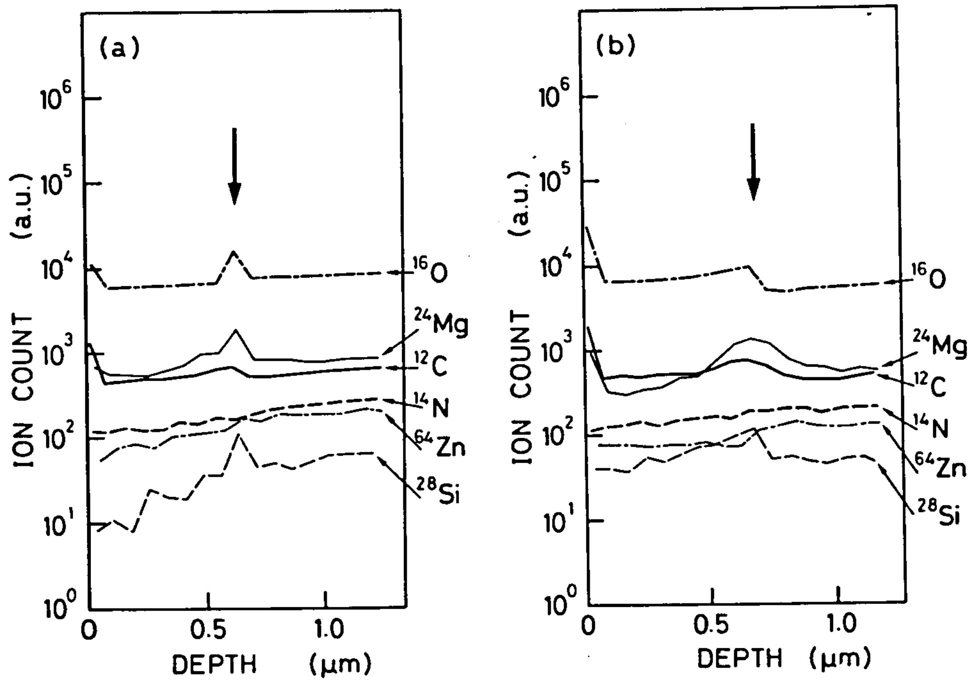

Fig. 3.29. Distribution of impurities in (a) n-type epilayer and (b) highly resistive epilayer. Down arrows represent the interface between the epilayer and the substrate.

electrical properties, probably due to the existence of carrier traps shown in Fig.3.28.

The incorporation of impurities was analyzed by secondary ion mass spectrometry (SIMS) for carbon, nitrogen oxygen, magnesium, silicon, and zinc. Any severe contamination was not observed for all the elements analyzed (Fig.3.29), even in a highly resistive epilayer. A little impurity-accumulation at the interface between substrate and epilayer suggest that the substrates were not perfectly cleaned before epitaxy, or contaminated at the initial stage of epitaxy.

3-5-4. Selective Epitaxy

To investigate the selective epitaxy of InGaP, SiO_2-masked substrates were prepared as follows. By photothermal chemical vapor deposition (CVD) using silane and oxygen, SiO_2 of 150 nm thick was deposited at 300℃ on a semi-insulating GaAs(001) substrate, which was previously etched with a solution of $8H_2SO_4:1H_2O_2:1H_2O$ for 1 min. By the use of conventional photolithographic technique, patterned photoresist was prepared on the SiO_2 layer (the pattern is given in Fig.3.30a). After etching SiO_2 with HF vapor and removing the photoresist with organic solvents, the substrate was etched with $20H_2SO_4:1H_2O_2:1H_2O$ solution to remove the damaged superficial part.

The epitaxy of $In_{0.5}Ga_{0.5}P$ on the masked substrate was carried out at 490℃. The epilayer thickness was monitored 'in-situ' by the laser monitor to stop the growth just when the patterned wells were buried. The surface feature before and after epitaxial growth is given in Figs. 3.30b and 3.30c, and the surface profile measured by a stylus profiler is shown in

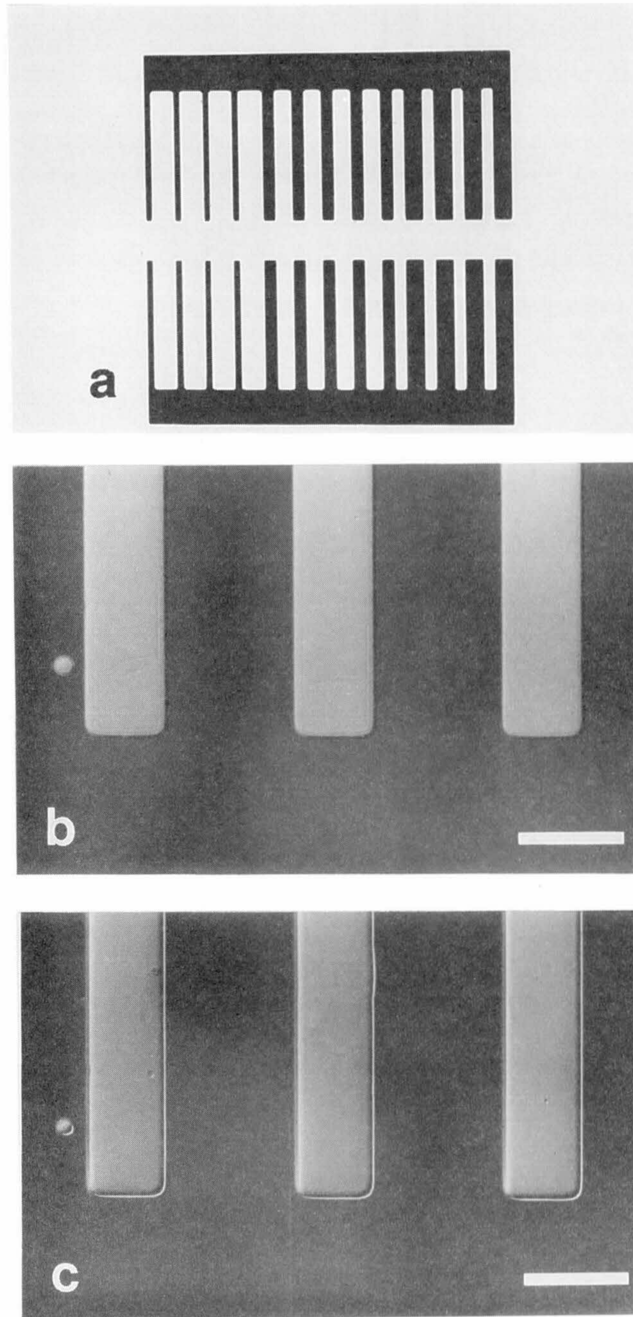

Fig. 3.30. Selective epitaxy of InGaP at 490℃; (a) SiO_2 pattern with a size of 2.5x2.5 mm^2, (b) patterned substrate before growth (darker part is SiO_2 mask), and (c) after growth. Markers in (b) and (c) represent 100μm.

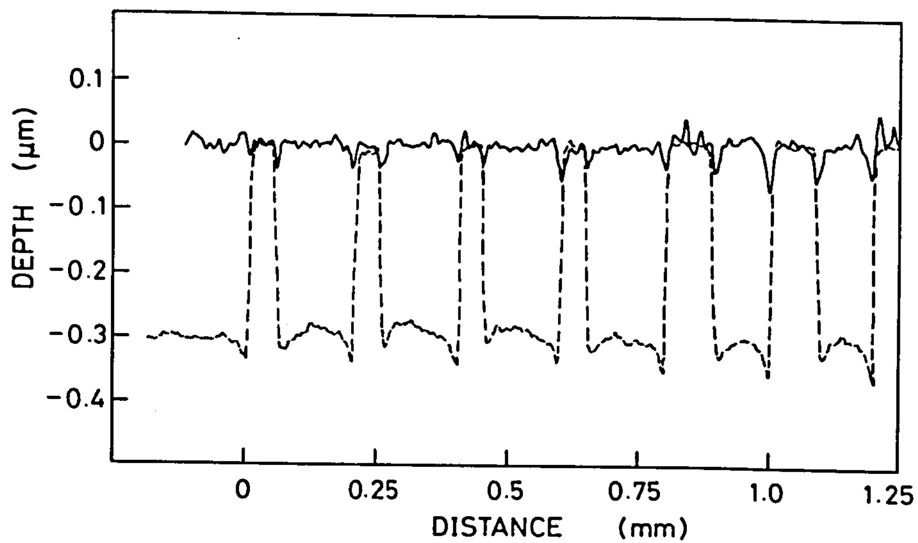

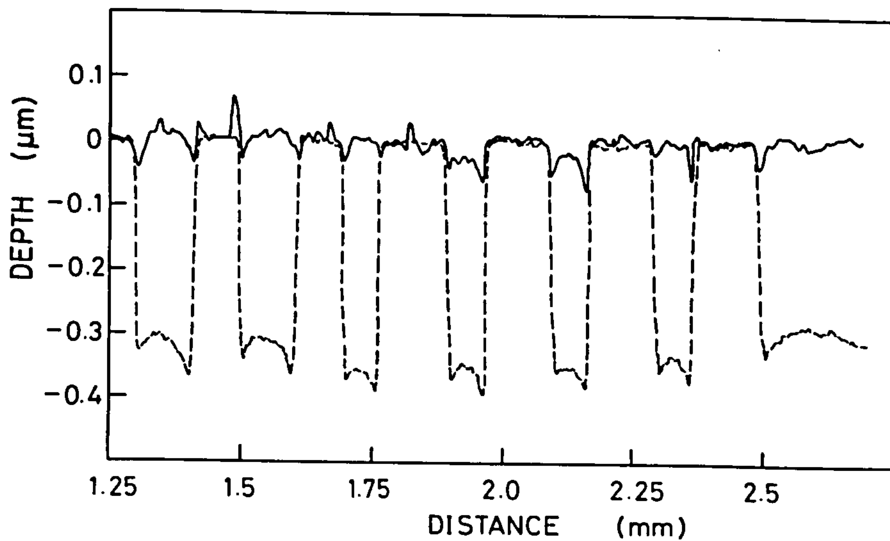

Fig. 3.31. Surface profile of selectively grown InGaP. Wells observed before growth (broken line) were buried by InGaP after growth (solid line).

Fig.3.31. As clearly shown in Fig.3.31, the wells of 0.3μm depth was perfectly buried after the epitaxial growth of 0.3μm, indicating that no deposition occurs on SiO_2. This suggests that metalorganic molecules are not adsorbed on SiO_2, since polycrystalline InGaP must be deposited on SiO_2 if the molecules were adsorbed and decomposed there.

3-6. Growth at Higher Temperatures

3-6-1. Shortage of Phosphorus

At higher temperatures above 520℃, the growth rate rapidly decreases and epilayers become GaP rich accompanied with defect (droplet) formation on the surface. These adverse affects are partially suppressed by using higher phosphine fluxes as shown in Figs. 3.10 and 3.11 with broken lines, suggesting that phosphorus shortage impedes normal growth. Figure 3.32 shows the growth rates of quasi-binaries (InP and GaP) above 420℃. The both growth rates fall rapidly above 520℃, and the decrease is much smaller for GaP compared with InP.

The shortage of phosphorus is caused by phosphorus evaporation from epilayers, or by the insufficient adsorption of phosphorus on the growth interface. The former means that phosphorus atoms already incorporated into the epilayer escape from the superficial part of the epilayer by getting high thermal energy. The latter means that phosphorus atoms impinged onto the growth interface do not stay long enough to be incorporated into the epilayer. In both cases, weaker In-P bonds than Ga-P bonds are responsible for the larger decrease in the growth rate of InP compared with GaP. More detailed discussion describing the analysis of growth at higher temperatures is given in the next

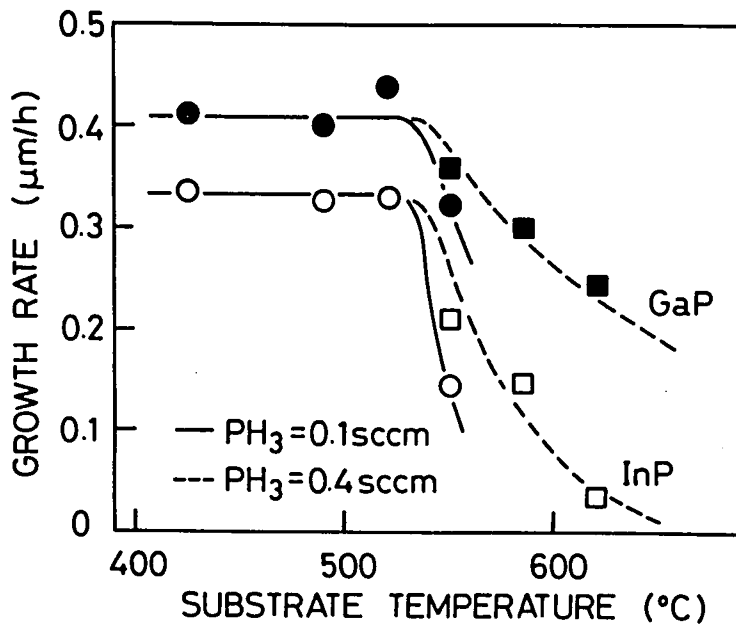

Fig. 3.32. Temperature dependence of growth rates of quasi-binaries (InP and GaP) above 420℃. ($TEIn=0.016$, $TEGa=0.020$ sccm).

chapter, and there the evaporation of phosphorus is concluded as the dominant factor of phosphorus shortage.

In contrast with InGaP MOMBE growth, decrease in the growth rate of GaAs and a constant growth rate of InAs at higher temperatures above 500℃ were reported in InGaAs MOMBE[46]. This significant difference suggests that the growth mechanism in MOMBE of arsenic-based III-V semiconductors is largely different from that of phosphorus-based III-V semiconductors, especially for high-temperature growth.

3-6-2. Immiscible Defects

The surface morphology obtained at higher temperatures was investigated by SEM observation and electron probe microanalyzer (EPMA) measurement, and three distinct types of surface features were found; (1) smooth surfaces as shown in Fig.3.33a, (2) a new type of defect (immiscible defect) as shown in Fig.3.33b, and (3) indium droplets on the surface as shown in Fig.3.33c. The EPMA observation revealed that the new type of defect in Fig.3.23b was a complex which had an InP crystallite partially surrounded by metal indium.

The temperature and the phosphine flux dependence of surface morphology (Fig.3.34) shows that higher temperature and smaller phosphine flux causes the formation of the complex defects on epilayers. When the temperature is extremely high and/or phosphine flux is extremely small, many indium droplets are formed instead of the complex defects. It is noteworthy that the complex defects are not observed below 520℃ even when insufficient phosphine flux for normal growth is used. Therefore, the phosphorus evaporation from epilayers is supposed to play an important role for the formation of the complex defects. The

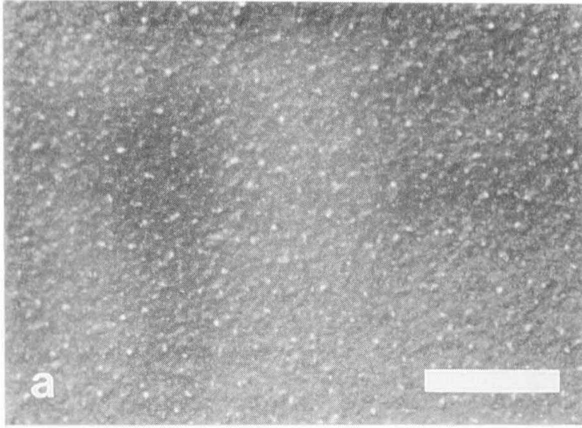

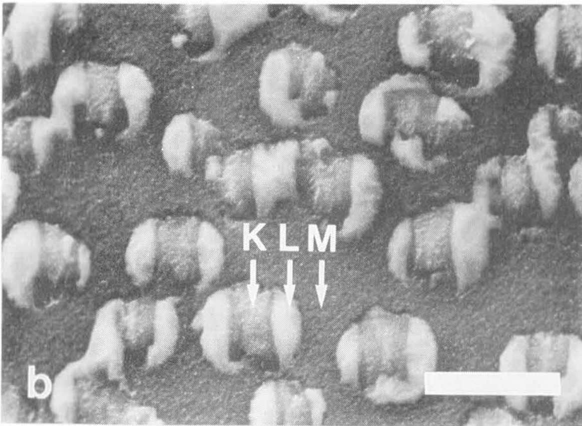

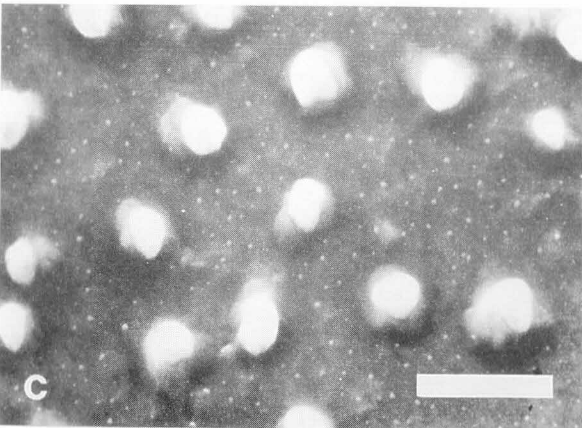

Fig. 3.33. Surface morphology obtained at 585℃ (SEM observation).
(a) PH_3=0.4sccm. Smooth surface of $In_{0.46}Ga_{0.54}P$.
(b) PH_3=0.3sccm. Complex defect (InP crystallite <K> partially surrounded by metal indium <L>) on $In_{0.29}Ga_{0.71}P$ <M>.
(c) PH_3=0.2sccm. Indium droplet on $In_{0.05}Ga_{0.95}P$.
Markers represent 5μm.

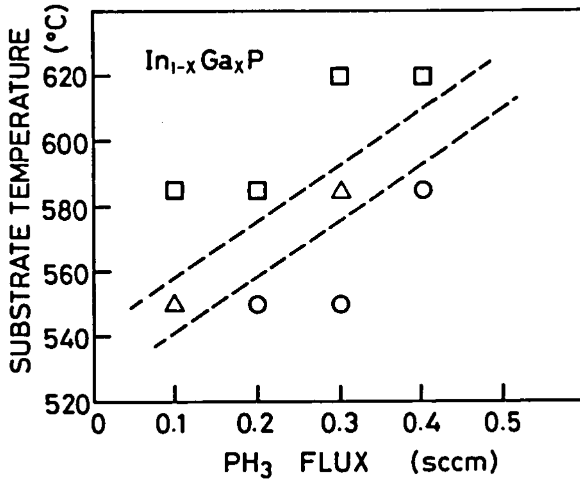

Fig. 3.34. Temperature and phosphine flux dependence of surface morphology grown with TEGa=TEIn=0.016 sccm. Smooth surface (○), complex defect (△), and indium droplet (□). Broken lines represent boundary of surface morphology.

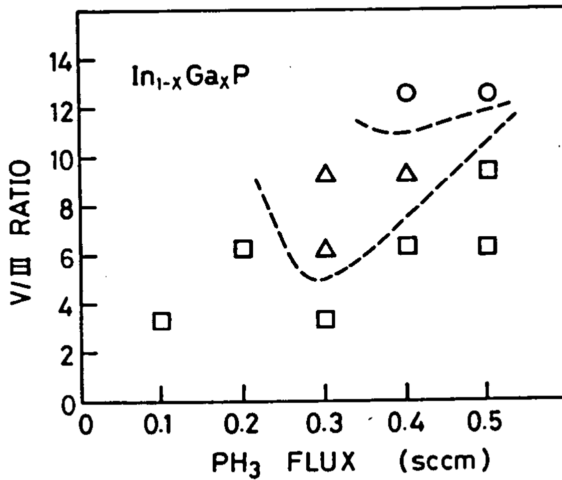

Fig. 3.35. V/III ratio and phosphine flux dependence of surface morphology grown at 585℃.
Smooth surface (○), complex defect (△), and indium droplet (□). Broken lines represent boundary of surface morphology.

V/III ratio and the phosphine flux dependence of the surface morphology at a constant temperature (585℃) is shown in Fig.3.35. The surface morphology was not governed simply by the V/III ratio nor the phosphine flux. Such immiscible defects indicates that very complicated surface kinetics are involved in the epitaxy of phosphorus-based III-V ternary semiconductors in MOMBE. The surface kinetics including the phosphorus incorporation into epilayers and the migration of adsorbed atoms/molecules at the growth interface must be made clear in order to explain the formation of immiscible defects.

3-7. Summary

For MOMBE growth of InGaP, the following were made clear.

(1) At lower temperatures below 390℃, the imperfect pyrolysis of TEGa limits the growth. An apparent activation energy of 39 kcal/mol for TEGa decomposition in InGaP MOMBE is considerably larger than that in GaAs MOMBE (20 kcal/mol). This indicates that the surface catalytic effect of phosphorus at the growth interface is considerably smaller compared with that of arsenic.

(2) In the moderate temperature region of 390-520℃, the growth rate and the composition x in $In_{1-x}Ga_xP$ epilayers are independent of temperature. The growth rate is proportional to the group-III total flux of TEGa+TEIn, and the gallium composition to the flux ratio of TEGa/(TEGa+TEIn). Smaller phosphine fluxes slightly improve the optical and electrical properties. Perfectly selective epitaxy of InGaP is achievable on SiO_2-masked substrates. This suggests that metalorganics are not adsorbed on the insulator surface.

(3) At higher temperatures above 520℃, phosphorus shortage impedes normal growth. A new type of complex defect (InP crystallite partially surrounded by metal indium) or indium droplets are formed when phosphorus shortage is severe. Rapid decrease in growth rate is much larger for InP constituent than for GaP constituent, corresponding to weak In-P bonds compared with Ga-P bonds.

(4) Epilayers grown at 490℃ have quite sharp band-edge PL peaks with a FWHM below to 16 meV at 77K, while two broad defect-related peaks are observed together. The epilayers exhibit n-type conduction, or are highly resistive. The carrier concentration of n-type epilayers is in the range of 10^{13}-10^{16} cm^{-3}, and the mobility is around 600 cm^2/Vs. These values indicate that impurities in the epilayers are compensated largely. Carrier traps with two different activation energy (approximately 140 meV and 1.5 eV) are probably responsible for the lower carrier concentration with the low mobility.

References

[1] F.J.Morris and H.Fukui, J.Vac.Sci.Technol. **11** (1974) 506.

[2] M.B.Panish, J.Electrochem.Soc. **127** (1980) 2729.

[3] M.B.Panish and H.Temkin, Appl.Phys.Lett. **44** (1984) 785.

[4] M.B.Panish and S.Sumski, J.Appl.Phys. **55** (1984) 3571.

[5] M.B.Panish, H.Temkin, and S.Sumski, J.Vac.Sci.Technol. **B3** (1985) 657.

[6] M.B.Panish, J.Cryst.Growth **81** (1987) 249.

[7] A.R.Calawa, Appl.Phys.Lett. **38** (1981) 701.

[8] R.Chow and Y.G.Chai, J.Vac.Sci.Technol. **A1** (1983) 49.

[9] B.J.Skromme, G.E.Stillman, A.R.Calawa, and G.M.Metze, Appl.Phys.Lett. **44** (1984) 240.

[10] L.W.Kapitan, C.W.Litton, G.C.Clark, and P.C.Colter, J.Vac.Sci.Technol. **B2** (1984) 280.

[11] C.Starck, L.Goldstein, M.Boulou, D.Bonnevie, M.Lambert, and C.Audry, J.Physique Colloq. **48** (1987) C5-175.

[12] E.Veuhoff, W.Pletschen, P.Balk, and H.Luth, J.Cryst.Growth **55** (1981) 30.

[13] N.Vodjdani, A.Lemarch, and H.Paradan, J.Physique Colloq. **43** (1982) C5-339.

[14] N.Putz, E.Veuhoff, H.Heinecke, M.Heyen, H.Luth, and P.Balk, J.Vac.Sci.Technol. **B3** (1985) 671.

[15] M.Weyers, N.Putz, H.Heinecke, M.Heyen, H.Luth, and P.Balk, J.Electron.Mater. **15** (1986) 57.

[16] N.Putz, H.Heinecke, M.Heyen, P.Balk, M.Weyers, and H.Luth, J.Cryst.Growth **74** (1986) 292.

[17] H.Heinecke, A.Brauers, F.Grafahrend, C.Plass, N.Putz, K.Werner, M.Weyers, H.Luth, and P.Balk, J.Cryst.Growth **77** (1986) 303.

[18] E.Tokumitsu, Y.Kudo, M.Konagai, and K.Takahashi, J.Appl.Phys. **55** (1984) 3163.

[19] E.Tokumitsu, Y.Kudo, M.Konagai, and K.Takahashi, Jpn.J.Appl.Phys. **24** (1985) 1189.

[20] E.Tokumitsu, T.Katoh, C.P.Sung, A.Sandhu, R.Kimura, M.Konagai, and K.Takahashi, Surf.Sci. **174** (1986) 43.

[21] E.Tokumitsu, T.Katoh, R.Kimura, M.Konagai, and K.Takahashi, Jpn.J.Appl.Phys. **25** (1986) 1211.

[22] K.Saito, E.Tokumitsu, T.Akatsuka, M.Miyauchi, T.Yamada, M.Konagai, and K.Takahashi, J.Appl.Phys. **63** (1988) 3975.

[23] See, for example, H.Ishikawa, K.Kondo, S.Sasa, H.Tanaka, and S.Hiyamizu, J.Cryst.Growth **76** (1986) 521.

[24] Y.Kawaguchi, H.Asahi, and H.Nagai, Jpn.J.Appl.Phys. **23** (1984) L737.

[25] Y.Kawaguchi, H.Asahi, and H.Nagai, Jpn.J.Appl.Phys. **24** (1985) L221.

[26] Y.Kawaguchi and H.Asahi, Appl.Phys.Lett. **50** (1987) 1243.

[27] W.T.Tsang, Appl.Phys.Lett **45** (1984) 1234.

[28] W.T.Tsang, J.Vac.Sci.Technol. **B3** (1985) 666.

[29] W.T.Tsang and R.C.Miller, J.Cryst.Growth **77** (1986) 55.

[30] W.T.Tsang, J.Electron.Mater. **15** (1986) 235.

[31] W.T.Tsang, B.Tell, J.A.Ditzenberger, and A.H.Dayman, J.Appl.Phys. **60** (1986) 4182.

[32] W.T.Tsang, J.Cryst.Growth **81** (1987) 261.

[33] N.Kobayashi, J.L.Benchimol, F.Alexandre, and Y.Gao, Appl.Phys.Lett. **51** (1987) 1907.

[34] A.Robertson Jr., T.H.Chiu, W.T.Tsang, and J.E.Cunningham, J.Appl.Phys. **64** (1988) 877.

[35] M.C.Paputa and S.J.W.Price, Can.J.Chem. **57** (1979) 3178.

[36] Y.Aoyagi, A.Doi, S.Iwai, and S.Namba, J.Vac.Sci.Technol. **B5** (1987) 1460.

[37] M.Ozeki, K.Mochizuki, N.Ohtsuka, and K.Kodama, Appl.Phys.Lett. **53** (1988) 1509.

[38] T.H.Chiu, W.T.Tsang, and J.E.Cunningham, J.Appl.Phys. **62** (1987) 2302.

[39] V.M.Donnelly, C.W.Tu, J.C.Beggy, V.R.McCrary, M.G.Lamont, T.D.Harris, F.A.Baiocchi, and R.C.Farrow, Appl.Phys.Lett. **52** (1988) 1065.

[40] Y.Aoyagi, S.Masuda, S.Namba, and A.Doi, Appl.Phys.Lett. **47** (1985) 95.

[41] Y.Aoyagi, M.Kanazawa, A.Doi, S.Iwai, and S.Namba, J.Appl.Phys. **60** (1986) 3131.

[42] A.Gomyo, K.Kobayashi, S.Kawata, I.Hino, and T.Suzuki, J.Cryst.Growth **77** (1986) 367.

[43] O.Ueda, M.Takikawa, J.Komeno, and I.Umebu, Jpn.J.Appl.Phys. **26** (1987) L1824.

[44] H.Asahi, Y.Kawamura, and H.Nagai, J.Appl.Phys. **53** (1982) 4928.

[45] P.Blood, J.S.Roberts, and J.P.Stagg, J.Appl.Phys. **53** (1982) 3145.

[46] Y.Kawaguchi, H.Asahi, and H.Nagai, Ext.Abstr. 18th Conf. Solid State Devices and Materials (Tokyo,1986) 619.

4. TEMPERATURE DEPENDENCE OF InAlP AND AlGaP GROWTH IN MOMBE

4-1. Introduction

InAlP and AlGaP are increasingly important to make full use of InGaP and GaP for visible lasers and light emitting diodes (LED's). Most of He-Ne lasers (632.8 nm) now widely used as convenient coherent-light sources will be replaced by heterostructure lasers of the InGaP-InAlP system lattice-matched to GaAs substrates[1-6]. The efficiency of light emission in GaP LED's (red-green) will be greatly improved by applying MQW/superlattice structures of the AlGaP-GaP system[7,8]. The investigation on such devices must be aggressively developed using the high performance of MOMBE in preparing heterostructures including superlattices. However, no work has been reported on MOMBE of InAlP and AlGaP.

This chapter describes the epitaxy of InAlP and AlGaP in MOMBE, focusing on the temperature dependence of growth rate and epilayer composition. As discussed in chapter 3, the epitaxy of InGaP in MOMBE is governed by the decomposition of TEGa at lower temperatures, the supply of metalorganics at moderate temperatures, and the shortage of phosphorus at higher temperatures. This suggests by analogy that the decomposition of TEAl plays an important role in the epitaxy of InAlP and AlGaP, especially at lower temperatures. Moreover, the epitaxy of AlGaP at higher temperatures must be fairly different from that of InGaP and InAlP, since weaker In-P bonds are not contained in AlGaP crystals. Therefore, the comparative analysis of MOMBE growth of InAlP and AlGaP is expected to bring much useful information for the understanding of the growth mechanisms in the MOMBE of phosphorus-based III-V semiconductors.

4-2. Epitaxy of InAlP and AlGaP

The InAlP epitaxy was carried out on GaAs(001) substrates, and epilayer compositions were determined by x-ray diffraction analysis. The temperature dependence of growth rate, epilayer composition x, surface morphology, and RHEED patterns of $In_{1-x}Al_xP$ epilayers are given in Figs. 4.1, 4.2, and 4.3. These dependencies are quite similar to those in InGaP epitaxy. Thus, as in the case of InGaP epitaxy, the InAlP growth is governed by the decomposition of TEAl at lower temperatures below 400℃, the supply of metalorganics at moderate temperatures of 400-500℃, and the shortage of phosphorus at higher temperatures above 500℃. However, there is a remarkable difference from the case of InGaP epitaxy that a larger flow of TEAl (0.016 sccm) compared with TEIn (0.0073 sccm) must be used to obtain the epilayer composition of 0.5 ($In_{0.5}Al_{0.5}P$) at the moderate temperatures. This difference indicates that the decomposition of TEAl differs greatly from that of TEGa in respect to decomposition efficiency.

The AlGaP epitaxy was carried out on GaP(001) substrates, and composition x in $Al_{1-x}Ga_xP$ epilayers was estimated by Auger electron spectrometry. The temperature dependence of AlGaP epitaxy is shown in Figs. 4.4, 4.5, and 4.6, obtained with a large flow of TEAl (0.037 sccm) compared with TEGa (0.014 sccm). Unlike the case of InGaP and InAlP epitaxy, the growth rate, epilayer composition, and surface morphology of AlGaP epilayers do not drastically change at higher temperatures up to 650℃, suggesting that phosphorus shortage is not severe in AlGaP epitaxy. Thus, the shortage of phosphorus at higher temperatures relates directly with the existence of indium atoms or In-P bonds in the epilayer. At lower temperatures below 400℃, the imperfect pyrolysis of TEGa and TEAl causes the rapid decrease in growth rate with decreasing temperature. The AlP-rich composition of

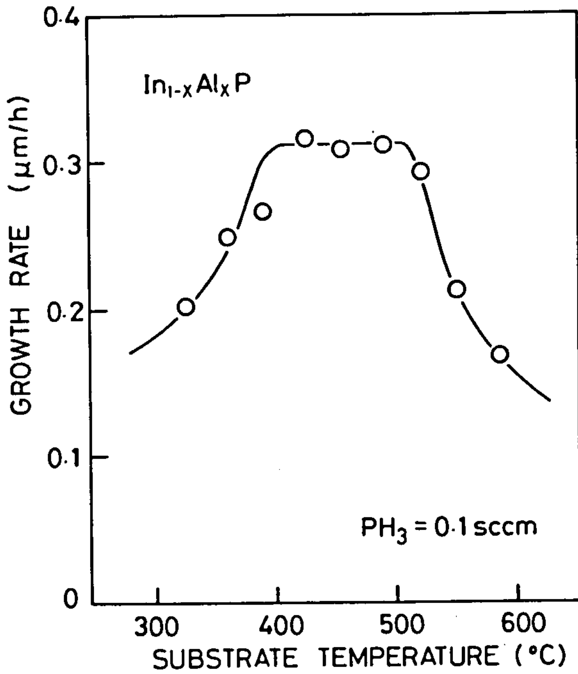

Fig. 4.1. Temperature dependence of growth rate of InAlP. (TEIn=0.0073, TEAl=0.016, PH_3=0.100 sccm).

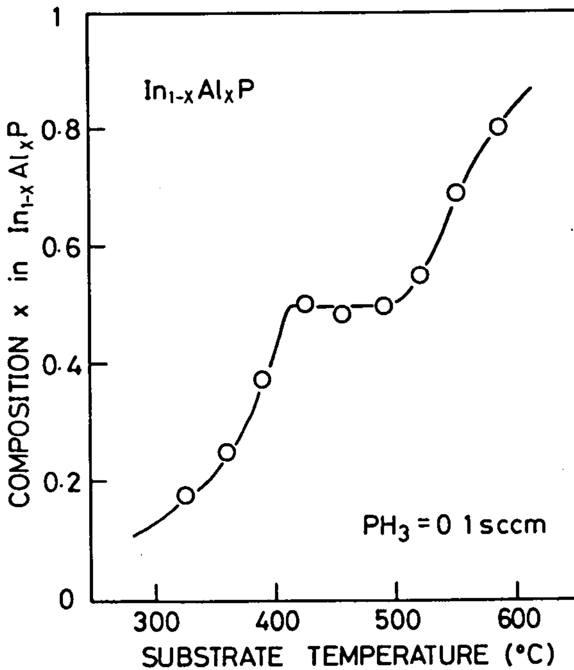

Fig. 4.2. Temperature dependence of epilayer composition x in $In_{1-x}Al_xP$. (TEIn=0.0073, TEAl=0.016, PH_3=0.100 sccm).

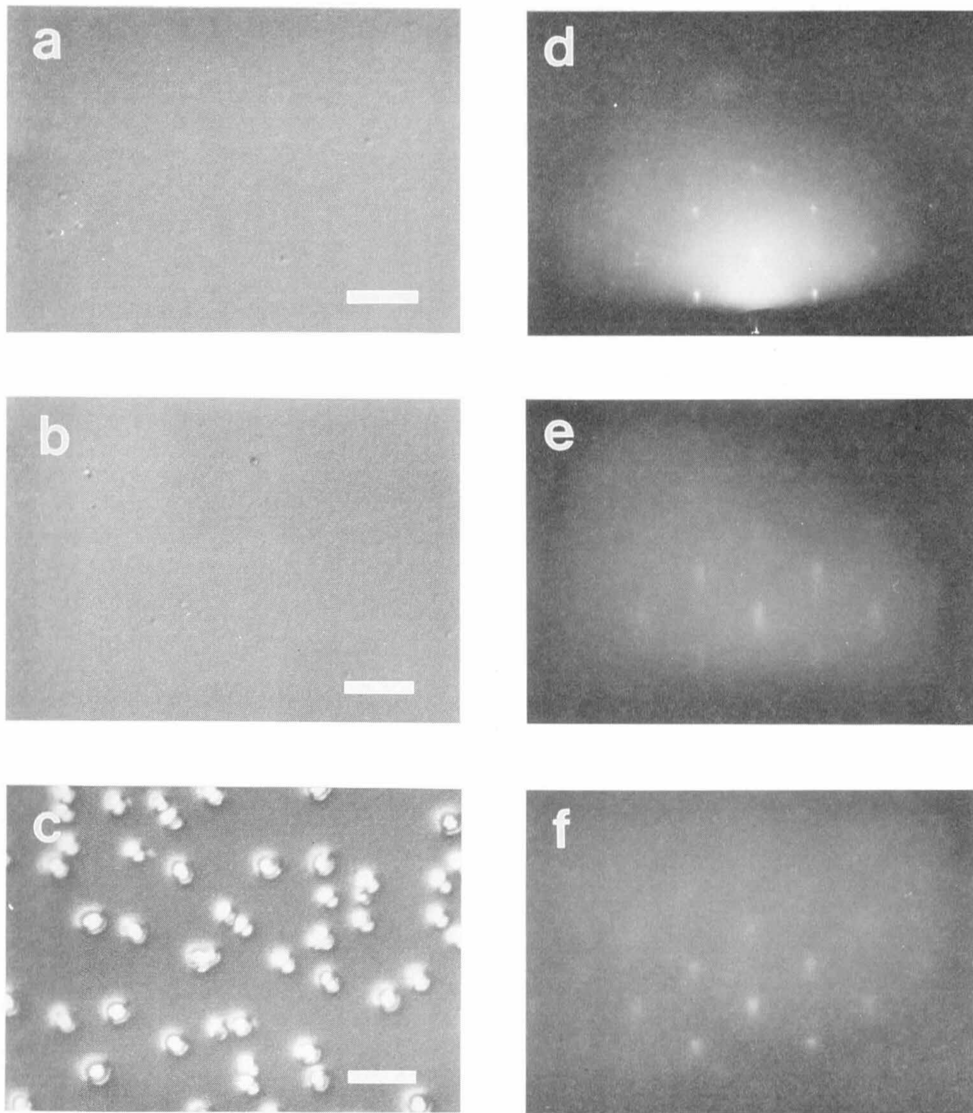

Fig. 4.3. Temperature dependence of surface morphology of InAlP epilayers observed by Nomarski phase contrast microscope (a)-(c), and RHEED patterns (d)-(f). (a),(d) 360℃; (b),(e) 490℃; (c),(f) 585℃. Markers in (a)-(c) represent 10μm.

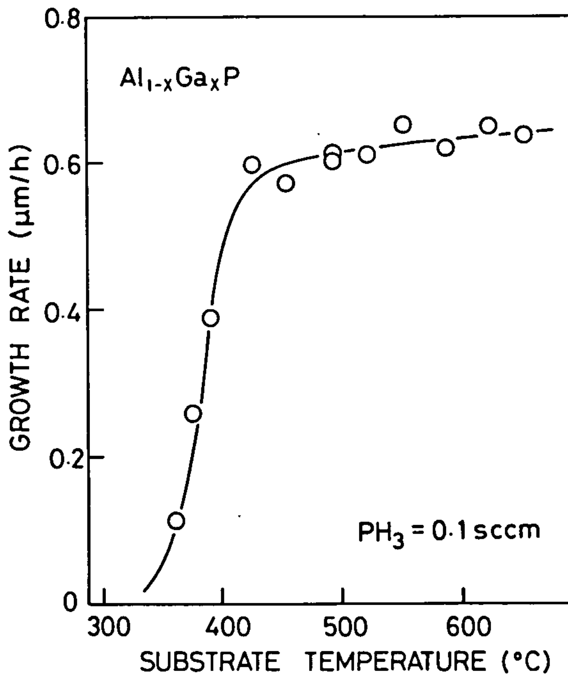

Fig. 4.4. Temperature dependence of growth rate of AlGaP. (TEAl=0.037, TEGa=0.014, PH_3=0.100 sccm).

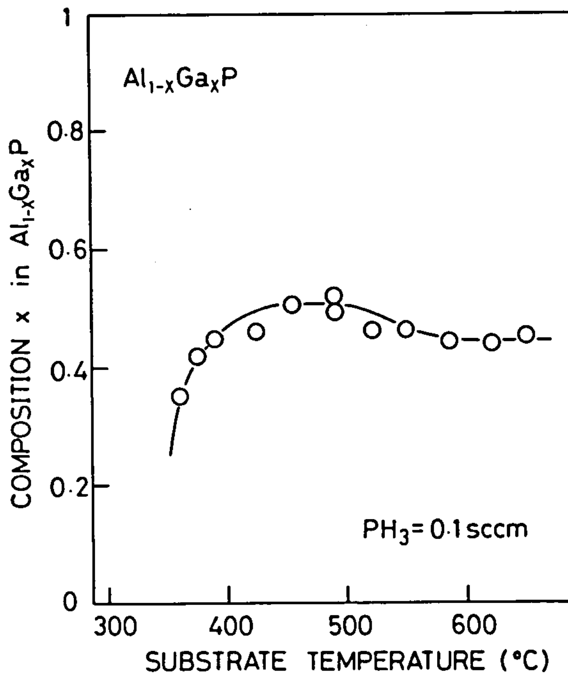

Fig. 4.5. Temperature dependence of epilayer composition x in $Al_{1-x}Ga_xP$. (TEAl=0.037, TEGa=0.014, PH_3=0.100 sccm).

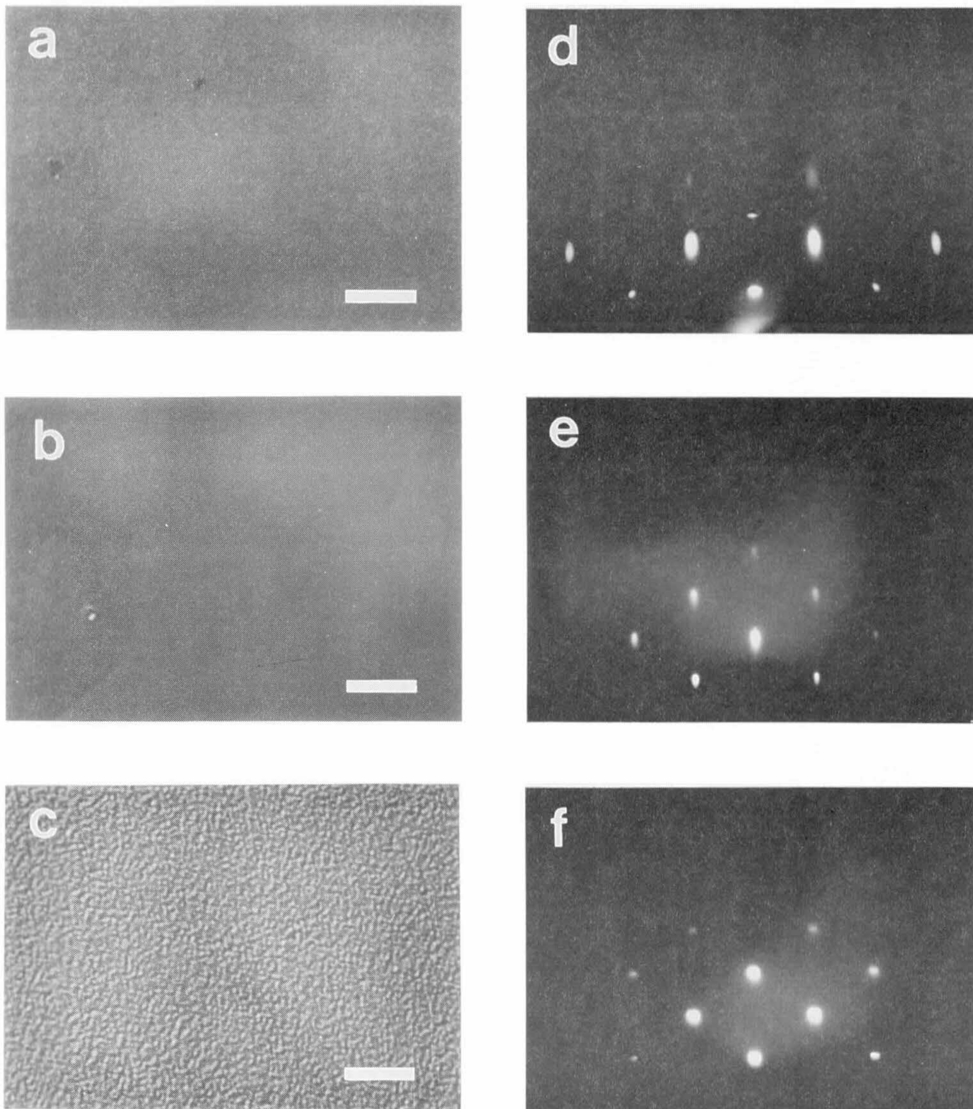

Fig. 4.6. Temperature dependence of surface morphology of AlGaP epilayers observed by Nomarski phase contrast microscope (a)-(c), and RHEED patterns (d)-(f). (a),(d) 360℃; (b),(e) 490℃; (c),(f) 620℃. Markers in (a)-(c) represent 10μm.

epilayers at these temperatures shows that the decomposition of TEGa is lowered much more than that of TEAl.

4-3. Co-decomposition of Metalorganics

As mentioned in the section 4-2, a large flow of TEAl (0.016 sccm) compared with TEIn (0.0073 sccm) is required for the epitaxy of $In_{0.5}Al_{0.5}P$ at the moderate temperatures. This reveals that only 45% of TEAl contributes to the epitaxy. The quite similar efficiency of 41% for TEAl decomposition is calculated for AlGaP epitaxy. Moreover, in AlP binary growth carried out for comparative study, a considerably smaller efficiency of TEAl decomposition was obtained; with an equivalent flux of TEAl and TEIn, the comparison of growth rate of AlP with that of InP shows that only 14% of TEAl is effectively used in AlP binary growth at 420-490℃. Therefore, it is obvious that the decomposition of TEAl is extremely ineffective in AlP binary epitaxy, and enhanced considerably by the existence of other metalorganics (TEIn or TEGa), or by the existence of other metal atoms (indium or gallium) at the growth interface.

The apparent activation energy (E_{act}) of TEAl decomposition obtained at lower temperatures is also unnatural. Figures 4.7 and 4.8 show the temperature dependence (Arrhenius' relation) of growth rates of quasi-binaries (InP-AlP for InAlP epitaxy, AlP-GaP for AlGaP epitaxy) at lower temperatures, calculated by the same scheme used in the analysis of InGaP epitaxy (section 3-4). The growth rate of AlP in AlP binary epitaxy is also plotted in Fig.4.7. The E_{act} of TEAl decomposition is 12 kcal/mol in InAlP epitaxy, 30 kcal/mol in AlGaP epitaxy, and 24 kcal/mol in AlP binary growth, while 29 kcal/mol was reported in direct pyrolysis experiment[9]. As indicated by the smaller E_{act} of TEAl

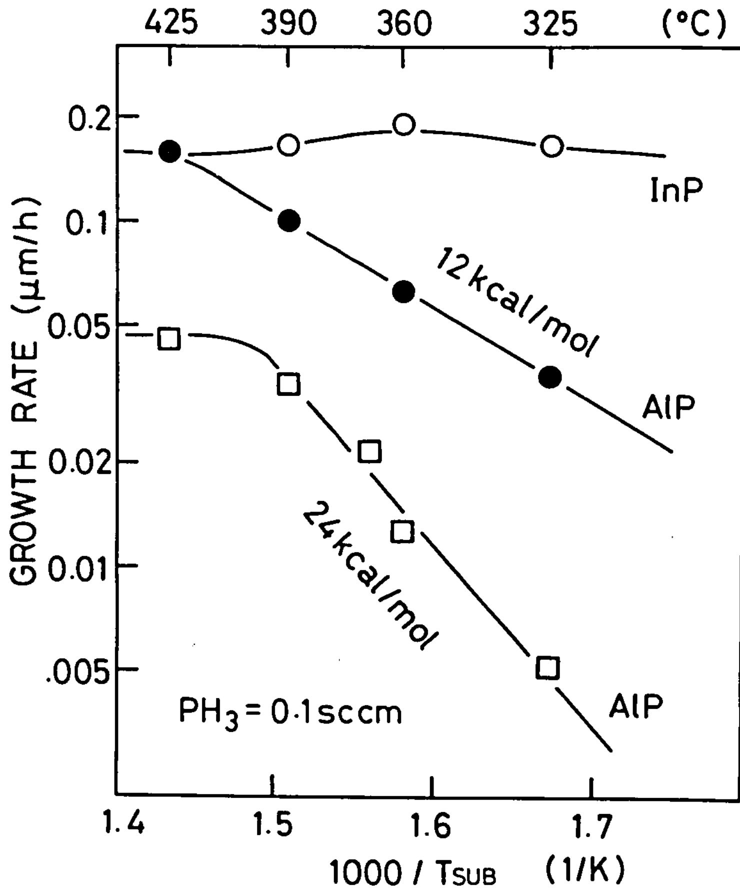

Fig. 4.7. Arrhenius plot of growth rates of quasi-binaries (InP (○) and AlP (●)) in InAlP epitaxy (TEIn=0.0073, TEAl=0.016 sccm), and of AlP (□) in binary growth (TEAl=0.016 sccm), at lower temperatures.

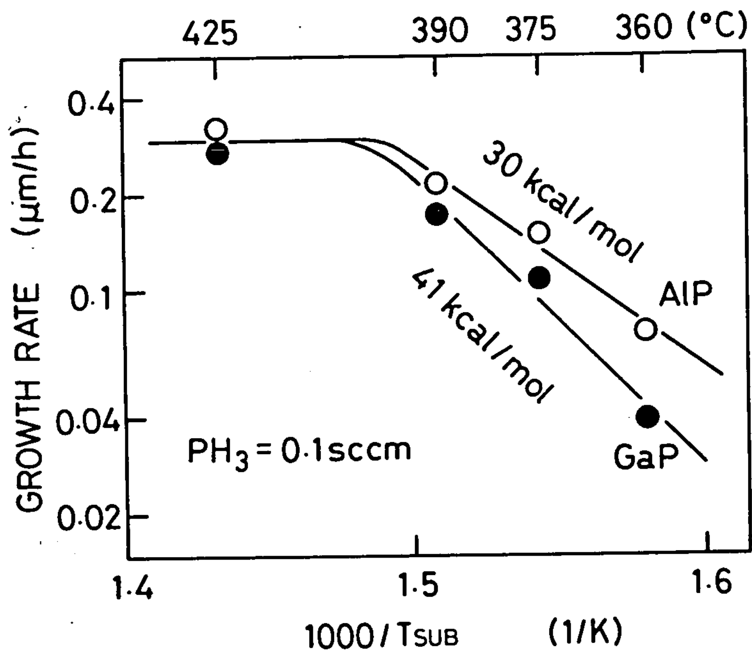

Fig. 4.8. Arrhenius plot of growth rates of quasi-binaries in AlGaP epitaxy at lower temperatures. (TEAl=0.037, TEGa=0.014 sccm).

decomposition in InAlP epitaxy, the enhancing influence of TEIn (or indium atoms) on TEAl decomposition is larger than that of TEGa (or gallium atoms) at lower temperatures, unlike that at moderate temperatures where the difference is very small. This strongly suggests that TEAl decomposition is enhanced by the decomposition of other metalorganics (TEIn or TEGa), but not by temperature-independent factors including surface catalytic effects of other metal atoms (indium or gallium) at the growth interface. The decomposition of TEIn and TEGa is consistent in each ternary growth, i.e., the pyrolysis of TEIn or TEGa is not influenced by the existence of other metalorganics; as in InGaP epitaxy, TEIn decomposes entirely as low as 320℃ in InAlP epitaxy, and a quite similar value of 41 kcal/mol is obtained for the E_{act} of TEGa in AlGaP epitaxy.

Here, an analogical model, "co-decomposition of metalorganics" is proposed as one possible mechanism to explain the strange aspects of TEAl decomposition. As is well known, TEAl molecules are mostly dimeric in the vapor phase, by making ethyl-bridged couplings as shown in Fig.4.9a[10]. It is probable that TEAl molecules make ethyl-bridged coupling also with other metalorganics, and form complexes like TEAl-TEIn or TEAl-TEGa, as illustrated in Fig.4.9b. The existence of such complexes is partly supported by the mass spectrometric observation of fragment molecules in low-pressure MOVPE[11]. In AlP binary growth, a small part of those TEAl molecules impinged onto the heated substrate are decomposed there and incorporated into the epilayer, but most of them escape without decomposition, since they cannot receive sufficient thermal energy to be decomposed. This ineffective decomposition is probably caused by the short residence of dimeric TEAl molecules, and results in the considerably smaller growth rates in AlP binary epitaxy. In InAlP epitaxy, since TEAl and TEIn are mixed in a source-transporting

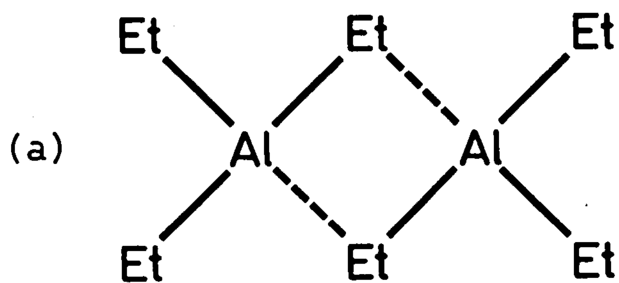

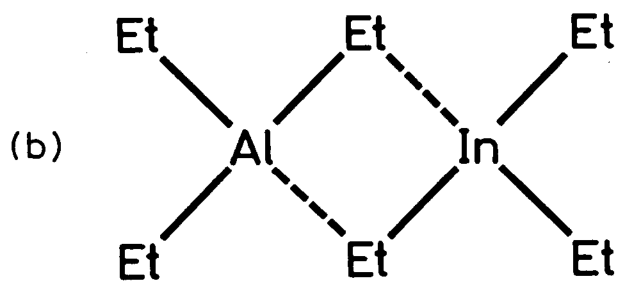

Fig. 4.9. Illustration of (a) TEAl dimer and (b) TEAl-TEIn complex.

line (Fig.1.1), a large part of TEAl molecules make the complex of TEAl-TEIn before they impinge to the substrate. On reaching the substrate, the TEIn part of the complex is decomposed, and releases the thermal energy of pyrolysis. The energy is transferred to the TEAl part, and induces its decomposition. Through this co-decomposition process, TEAl decomposition is enhanced by the existence of TEIn in InAlP epitaxy. The same process happens in AlGaP epitaxy, but the imperfect pyrolysis of TEGa below 390℃ results in the relatively large E_{act} of TEAl decomposition in AlGaP epitaxy compared with that in InAlP epitaxy. The co-decomposition model proposed here is rather speculative, and must be examined in future investigations.

4-4. Phosphorus Evaporation

The rapid change of growth rate and epilayer composition in InAlP epitaxy above 500℃ (Figs. 4.1 and 4.2) indicates that the shortage of phosphorus occurs at higher temperatures, just as in InGaP epitaxy. The phosphorus shortage also causes many indium-rich droplets on the surface of InAlP epilayers (Fig.4.3c), but no immiscible defect was observed unlike in InGaP epitaxy. However, in AlGaP epitaxy, the growth rate does not decrease at higher temperatures up to 650℃ (Fig.4.4). The surface of AlGaP epilayers is somewhat deteriorated above 585℃ (Fig.4.6c), but no metal droplets are formed. The difference in this dependence strictly indicates that the shortage of phosphorus observed at higher temperatures in InGaP and InAlP epitaxy is caused by the evaporation of phosphorus from the superficial part of epilayers, by breaking weak In-P bonds. In clear contrast with these observations, the insufficient adsorption of phosphorus atoms on the growth interface must

reduce the growth rate of AlGaP at higher temperatures as much as that of InGaP or InAlP. Thus, the insufficient adsorption of phosphorus is not a dominant factor responsible for the phosphorus shortage. Phosphorus atoms impinging on the growth interface at higher temperatures are therefore once incorporated into the epilayer. Then weak In-P bonds are broken thermally, and phosphorus atoms evaporate from the epilayer, leaving indium atoms on the surface. Since the temperatures are much higher than the upper limit for the congruent sublimation of InP, the residual free indium atoms do not evaporate from the surface, but form droplets.

Comparative study on the temperature dependence of the growth rates of quasi-binaries in each ternary brings much more information on the behavior of group-III atoms at the growth interface. As in InGaP epitaxy (Fig.3.32), the growth rate of InP decreases rapidly above 520℃ in InAlP epitaxy (Fig.4.10). Those remarkable decrease are well explained by phosphorus evaporation from epilayers as discussed above. However, the growth rate of GaP falls in InGaP epitaxy above 520℃, but remains constant up to 650℃ in AlGaP epitaxy (Fig.4.11). The growth rate of AlP decreases slightly above 520℃ in InAlP epitaxy, but increases approximately 20% in AlGaP epitaxy. These results reveal that Ga-P and Al-P bonds are stable up to 650℃ under a phosphine flux of 0.1 sccm. The decrease in GaP and AlP growth rates observed in InGaP or InAlP epitaxy is therefore a secondary affect due to phosphorus evaporation. Free gallium and aluminum atoms produced by the decomposition of metalorganics migrate/diffuse on the growth interface until they are caught at growth sites or into droplets. Their incorporation into droplets causes the decrease in the growth rate of GaP in InGaP epitaxy, or of AlP in InAlP epitaxy. The longer migrating/diffusing distance of gallium atoms than aluminum atoms[12,13] corresponds to the larger decrease in

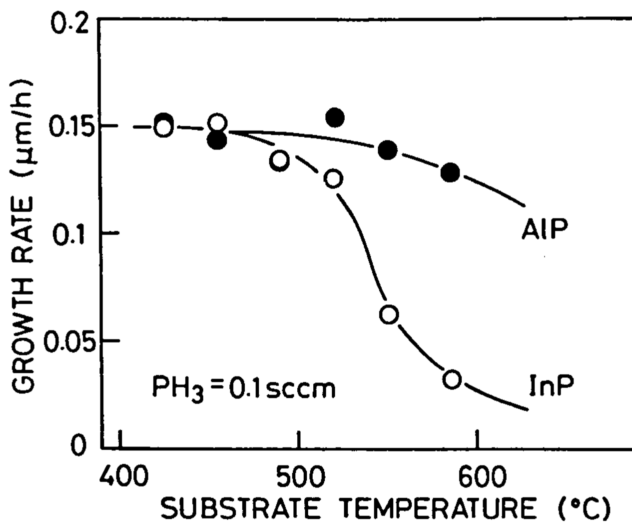

Fig. 4.10. Temperature dependence of growth rates of quasi-binaries in InAlP epitaxy above 420℃.

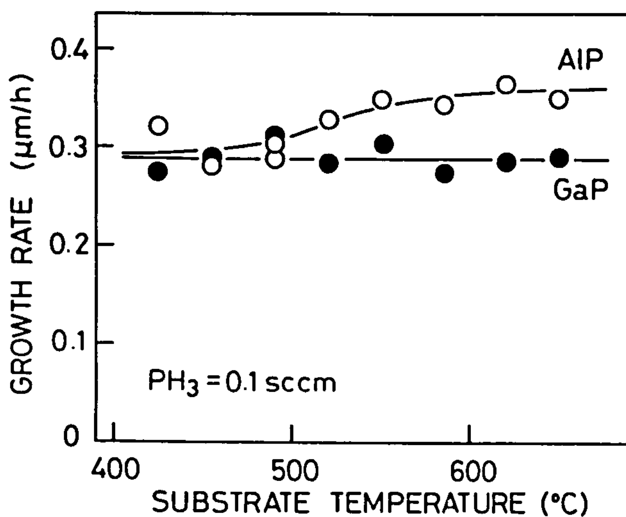

Fig. 4.11. Temperature dependence of growth rates of quasi-binaries in AlGaP epitaxy above 420℃.

GaP growth rate in InGaP epitaxy than the decrease in AlP growth rate in InAlP epitaxy. In AlGaP epitaxy, since no droplets are formed on the surface by the absence of weak In-P bonds, migrating/diffusing gallium and aluminum atoms are all incorporated in the epilayer. Therefore, the growth rate of AlGaP does not decrease up to 650℃. The increase in AlP growth rate in AlGaP epitaxy above 520℃ is probably due to the thermal enhancement of TEAl decomposition. Slightly inferior surfaces above 585℃ may suggest that a smaller amount of phosphorus evaporates from the epilayer by breaking Ga-P or Al-P bonds.

4-5. Impurity Incorporation

All InAlP epilayers grown in this study were highly resistive and showed no photoluminescence. AlGaP epilayers grown at 400-520℃ were low-resistive of p-type conduction (e.g., carrier concentration of 4.9×10^{19} cm^{-3} and Hall mobility of 1.6 cm^2/Vs), while those grown at other temperatures were highly resistive. Those electrical properties, especially p-type AlGaP epilayers with high carrier concentration, suggest the large incorporation of impurities.

Impurity incorporation in InAlP and AlGaP epilayers was measured by SIMS analysis. Figures 4.12 shows the depth profiles of impurities (nitrogen, carbon, oxygen, magnesium, silicon, and zinc) for a typical InAlP epilayer (Fig.4.12a) and for a typical AlGaP epilayer (Fig.4.12b). The large incorporation of carbon, oxygen, and silicon was detected in the InAlP epilayer. The high resistivity of InAlP epilayers is probably due to considerable contamination by oxygen. In the AlGaP epilayer, the fairly high incorporation of carbon, oxygen, magnesium, and silicon was observed with the pile up of oxygen and silicon at the interface

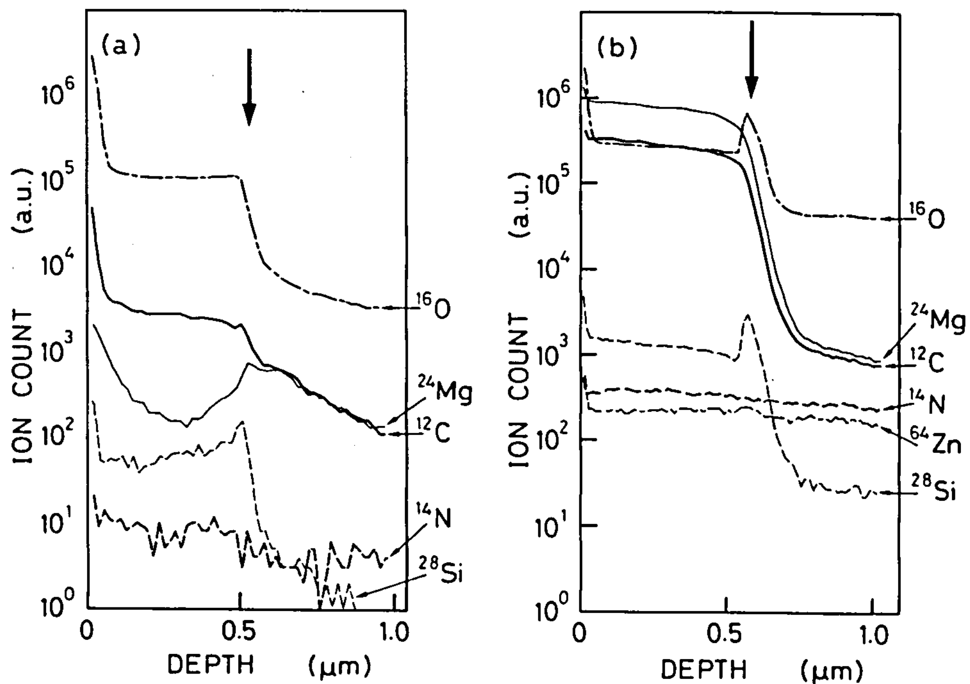

Fig. 4.12. Distribution of impurities in (a) InAlP epilayer and (b) AlGaP epilayer. Down arrows represent the interface between the epilayer and the substrate.

between the epilayer and the substrate. The low resistivity of p-type AlGaP epilayers is clearly due to heavy contamination by carbon. The pile up of impurities at the interface is probably due to the insufficient cleaning temperature of 700℃ for GaP substrates.

Since such contaminations are not detected in InGaP epilayers (section 3-5-3), it is obvious that active aluminum atoms are responsible for the large impurity incorporation into InAlP and AlGaP epilayers. The baking of the growth chamber possibly reduces the incorporation of impurities except carbon. The carbon impurities are derived mainly from the imperfect decomposition of TEAl. Thus, some other assistance to decompose TEAl perfectly (e.g., photo-irradiation) must be employed to lower carbon impurities.

4-6. Summary

The following were concluded by the comparative analysis of MOMBE growth of InGaP, InAlP and AlGaP.

(1) Three distinct stages are observed in the temperature dependence of growth rate and epilayer composition in MOMBE of InAlP and AlGaP, while a higher-temperature region for AlGaP epitaxy is relatively unclear. As in InGaP growth, the MOMBE growth of InAlP and AlGaP is governed by the imperfect decomposition of TEGa and TEAl at lower temperatures, by the supply of metalorganics at moderate temperatures, and by phosphorus evaporation at higher temperatures.

(2) The decomposition of TEAl is imperfect at all the temperatures studied, and is enhanced by the existence of other

metalorganics (TEIn or TEGa). The apparent activation energy of TEAl decomposition is 12 kcal/mol in InAlP epitaxy, 30 kcal/mol in AlGaP epitaxy, and 24 kcal/mol in AlP binary epitaxy. Such strange decomposition of TEAl can be explained by the co-decomposition mechanism, in which the thermal energy produced by the pyrolysis of TEIn or TEGa is transferred to TEAl and induces its decomposition.

(3) The evaporation of phosphorus atoms from epilayers by breaking weak In-P bonds is responsible for the shortage of phosphorus (decrease in growth rate and droplet formation) observed above 520℃ in InGaP and InAlP epitaxy. The incorporation of gallium or aluminum atoms into indium droplets on the epilayer surface reduces the growth rate of the GaP and AlP constituents in InGaP and InAlP epitaxy at higher temperatures. By the absence of In-P bonds, the growth rate of AlGaP does not decrease up to 650℃, and no droplets are formed on the surfaces.

(4) InAlP epilayers obtained in this study are highly resistive, caused by the large incorporation of impurities, especially oxygen. AlGaP epilayers grown at moderate temperatures are heavily contaminated by carbon, and show low-resistivity of p-type conduction. Active aluminum atoms seem to cause the incorporation of ambient impurities into the epilayers, while the imperfect decomposition of TEAl causes carbon contamination.

References

[1] H.Asahi, Y.Kawamura, H.Nagai, and T.Ikegami, Electron.Lett. **18** (1982) 62.

[2] K.Kobayashi, S.Kawata, A.Gomyo, I.Hino, and T.Suzuki, Electron.Lett. **21** (1985) 931.

[3] Y.Ohba, M.Ishikawa, H.Sugawara, M.Yamamoto, and T.Nakanisi, J.Cryst.Growth **77** (1986) 374.

[4] M.Ikeda, K.Nakano, Y.Mori, K.Kaneko, and N.Watanabe, J.Cryst.Growth **77** (1986) 380.

[5] M.Ikeda, H.Sato, T.Ohata, K.Nakano, A.Toda, O.Kumagai, and C.Kojima, Appl.Phys.Lett. **51** (1987) 1572.

[6] D.P.Bour and J.R.Shealy, Appl.Phys.Lett. **51** (1987) 1658.

[7] J.Y.Kim and A.Madhukar, J.Vac.Sci.Technol. **21** (1982) 528.

[8] M.Kumagai and T.Takagahara, Phys.Rev. **B37** (1988) 898.

[9] W.L.Smith and T.Wartik, J.Inorg.Nucl.Chem. **29**, 629 (1967).

[10] T.Mole and E.A.Jeffery, "Organoaluminum Compounds", Elsevier Pub., Amsterdam (1972) 93.

[11] M.Mashita, S.Horiguchi, M.Shimazu, K.Kamon, M.Mihara, and M.Ishii, J.Cryst.Growth **77** (1986) 194.

[12] B.A.Joyce, P.J.Dobson, J.H.Neave, K.Woodbridge, J.Zhang, P.K.Larsen, and B.Bolger, Surf.Sci. **168** (1986) 423.

[13] M.Tanaka and H.Sakaki, Superlattices Microstruct. **4** (1988) 237.

5. EFFECTS OF LATTICE MISMATCH

5-1. Introduction

Lattice matching to substrates is extremely important in preparing various heterostructures with high quality, and thus is the most restrictive condition in device design. The AlGaAs/GaAs system is free from this restriction, since $Al_xGa_{1-x}As$ is almost perfectly lattice-matched to GaAs substrates for the entire range of composition x. Hence, most of heterostructure devices have been developed mainly in the AlGaAs/GaAs system, while a large difference of lattice parameter among InP, GaP, and GaAs (Table 5.1) has kept the InGaP/GaAs system far behind in device application. A large mismatch of lattice parameters between epilayer and substrate causes many misfit dislocations (or cracks) with interfacial states, which causes nonradiative recombination of free carriers in the epilayer. However, when the lattice-mismatched epilayer is thin enough, a misfit strain can be accommodated elastically by the tetragonal deformation of the epilayer lattice without generating dislocations. By using such strained epilayers, the device application of phosphorus-based III-V ternary semiconductors including InGaP will surely become advanced to the state of AlGaAs.

As increasing the thickness of strained epilayers, misfit strains beyond accommodation limit are released by generating dislocations (strain relaxation). The accommodation limit, i.e. the critical thickness of strained epilayers, has been predicted as a function of strain, by Matthews and Blakeslee with a force-balancing model[1] and by People and Bean with an energy-balancing model[2]. In the force-balancing model, mechanical equilibrium of a grown-in threading dislocation determines the onset of interfacial misfit dislocations, i.e.,

the grown-in threading dislocations begin to elongate in the plane of the interface when the force exerted by the misfit strain becomes larger than the tension in the dislocation line. In the energy-balancing model, it is assumed that the growing layer is initially free of threading dislocations, and that interfacial misfit dislocations will be generated when the areal strain energy density exceeds the self-energy of an isolated dislocation. The force-balancing model gives a considerably smaller critical thickness than the energy-balancing model. The experimental determination of the critical thickness has been reported for the heterosystem of SiGe/Si[3,4] or InGaAs/InP[5,6], but it has not been confirmed yet which model is more accurate.

Elastic strain is known to influence the energy band gap of III-V semiconductors. Olsen et al. studied strain-induced energy-band-gap shift in strained $In_{1-x}Ga_xP$ grown on GaAs(001) by VPE[7]. Asai and Oe gave a quantitative explanation on the strain-induced gap-shift, and showed that their experimental results for compressively strained $In_{1-x}Ga_xP$ grown on GaAs(001) by LPE were in quite good agreement with the calculated values[8]. Kuo et al. have reported the energy-band-gap shifts in strained $In_{1-x}Ga_xAs$ on InP(001) and $In_{1-x}Ga_xP$ on GaAs(001), both grown by MOVPE[9]. However, the relationship between the strain relaxation and the energy-band-gap shift, inevitably required in applying strain-induced physics like energy-band-gap shift to devices, has been unclear in these reports.

In this chapter, misfit-strain effects on lattice parameters, energy band gap, and electrical properties are described for $In_{1-x}Ga_xP$ epilayers grown on GaAs(001) substrates by MOMBE. The strain accumulation/relaxation and the energy-band-gap shift are discussed for the wide range of epilayer composition x with a constant epilayer thickness of 0.75μm.

5-2. Experiments

$In_{1-x}Ga_xP$ epilayers (0.75μm) were grown on GaAs(001) substrates by MOMBE at 490℃. Epilayer composition was determined by standard x-ray diffraction analysis on the (002) plane, together with the estimation of strain accumulation/relaxation. Since the scattering factor of gallium atoms is very close to that of arsenic atoms, x-ray diffraction is quasi-forbidden for the (002) plane of GaAs. Thus, (002) diffraction from the epilayers is always observed clearly, though the resolution of standard x-ray diffraction analysis is relatively poor; the resolution-minimum of FWHM of rocking curves for the standard x-ray apparatus used in this study was 0.05 degree. In order to discuss lattice distortion more strictly, the lattice parameters of nearly lattice-matching epilayers were measured by double-crystal x-ray diffraction analysis on the (004) and (115) planes. The resolution-minimum of FWHM in double-crystal x-ray diffraction is 15 msec. The band-gap energy of the epilayers was determined by PL measurement performed at 77K with a conventional grating monocromator and a photomultiplier. An argon ion laser of 6 mW was used as an excitation beam. An energy-resolution in the PL apparatus is approximately 5 meV for the energy range of 1.85-2.05 eV in this study. Carrier concentration and mobility were obtained by Hall measurement at room temperature. Table 5.1 shows the list of numerical values used in this investigation.

5-3. Strain Effects

5-3-1. Lattice Parameters

Misfit strain in heterostructures of zinc-blende type

Table 5.1. List of numerical values used in this study.

	InP	GaP	GaAs
lattice parameter (Å)	5.86875 [10]	5.45117 [11]	5.65325 [12]
thermal expansion coefficient [13] ($\times 10^{-6}$/℃)	4.75	5.91	6.63
elastic stiffness [8]			
C_{11}	1.022	1.412	-
C_{12}	0.576	0.625	-
($\times 10^{12}$ dyn/cm^2)			
deformation potential			
hydrostatic (eV)	-0.8	-9.5	-
shear (eV) [8]	-1.55	-1.3	-
energy band gap of $In_{1-x}Ga_xP$ at 77K [14]: $1.414 + 1.452x + 0.758x(x-1)$ (eV)			

semiconductors including $In_{1-x}Ga_xP$ is generally accommodated only by the tetragonal deformation of the epilayer lattice. Thus, the lattice parameters of strained epilayers, normal ($a_\perp$) and parallel ($a_\parallel$) to the substrate surface, deviate from the natural strain-free lattice parameter (a). For an ideally strained epilayer on a (001) substrate, the parameter $a_\parallel$ is equal to the lattice parameter of the substrate (a_0). The parameter $a_\perp$ in this case is related to a by the following equation[15];

$$\frac{\Delta a}{a_0} = \frac{C_{11}}{C_{11}+2C_{12}} \cdot \frac{\Delta a_\perp}{a_0} , \qquad (5\text{-}1)$$

where the misfit strain $\Delta a/a_0$ is defined as $(a-a_0)/a_0$, $\Delta a_\perp/a_0$ as $(a_\perp-a_0)/a_0$, and C_{ij}'s are the elastic stiffness coefficients for the epilayer. By the equation (5-1) and Vegard's law, the composition x of ideally strained $In_{1-x}Ga_xP$ epilayers is determined from the parameter $a_\perp$, which can be directly measured by x-ray diffraction analysis on the epilayer (002) or (004) plane. The parameter $a_\parallel$ is experimentally obtained from the angle ϕ between the epilayer (115) plane and the substrate (115) plane, using a relation written below (scalar product of normal vectors of the (115) planes);

$$\left(\frac{1}{a_\parallel},\frac{1}{a_\parallel},\frac{5}{a_\perp}\right)\cdot\left(\frac{1}{a_0},\frac{1}{a_0},\frac{5}{a_0}\right)$$
$$= \left|\left(\frac{1}{a_\parallel},\frac{1}{a_\parallel},\frac{5}{a_\perp}\right)\right|\cdot\left|\left(\frac{1}{a_0},\frac{1}{a_0},\frac{5}{a_0}\right)\right|\cdot\cos\phi \quad . \qquad (5\text{-}2)$$

The angle ϕ can be measured also by x-ray diffraction analysis on the (115) plane. On the other hand, when the misfit strain is completely relaxed by generating dislocations, both $a_\perp$ and $a_\parallel$ are equal to a.

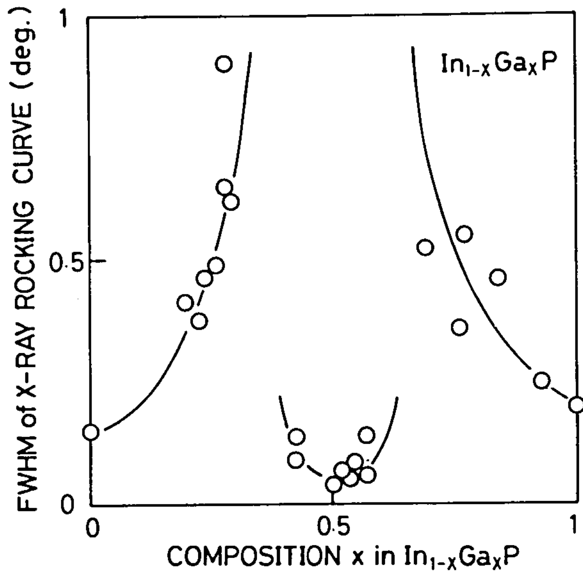

Fig. 5.1. Dependence of FWHM of x-ray rocking curve on epilayer composition x in $In_{1-x}Ga_xP$.

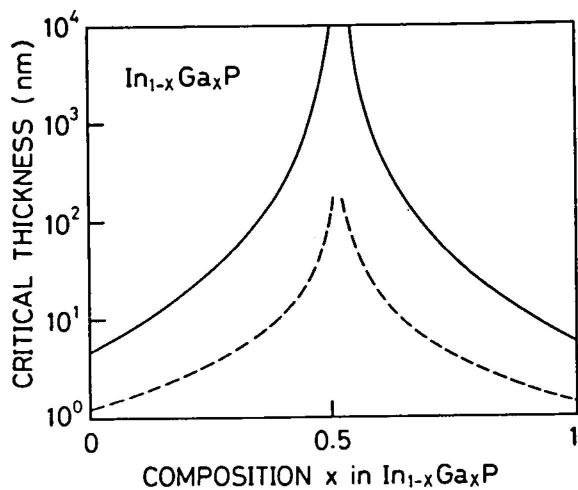

Fig. 5.2. Theoretical calculation of critical thickness; with energy-balancing model (solid line) and with force-balancing model (broken line).

The accumulation and relaxation of misfit strain are clearly shown in the dependence of FWHM of the x-ray (002) rocking curve on the composition x of $In_{1-x}Ga_xP$ epilayers (Fig.5.1). For the epilayer composition x of 0.40-0.60, near lattice-matching to GaAs at x=0.516, the misfit strain is accumulated in the epilayer elastically; a lower FWHM corresponds to homogeneous lattice deformation. A remarkable increase in FWHM at x=0.35-0.40 and x=0.60-0.65 indicates that the lattice deformation is no longer homogeneous, since a large amount of misfit dislocation is introduced into the epilayer to relax over-threshold strain. As epilayer composition approaches to x=0 (InP) or x=1 (GaP), the homogeneity of lattice deformation is recovered as shown by steady decrease in FWHM. Since lattice mismatch is quite large (3-4%) when x is close to 0 or 1, most of the misfit strain is released by generating dislocations at the very early stage of growth. Thus, the upper part of the epilayer has very small strain, contributing to the reduction of FWHM near x=0 or x=1. Based on this analysis, the epilayer composition x in this study is calculated by assuming that the epilayer is ideally strained at x=0.35-0.65, and strain-free elsewhere. The critical thickness (h_c) of $In_{1-x}Ga_xP$ epilayers on GaAs(001) is theoretically calculated using equation (5-3) derived from the force-balancing model[1], and using equation (5-4) derived from the energy-balancing model[2];

$$h_c = \frac{b(1-\nu\cos^2\theta)}{8\pi f(1+\nu)\cos\alpha}\cdot\left[\ln\left(\frac{h_c}{b}\right)+1\right] \quad , \qquad (5\text{-}3)$$

$$h_c = \left(\frac{1-\nu}{1+\nu}\right)\cdot\left(\cos^2\theta+\frac{\sin^2\theta}{1-\nu}\right)\cdot\left(\frac{1}{16\pi\sqrt{2}}\right)\cdot\left(\frac{b^2}{a}\right)\cdot\left[\left(\frac{1}{f^2}\right)\cdot\ln\left(\frac{h_c}{b}\right)\right] \quad , \qquad (5\text{-}4)$$

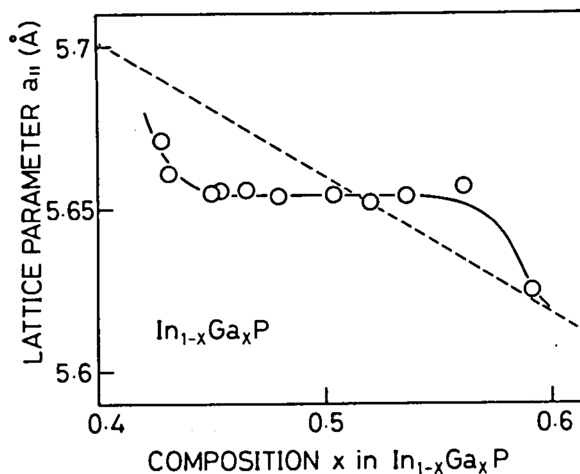

Fig. 5.3. Dependence of lattice parameter $a_{\parallel}$ on epilayer composition x in $In_{1-x}Ga_xP$. Broken line represents lattice parameter for strain-free $In_{1-x}Ga_xP$.

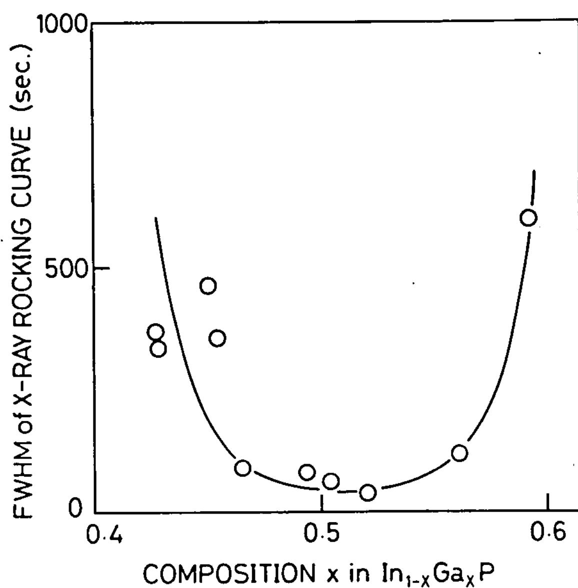

Fig. 5.4. Dependence of FWHM of x-ray rocking curve on epilayer composition x in $In_{1-x}Ga_xP$.

where b is the magnitude of the Burgers vector of the dislocation ($a/\sqrt{2}$), ν is the Poisson ratio equal to $C_{12}/(C_{11}+C_{12})$, θ is the angle between the dislocation line and its Burgers vector (60° for most III-V semiconductors), α is the angle between the slip direction and that direction in the epilayer plane which is perpendicular to the line of intersection of the slip plane and the interface (60°), and f is the absolute value of the misfit between the stress-free epilayer and the substrate ($|a-a_0|/a_0$). As shown in Fig.5.2, the force-balancing model gives considerably smaller h_c than the energy-balancing model does. For the epilayer thickness of 0.75μm in this study, the energy-balancing model gives the critical composition of x=0.45 and x=0.59, fairly close to the observation.

For the more strict analysis of lattice distortion, double-crystal x-ray diffraction measurement was performed for epilayers with x=0.4-0.6, and the lattice parameter $a_{\parallel}$ was calculated by the equation (5-2). As shown in Fig.5.3, the parameter $a_{\parallel}$ is equal to the lattice parameter of GaAs (the substrate) at x=0.44-0.57, clearly indicating that the strain is perfectly accommodated elastically by tetragonal lattice deformation. The critical composition of x=0.44 and x=0.57 obtained from $a_{\parallel}$ measurement also agrees quite well with the calculation based on the energy-balancing model. However, the relaxation of lattice deformation under tensile strain and that under compressive strain is not symmetrical; the value of $(a_{\parallel}-a)/a$, which represents deviation from Vegard's law (broken line in Fig.5.3), is 0.35% at x=0.43 (lattice mismatch $\Delta a/a_0$=0.65%), but only 0.035% at x=0.59 ($\Delta a/a_0$=0.50%). By the thermal expansion of the lattice parameters (Table 5.1), the lattice-matching condition is changed to x=0.507 at the growth temperature of 490℃, but the change is too small to explain the asymmetrical dependence observed. Therefore, the observation

indicates that the tensile strain in the epilayer is relaxed more easily than the compressive strain. Similar an asymmetrical dependence has been reported in InGaAs/InP heterostructures[5,6]. The dependence of FWHM on the epilayer composition measured by double-crystal x-ray diffraction analysis on the (004) plane is given in Fig.5.4. Small values of FWHM under 100 sec were obtained for the epilayers at x=0.46-0.56, where the parameter $a_{\parallel}$ is equal to the lattice parameter of GaAs.

5-3-2. Photoluminescence

The strain-induced shift of the energy band gap in $In_{1-x}Ga_xP$ epilayers on GaAs has been calculated from the orbital-strain Hamiltonian[8]. The dependence of the energy-band-gap shift on misfit strain is expressed as follows[8];

$$\Delta E_{lh} = \left[\frac{-2A(C_{11}-C_{12})}{C_{11}} + \frac{B(C_{11}+2C_{12})}{C_{11}} \right] \cdot f \quad , \qquad (5\text{-}5)$$

$$\Delta E_{hh} = \left[\frac{-2A(C_{11}-C_{12})}{C_{11}} - \frac{B(C_{11}+2C_{12})}{C_{11}} \right] \cdot f \quad , \qquad (5\text{-}6)$$

where ΔE_{lh} is the change of gap between the conduction band and the light-hole valence-band, ΔE_{hh} is that between the conduction band and the heavy-hole valence-band, A is the hydrostatic deformation potential, and B is the shear deformation potential (Table 5.1). Valence-band splitting and shift calculated with the equations are representatively shown in Fig.5.5. The top of valence band at k=0 is on the heavy-hole band in tension, and on the light-hole band in compression. Therefore, for band-to-band recombination processes, electrons at the bottom of conduction

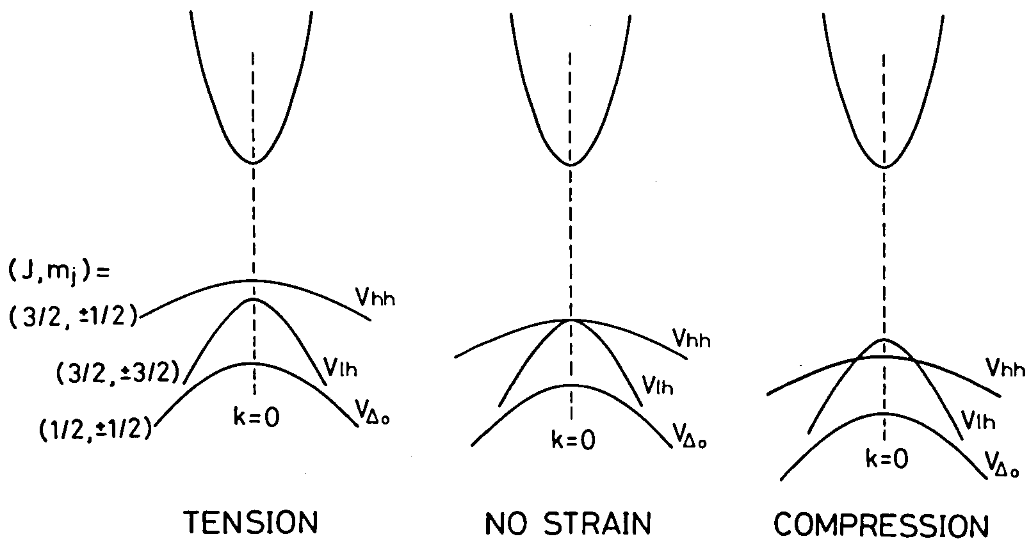

Fig. 5.5. Representations of change (splitting and shift) of energy-band-gap by misfit strain in $In_{1-x}Ga_xP$. (After Kuo et al.[9]).

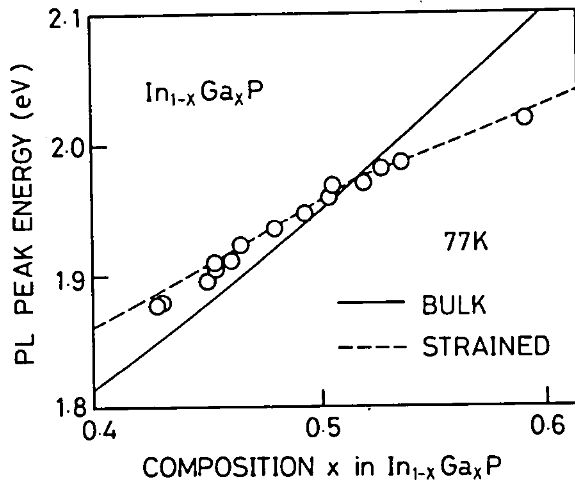

Fig. 5.6. Dependence of photoluminescence peak energy on epilayer composition x in $In_{1-x}Ga_xP$.

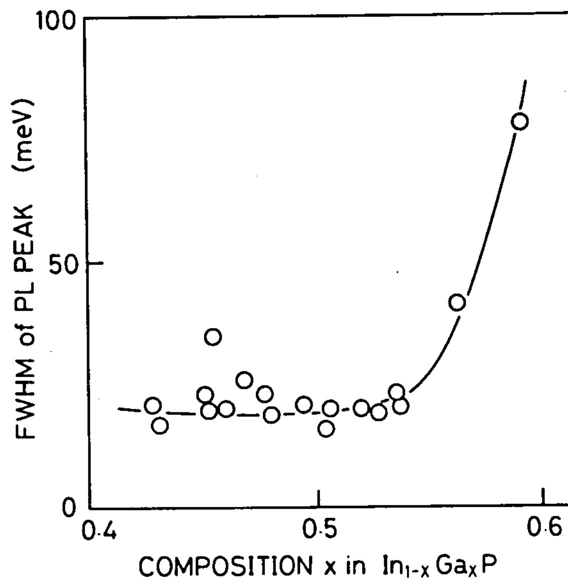

Fig. 5.7. Dependence of FWHM of photoluminescence peak on epilayer composition x in $In_{1-x}Ga_xP$.

valley recombine with heavy-holes in tensively strained epilayers, and with light-holes in compressively strained epilayers. Since the heavy-hole valence-band is more strongly affected by misfit strain than the light-hole valence-band, the energy-band-gap shift is larger in tensile than in compression.

Figure 5.6 shows the dependence of PL peak energy on epilayer composition in the rage x of 0.4-0.6. The solid line in Fig.5.6 represents the energy band gap of strain-free $In_{1-x}Ga_xP$ at 77K[14], and the broken line represents that of ideally strained $In_{1-x}Ga_xP$ epilayers derived from the shift calculation described above. The experimental results agree quite well with the calculation for ideally strained epilayers. It is noteworthy that epilayers with a considerably relaxed lattice at x=0.43 and x=0.59 also show the ideal energy-band-gap shift. This reveals that the energy-band-gap shift is not sensitive to the relaxation of lattice deformation, i.e. the generation of dislocations. The dependence of FWHM of PL peak on epilayer composition is plotted in Fig.5.7. A small value of approximately 20 meV is observed at the range of x=0.43-0.54, while it increases above x=0.55. This asymmetrical dependence is fairly different from the strain-symmetrical change of FWHM of the x-ray rocking curve (Fig.5.4), but corresponds well to the asymmetrical dependence of the lattice parameter $a_{\parallel}$.

5-3-3. Electrical Properties

The dependence of carrier concentration and electron mobility on epilayer composition x in the $In_{1-x}Ga_xP$ epilayers is given in Figs. 5.8 and 5.9, respectively. The low carrier concentration, which is less than 10^{16} cm^{-3}, with a low mobility around 500 cm^2/Vs indicates large compensation in these

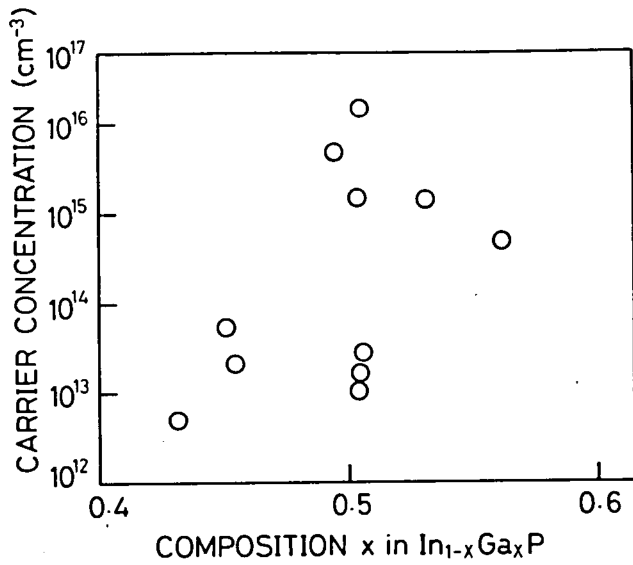

Fig. 5.8. Dependence of carrier concentration on epilayer composition x in $In_{1-x}Ga_xP$.

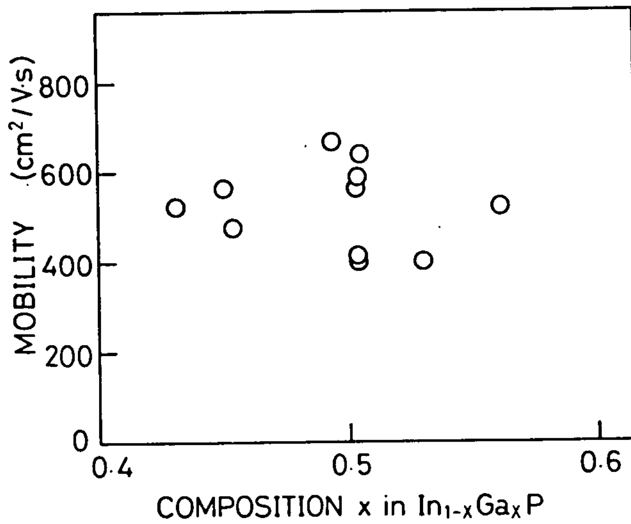

Fig. 5.9. Dependence of mobility on epilayer composition x in $In_{1-x}Ga_xP$.

epilayers. However, it is clear that strain-induced defects (e.g., dislocations) do not cause the large compensation, since the affect of misfit strain on mobility is not observed in Fig.5.9. Therefore, the origin of the carrier traps discussed in the section 3-5-3 (Fig.3.28) is not the strain-induced defects. Since no degradation is observed for lattice parameters and photoluminescence as described in previous sections, the effect of misfit strain is probably negligible for x=0.44-0.57.

5-4. Summary

The following results were obtained for strained $In_{1-x}Ga_xP$ epilayers with a constant thickness of 0.75μm grown on GaAs(001) by MOMBE;

(1) Accumulation and relaxation of misfit strain are clearly observed in the dependence of FWHM of the x-ray rocking curve on epilayer composition. For the upper limit of strain accommodation (critical thickness), the energy-balancing model gives calculated values close to the experimental results. The tensile strain is relaxed more easily than the compressive strain, as suggested in the asymmetrical dependence of $a_{\parallel}$ on misfit strain.

(2) The strain-induced shift of the energy band gap in $In_{1-x}Ga_xP$ epilayers is clearly observed by PL measurements, and it agrees well with theoretical calculation, both for compressively and tensively strained epilayers. Epilayers with considerably relaxed lattice also show the ideal energy-band-gap shifts induced by strain, revealing that the shift is not sensitive to the relaxation of lattice deformation, i.e. the generation of dislocations. The effect of misfit on the FWHM of PL peak is

smaller for compressive strain than for tensile strain.

(3) The origin of the large compensation in electrical properties described in the section 3-5-3 is not strain-induced defects, since mobility does not depend on misfit strain. The small effect of misfit strain on electrical properties was screened by the large compensation, and not observed.

References

[1] J.W.Matthews and A.E.Blakeslee, J.Cryst.Growth **27** (1974) 118.

[2] R.People and J.C.Bean, Appl.Phys.Lett. **47** (1985) 322.

[3] Y.Kohama, Y.Fukuda, and M.Seki, Appl.Phys.Lett. **52** (1988) 380.

[4] R.H.Miles, T.C.McGill, P.P.Chow, D.C.Johnson, R.J.Hauenstein, C.W.Nieh, and M.D.Strathman, Appl.Phys.Lett. **52** (1988) 916.

[5] K.Nakajima, S.Komiya, K.Akita, T.Yamaoka, and O.Ryuzan, J.Electrochem.Soc. **127** (1980) 1568.

[6] K.Nakajima, S.Yamazaki, S.Komiya, and K.Akita, J.Appl.Phys. **52** (1981) 4575.

[7] G.H.Olsen, C.J.Nuese and R.T.Smith, J.Appl.Phys. **49** (1978) 5523.

[8] H.Asai and K.Oe, J.Appl.Phys. **54** (1983) 2052.

[9] C.P.Kuo, S.K.Vong, R.M.Cohen, and G.B.Stringfellow, J.Appl.Phys. **57** (1985) 5428.

[10] G.Giesecke and H.Pfister, Acta Crystallogr. **11** (1985) 369.

[11] H.C.Casey Jr. and M.B.Panish, "Heterostructure Lasers part B", Academic Press, New York (1978) 8.

[12] C.M.H.Driscoll, A.F.W.Willonghby, J.B.Mullin, and B.W.Straughan, "Proc. of Symposium on Gallium Arsenide and Related Compounds 1974", Inst.Phys., London (1975) 275.

[13] I.Kudman and R.J.Paff, J.Appl.Phys. **43** (1972) 3760.

[14] R.J.Nelson and N.Holonyak Jr., J.Phys.Chem.Solids **37** (1976) 629.

[15] J.Hornstra and W.J.Bartels, J.Cryst.Growth **44** (1978) 513.

6. CONCLUSION

In this thesis, the growth characteristics and mechanisms of low-vacuum MOVPE and MOMBE have been investigated for phosphorus-based III-V ternary semiconductors (InGaP, InAlP, and AlGaP) by using ethyl-based metalorganics (TEIn, TEGa, and TEAl) and phosphine. The investigation provides much useful information on the surface reaction of metalorganics, the evaporation of phosphorus atoms at higher temperatures, the influence of phosphorus flux on epilayer quality, and the selective epitaxy of InGaP on SiO_2-masked GaAs substrates. Such information has been inevitably required to apply MOMBE, the most promising technique in preparing various heterostructure devices with high quality, to the epitaxy of the phosphorus-based III-V semiconductors. The effects of misfit strain on physical properties (lattice parameters, photoluminescence, and electrical properties) have also been discussed for $In_{1-x}Ga_xP$ epilayers grown on GaAs(001) by MOMBE. Experimental results indicate that strained $In_{1-x}Ga_xP$ epilayers can be used as an active layer in heterostructures, unless the epilayer thickness is beyond the upper limit of the elastic accommodation of misfit strain. Therefore, the application of the phosphorus-based III-V semiconductors to strained active layers in various heterostructures shows great potential for realizing high-speed devices and visible light-emitting devices with excellent performance.

In chapter 2, the investigation on low-vacuum MOVPE was described. The crystal growth in low-vacuum MOVPE is controlled by the supply of group-III sources, but the composition x in $In_{1-x}Ga_xP$ layers is not proportional to the flow ratio of TEGa/(TEGa+TEIn); since involatile materials are formed by vapor-phase reactions between TEIn and phosphine, the use of TEIn is highly inefficient compared with that of TEGa. The

decomposition of metalorganics in the vapor phase is enhanced by substrate temperature. Thus, the effective supply of metalorganics, which governs the growth rate, is lowered with increasing temperature, but the composition is not affected by the temperature. The crystal quality is improved by higher temperatures. The influence of other factors such as growth rate or phosphine flow on the crystal quality was not observed. The vapor-phase reactions, such as the decomposition of metalorganics and the parasitic reactions between TEIn and phosphine, are undesirable for the precise control of growth rate and epilayer composition. In some cases below 620℃, two separate peaks of (002) diffraction observed in x-ray analysis indicate that immiscible growth occurs in the low-vacuum MOVPE of InGaP. EPMA analysis on the immiscible layers revealed that many InP-rich crystallites are formed in GaP-rich flat area. A growth model based on the thermodynamic explanation of immiscibility was proposed to explain the immiscible growth of InGaP and its surface morphology consistently.

Detailed discussion on InGaP growth in MOMBE was made in chapter 3. Three distinct stages are observed in the temperature dependence of growth rate and epilayer composition. The growth is limited by the imperfect pyrolysis of TEGa at lower temperatures below 390℃, by the supply of metalorganics at moderate temperatures of 390-520℃, and by the shortage of phosphorus at higher temperatures above 520℃. For the moderate temperatures, the growth rate is proportional to the group-III total flux of TEGa+TEIn, and the composition x in $In_{1-x}Ga_xP$ epilayers to the flux ratio of TEGa/(TEGa+TEIn), revealing that the vapor-phase reactions observed in low-vacuum MOVPE are completely removed in MOMBE. Optical and electrical properties are slightly improved by smaller phosphine fluxes. Perfectly selective epitaxy of InGaP was demonstrated at 490℃ on SiO_2-masked substrates, suggesting

that metalorganics are not adsorbed on the insulator surface. The surface catalytic effect of phosphorus at the growth interface on TEGa decomposition is considerably smaller than that of arsenic; an apparent activation energy of 39 kcal/mol was observed for TEGa decomposition in InGaP MOMBE, which is much larger than in GaAs MOMBE (20 kcal/mol). With increasing temperature above 520℃, the growth rate of InP constituent is substantially decreased compared with that of GaP constituent, corresponding to weaker In-P bonds than Ga-P bonds. A new type of complex defect (InP crystallite partially surrounded by metal indium) or indium droplets are found on the epilayer surface, when phosphorus shortage is severe. Each epilayer grown at 490℃ shows a quite sharp band-edge peak (with FWHM as low as 16 meV) and two broad defect-related peaks in PL spectrum at 77K. The undoped epilayers exhibit n-type conduction ($n=10^{13}-10^{16}$ cm^{-3}, $\mu_H=500-600$ cm^2/Vs), or are highly resistive, indicating that carriers in the epilayers are compensated largely. Carrier traps with two different activation energies (approximately 140 meV and 1.5 eV) found in the temperature dependence of carrier concentration and in photocurrent spectrum are probably responsible for the compensation.

Chapter 4 was devoted to a discussion of MOMBE growth of InAlP and AlGaP. As in InGaP growth, the MOMBE growth of InAlP and AlGaP is governed by the imperfect decomposition of TEGa and TEAl at lower temperatures, while the decomposition of TEAl is imperfect at all the temperatures studied. The existence of other metalorganics (TEIn or TEGa) gives an enhancing influence on TEAl decomposition and changes the apparent activation energy of TEAl decomposition (12-30 kcal/mol). A co-decomposition model proposed in this study, though it is rather speculative, can explain the strange decomposition of TEAl; the thermal energy produced by the pyrolysis of TEIn or TEGa is transferred to TEAl and induces its

decomposition. The shortage of phosphorus (decrease in growth rate and indium droplet formation) observed above 520℃ in InGaP and InAlP epitaxy is caused by the evaporation of phosphorus atoms from epilayers by breaking weak In-P bonds. The incorporation of gallium or aluminum atoms into indium droplets is responsible for the reduced growth rate of GaP or AlP constituent at higher temperatures. The growth rate of AlGaP does not decrease up to 650℃ because of the absence of weak In-P bonds. The large incorporation of impurities, especially oxygen, causes highly resistive InAlP epilayers in this study. AlGaP epilayers (p-type and low resistive) are heavily contaminated by carbon. Active aluminum atoms induce the incorporation of ambient impurities, and the imperfect decomposition of TEAl results in the carbon contamination.

In chapter 5, effects of misfit strain on physical properties (lattice parameters, photoluminescence, and electrical properties) were discussed for strained $In_{1-x}Ga_xP$ epilayers grown on GaAs(001) by MOMBE. In the dependence of FWHM of x-ray rocking curves on epilayer composition, accumulation and relaxation of misfit strain are clearly observed. The upper limit of strain accommodation (critical thickness) obtained by the energy-balancing model agrees well with the experimental results. The asymmetrical dependence of $a_{\parallel}$ (lattice parameter parallel to the substrate surface) on misfit strain suggests that the tensile strain is relaxed more easily than the compressive strain. The strain-induced shift of energy band gap in $In_{1-x}Ga_xP$ epilayers, clearly observed in PL spectra, fits well with theoretical calculation, both in compression and in tension. The ideal energy-band-gap shifts are observed also for epilayers with considerably relaxed lattice, indicating that the shift is not sensitive to the generation of dislocations. Tensile strain shows a larger influence on the FWHM of PL peak than compressive

strain. The carrier traps described in chapter 3 is not originated from strain-induced defects, since electron mobility is independent of misfit strain. The small effect of misfit strain on electrical properties was screened by the large compensation, and not observed.

In the future, more effort should be given to improve the electrical properties of phosphorus-based III-V semiconductors grown by MOMBE. The baking of the growth chamber will surely contribute to the improvement of electrical and optical properties of InGaP epilayers, while some other special techniques should be employed to decompose TEAl perfectly in order to reduce the incorporation of carbon impurities into InAlP and AlGaP epilayers. In preparing three-dimensional heterostructures, which have unique characteristics in the optical and electrical properties, the advanced growth techniques, such as photocontrolled MOMBE, atomic layer MOMBE, migration-enhanced MOMBE, and electron-beam drawing MOMBE, shows great promise, as well as the selective epitaxy in MOMBE demonstrated in this investigation. For these evolutions of MOMBE, the analysis of adsorbed species on the growth interface and the characterization of their migration must be investigated further. For realizing high-speed devices and visible light-emitting devices with high performance, strained layer superlattices and graded composition epilayers of phosphorus-based III-V semiconductors show great potential, as well as thin strained epilayers investigated in this study. Intensive investigation on these advanced structures promises that optical devices with excellent performance, including integrated optical neuro-devices, can be realized and may contribute towards the achievement of artificial intelligence.

LIST OF PUBLICATION

(1) "LOW-VACUUM METALORGANIC VAPOR PHASE EPITAXY OF InGaP AND ITS IMMISCIBLE GROWTH",
Kazunari OZASA, Masaaki YURI, Shigehiro NISHINO, and Hiroyuki MATSUNAMI,
Journal of Crystal Growth **89** (1988) 485-495.

(2) "IMMISCIBLE GROWTH OF $In_{1-x}Ga_xP$ IN LOW-VACUUM MOVPE",
Kazunari OZASA, Masaaki YURI, Shigehiro NISHINO, and Hiroyuki MATSUNAMI,
Journal of Crystal Growth **93** (proceedings of the fourth International Conference on Metalorganic Vapor Phase Epitaxy) (1988) 177-181.

(3) "GROWTH MECHANISM OF $In_{1-x}Ga_xP$ AND $In_{1-x}Al_xP$ IN METALORGANIC MOLECULAR BEAM EPITAXY",
Kazunari OZASA, Masaaki YURI, Shigehisa TANAKA, and Hiroyuki MATSUNAMI,
Journal of Crystal Growth **95** (proceedings of the fifth International Conference on Molecular Beam Epitaxy) (1989) 171-175.

(4) "Metalorganic molecular-beam epitaxy of InGaP",
Kazunari OZASA, Masaaki YURI, Shigehisa TANAKA, and Hiroyuki MATSUNAMI,
Journal of Applied Physics **65** (1989) 2711-2716.

(5) "Temperature dependence of InGaP, InAlP, and AlGaP growth in metalorganic molecular-beam epitaxy",
Kazunari OZASA, Masaaki YURI, and Hiroyuki MATSUNAMI,
To be submitted in Journal of Applied Physics.

(6) "Effect of misfit strain on physical properties of InGaP grown by metalorganic molecular beam epitaxy",
Kazunari OZASA, Masaaki YURI, Shigehisa TANAKA, and Hiroyuki MATSUNAMI,
To be submitted in Journal of Applied Physics.